Journal of Sound and Vibration 534 (2022) 117002

Contents lists available at ScienceDirect

Journal of Sound and Vibration

journal homepage: www.elsevier.com/locate/jsvi

Aeroacoustics research in Europe: The CEAS-ASC report on 2020 & 2021 highlights

Attila Balázs Nagy [a], Jan Delfs [b], Gareth J. Bennett [c,*]

[a] Department of Building Constructions, Budapest University of Technology and Economics, Muegyetem rkp. 3., Budapest, 1111, Hungary
[b] Deutsches Zentrum für Luft- und Raumfahrt (DLR), Braunschweig, 38108, Germany
[c] Department of Mechanical, Manufacturing and Biomedical Engineering, School of Engineering, Trinity College Dublin, the University of Dublin, D02 PN40, Ireland

ARTICLE INFO

Keywords:
Aeroacoustics

ABSTRACT

The Council of European Aerospace Societies (CEAS) Aeroacoustics Specialists Committee (ASC) supports and promotes the interests of the scientific and industrial aeroacoustics community on a European scale and European aeronautics activities internationally. In this context, "aeroacoustics" encompasses all aerospace acoustics and related areas. Each year the committee highlights some of the research and development projects in Europe.

Due the effects of the Covid 19 pandemic it was not possible to publish an edition in 2021 and so this paper is a report on highlights of aeroacoustics research in Europe in both 2020 and 2021, compiled from information provided to the ASC of the CEAS. In addition, during 2020 and 2021, a number of research programmes involving aeroacoustics were funded by the European Commission. Some of the highlights from these programmes are also summarized in this article.

Enquiries concerning all contributions should be addressed to the authors who are given at the end of each subsection.

1. Propeller noise

1.1. Surrogate tone noise emission models for propellers

This work deals with the innovative development of surrogate models suitable for the simulation of aerodynamic performance and acoustic emission in terms of tonal components, of multi-propeller systems like those applicable in urban air-mobility vehicles [1]. These can be of great help particularly when designing distributed-electric-propulsion configurations, as they provide an agile tool that avoids the need for computationally expensive CFD/CAA predictions. Without losing the generality of the conclusions that can be drawn about the capability of the proposed surrogate models to accurately describe multi-propeller aerodynamic and aeroacoustic responses, applications to a single propeller configuration are examined. Focusing on the simulation of the effects due to the spanwise distribution of blade twist and chord length, two surrogate modelling techniques are examined: one based on Artificial Neural Networks and one based on Genetic Programming. The numerical database for the identification of these models is determined by the combined application of a boundary integral formulation suitable for the potential aerodynamics solution around lifting/thrusting bodies, and the Farassat 1 A formulation for the evaluation of the noise field [2]. The numerical investigation demonstrates that

* Corresponding author.
E-mail address: gareth.bennett@tcd.ie (G.J. Bennett).

https://doi.org/10.1016/j.jsv.2022.117002
Received 18 March 2022; Received in revised form 25 April 2022; Accepted 4 May 2022
Available online 27 May 2022

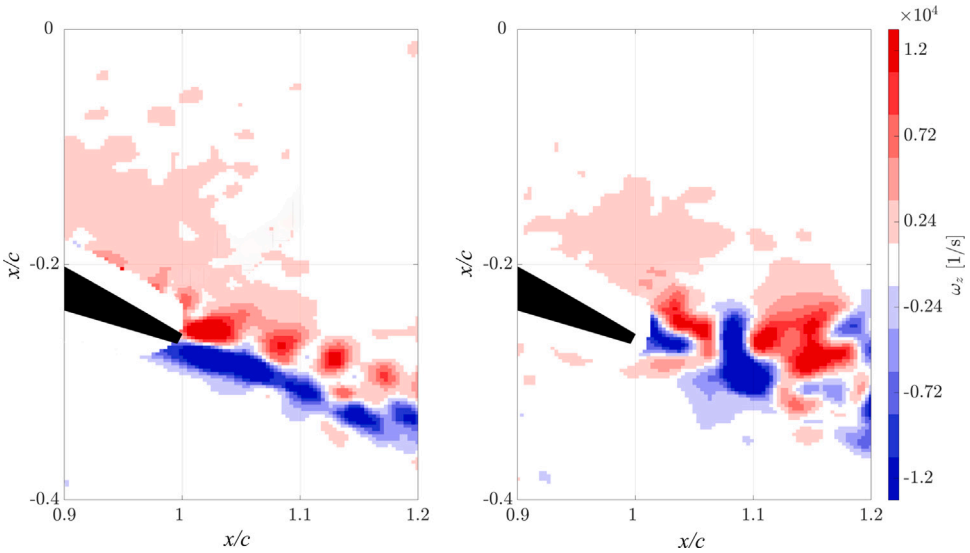

Fig. 1. Instantaneous spanwise vorticity around the trailing edge of the blade section (r/R = 0.6) at 4000 rpm and an advance ratio J = 0.4 (left) and J = 0.6 (right).

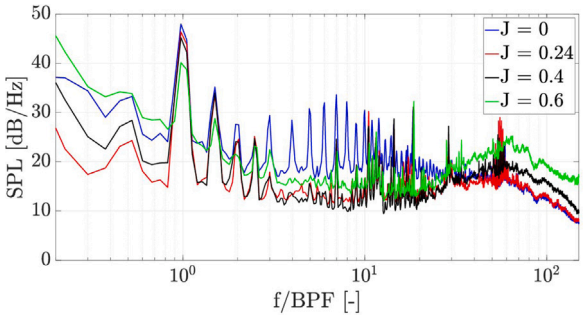

Fig. 2. Comparison of noise spectra at 4000 rpm by varying the advance ratio J from 0 to 0.6.

both metamodelling techniques are able to reproduce propeller aerodynamic performance and radiated noise with a very good level of accuracy, certainly suitable for preliminary design applications.

Written by: Massimo Gennaretti: massimo.gennaretti@uniroma3.it, Roma Tre University, Rome, Italy

1.2. On the aeroacoustic behaviour of propellers operating at low-Reynolds number.

Studies conducted at Delft University of Technology have shed more light on the role of low-Reynolds aerodynamic phenomena on the noise emissions of propeller rotors [3]. The employed configuration has been proposed as a benchmarking database for the assessment of low-order methods [4] and high-fidelity numerical simulations [5].

Casalino et al. [4] have used an aerodynamic low-order method, based on blade element momentum theory (BEMT), coupled with analytical methods for noise prediction, both tonal and broadband, to estimate the aerodynamic forces and the far-field noise. Results agree well with both experiments and high-fidelity numerical simulations. However, it was found that the broadband noise predictions are very sensitive to the wall pressure spectra model used. In addition, it was proposed that the broadband noise could be potentially affected by the presence of a laminar separation (LSB) over the blade surface. Grande et al. [3] has visualized the flow field over the blade surface and confirmed the presence of a LSB on the blade suction side. At high advance ratios, the vortex shedding from the LSB, shown in Fig. 1, is responsible for a high-frequency hump found in the noise spectra (see Fig. 2).

To reproduce the acoustic far-field noise caused by the flow development on the blade, an engineering approach, using the lattice-Boltzmann Very Large Eddy Simulations method, has been proposed by Romani et al. [5]. A zig-zag trip was placed on the blade surface to force the switch from modelled to resolved turbulence. Results show that both aerodynamic forces and tonal noise are in good agreement with the experiments and that they are not significantly affected by the trip location. The broadband noise is more sensitive to the trip location, and it exhibits the best agreement with the experiments at intermediate advance ratios.

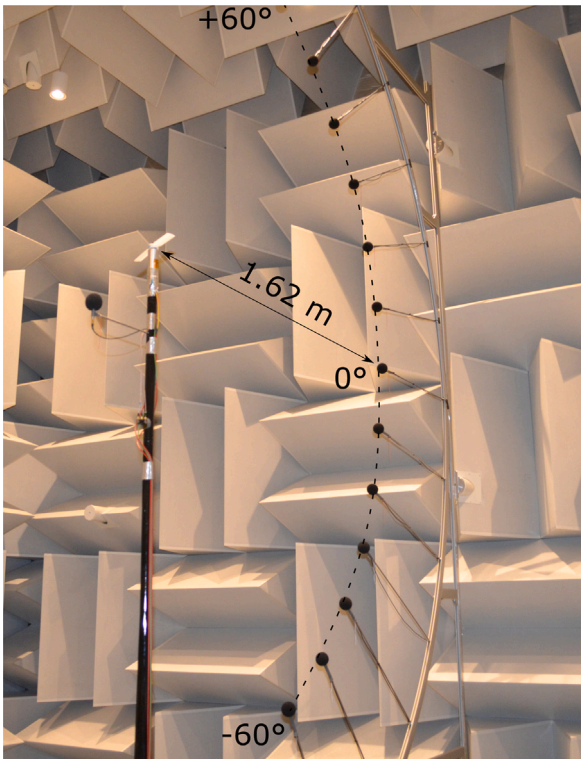

Fig. 3. Photograph of the experimental setup.

Written by: Edoardo Grande (e.grande@tudelft.nl), Damiano Casalino, Gianluca Romani, Daniele Ragni, Francesco avallone, Delft University of Technology, The Netherlands.

1.3. Experimental investigation of low Reynolds number rotor noise

Small UAVs are now used in a wide range of applications, thus raising the question of public acceptance associated, in part, with noise emission. In line with ongoing efforts at ISAE-SUPAERO to investigate the noise generated by small scale isolated UAV rotors operating under hovering conditions, an experimental database that may serve as a benchmark for the assessment of numerical approaches has been created [6,7].

The experimental setup, consisting of an isolated rotor positioned at the centre of ISAE-SUPAERO anechoic room, is presented Fig. 3. Thrust, torque and far field acoustic radiation generated by several rotors were measured at rotational speeds from 2000 to 9000 RPM. First, the quality of the experimental setup was assessed and results obtained on well-known commercial rotors were validated against literature data [8]. Secondly, homemade 3D printed rotors with blade numbers ranging from 2 to 5, NACA0012 blade section profiles, constant chord of 25 mm, constant pitch of 10° and a diameter of 25 cm were tested. These data are currently used to validate in-house numerical methods and are available as an open database for the UAV acoustic community [6,7].

For all the rotors studied, far field spectra are dominated by tones at the blade passing frequency (BPF) together with its harmonics, and present a high frequency broadband noise related to trailing edge noise (see Fig. 4). All these noise components, and hence the overall sound pressure level (OASPL), increase with the rotational speed. An interesting change of directivity pattern is observed for the amplitudes of the BPF and of its first harmonic, with a minimum value at $\theta \sim -10°$ for low RPMs and high numbers of blades, and a maximum value at $\theta \sim 10°$ for high RPMs and low numbers of blades (see Fig. 5). Comparable trends have been observed in the literature [9] and were attributed to phase cancellation of thickness and loading noise sources. Finally, the directivity of the broadband noise presents a dipole like pattern with a minimum value at $\theta = -10°$, as expected for trailing edge noise.

Written by: Romain Gojon (romain.gojon@isae-supaero.fr), Thierry Jardin and Hélène Parisot-Dupuis, ISAE-SUPAERO, Université de Toulouse, France.

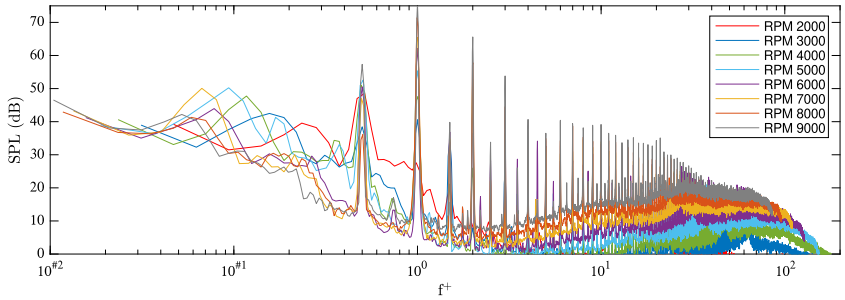

Fig. 4. Sound pressure Levels (SPL) as functions of the frequency normalized by the blade passing frequency of the two-bladed NACA0012 rotor in the rotor disk plane.

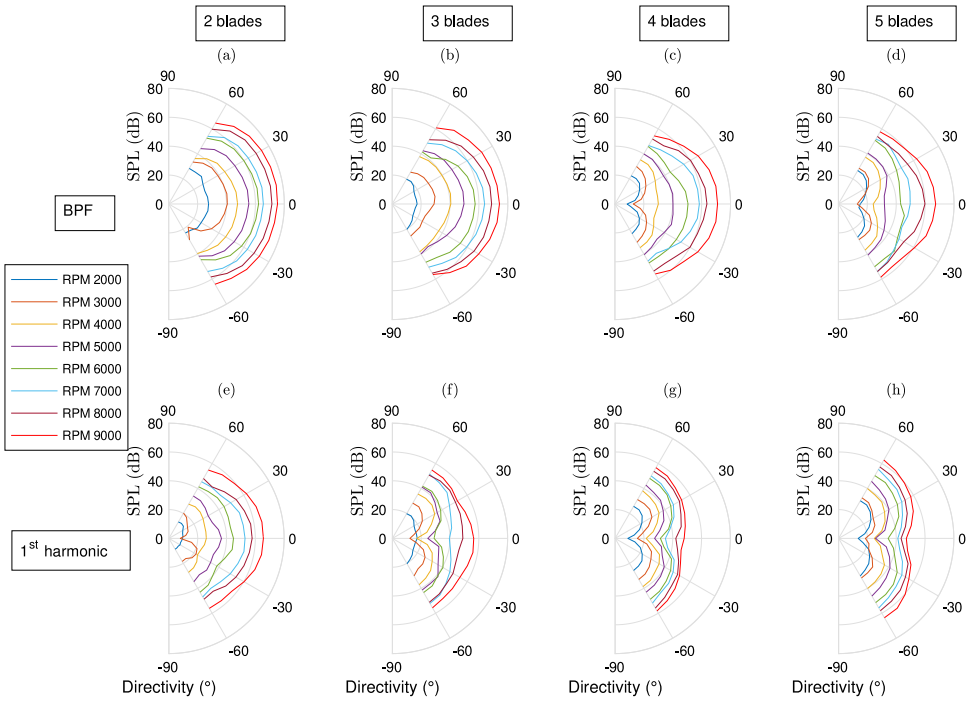

Fig. 5. Directivity of the BPF (a, b, c, d), and of its first harmonic (e, f, g, h) for NACA0012 rotors with 2(a, e)-3(b, f)-4(c, g)-5(d, h) blades in the rotor disk plane.

1.4. Numerical characterization of the aeroacoustic signature of propeller arrays for distributed electric propulsion

This work presents an investigation of the aerodynamic and aeroacoustic interaction of propellers for distributed electric propulsion applications. The rationale underlying the research is related to the key role that aeroacoustics plays in the establishment of the future commercial aviation scenario. The sustainable development of airborne transportation system is currently constrained by community noise, which limits the operations of existing airports and prevents the building of new ones. In addition, the substantial saturation of the existing noise abatement technologies inhibits the further development of the existing fleet, and imposes the adoption of disruptive configurations in terms of airframe layout and propulsion technology. Simulation-based data may help in clarifying many aspects related to the acoustic impact of such innovative concepts. Blended-wing-body equipped with distributed electric propulsion is one of the most promising, due to the beneficial effect of the substantial shielding induced by its geometry. Nevertheless, the novelty of the layout requires a thorough investigation of specific aspect for which no previous experience is available. Herein, the interaction between propellers is analysed for a fixed propeller geometry, as a function of their mutual distance and compared to the acoustic pattern of the isolated one. The aerodynamic results have been obtained using a boundary integral formulation for unsteady, incompressible, potential flows which accounts for the interaction between free wakes and propellers. For the aeroacoustic analyses, the Farassat 1 A boundary integral formulation for the solution of the Ffowcs Williams and Hawkings equation has been used. These results provide an insight into the minimum distance between propellers to avoid

aerodynamic/aeroacoustic interaction effects, which is an important starting point for the development of distributed propulsion systems, see also [10].

Written by Giovanni Bernardini: giovanni.bernardini@uniroma3.it, Fr. Centracchio, M. Gennaretti, U. Iemma, C. Pasquali, C. Poggi, M. Rossetti and J. Serafini, Università Roma Tre, Italy.

2. Techniques and methods in aeroacoustics

2.1. Study of velocity-potential integral formulations for sound scattered by moving bodies

This work deals with the theoretical–numerical study of integral formulations for the prediction of noise scattered by moving bodies, through the velocity-potential description of flow disturbance [11]. Three potential-flow acoustic scattering integral formulations are examined: a linearized boundary-field integral formulation (VP) [12] is compared with two widely applied boundary integral approaches based on Taylor (T) and Taylor–Lorentz (TL) transformations [13,14]. The objective of the work is to give a detailed analysis of the theoretical differences among these formulations and their limits of applicability and to assess their capability of capturing the influence of nonuniform mean flow around moving sound scatterers. This is accomplished by a numerical investigation on a rigid, rectangular, non-lifting wing in uniform rectilinear translation impinged by sound waves emitted by a co-moving pulsating point source. Three boundary integral formulations (linear VP, TL, and T) have been used to predict the scattered noise, and they have been compared with two nonconventional boundary-field integral formulations (linearized VP and VP-A 4). The formulation VP-A 4 is, in principle, equivalent to the Taylor–Lorentz solution of the convective wave equation in nonuniform mean flows. The linearized VP formulation is the most complete linear description of sound scattered in nonuniform mean flow. The numerical results show that the discrepancies of the predictions by the linear VP, T, and TL formulations with respect to those by the linearized VP approach increase as the scatterer velocity and the incident perturbation wave number increase. Furthermore, the use of a non-exact fundamental solution in the TL formulation makes it less accurate than the VP-A4 one, although, at least for the case examined, the greater computational burden of the VP-A4 approach seems to be not compensated for by the slightly increased computational accuracy.

Written by: Giovanni Bernardini: giovanni.bernardini@uniroma3.it, Department of Engineering, Roma Tre University, Italy, Caterina Poggi, Department of Engineering, Roma Tre University, Italy, Massimo Gennaretti, Department of Engineering, Roma Tre University, Italy, Claudio Testa, Rotary-Wing Propulsion and Hydroacoustics Department, Institute of Marine Engineering - National Research Council of Italy, Italy.

2.2. Investigation of extended-tube liners for control of low-frequency duct noise

For noise control of future UHBR aeroengines size and weight constraints on the liners will be more stringent. This work [15] investigated a liner based on the concept of extended tubes which features a number of hollow tubes protruding into the honeycomb cells from the holes of the covering perforated panel. Comparing with the conventional liner, the presence of extended tube can significantly reduce the resonance frequency which is inversely proportional to the extended tube length. An impedance model was developed using the transfer matrix method and end corrections were introduced to account for the grazing flow effect. The proposed impedance model was validated against measured impedance educed from a grazing flow duct test of two 3D printed extended tube liners and a favourable agreement was obtained. The experiments also demonstrated that the extended tube liner exhibits a more linear acoustic behaviour at high SPL compared to a conventional perforated liner. Unsteady numerical simulations showed that the extended tube confines the flow evolution in the perforation and reduce the creation and interaction of vortices. Compared with a conventional liner the acoustic-induced vortex shedding is weaker for the extended tube liner, so its impedance is less affected by a high SPL.

Written by: Cheng Yang: cheng.yang@sjtu.edu.cn, Shanghai Jiao Tong University, Shanghai, People's Republic of China, Penglin Zhang Shanghai Jiao Tong University, Shanghai, People's Republic of China, Stefan Jacob, KTH Royal Institute of Technology, Stockholm, Sweden, Emelie Trigell, KTH Royal Institute of Technology, Stockholm, Sweden, Mats Åbom, KTH Royal Institute of Technology, Stockholm, Sweden.

2.3. In-flight MEMS microphone array measurements of fuselage surface pressure fluctuations

The characteristics of pressure fluctuations on the aeroplane fuselage govern the vibro-acoustic excitation of surface panels exposed to the boundary layer flow. Preparing an experimental setup for measuring the excitation under real flight conditions this study compares small and inexpensive acoustic Micro-Electro-Mechanical Systems (MEMS) to large and proven surface-mounted condenser microphones [16]. The applicability study was carried out in successive steps starting with the comparison of spectra in low-speed wind tunnel environments followed by similar comparisons in a transonic wind tunnel. In a final step, in-flight measurements were performed on the outside fuselage of a twin-engine turboprop aircraft. A slim array of 45 MEMS microphones was used with additional large 1/4-inch microphones installed on the same carrier for comparison. Fig. 6 shows a sketch of the MEMS microphone array mounting. It should be noted that in order to attenuate the pressure excitation, the MEMS microphone array was also coated with a Kapton foil. The acquired data were corrected with regard to influence of the Kapton foil coating. Fig. 7 compares the mean spectra of the reference microphones to the MEMS microphones obtained from one in-flight measurement. While the dominant tonal components (which are assumed to be of acoustic nature as they coincide with multiples of the BPF) measured with both the reference microphone and the MEMS microphone are very similar, some differences are visible for the broadband

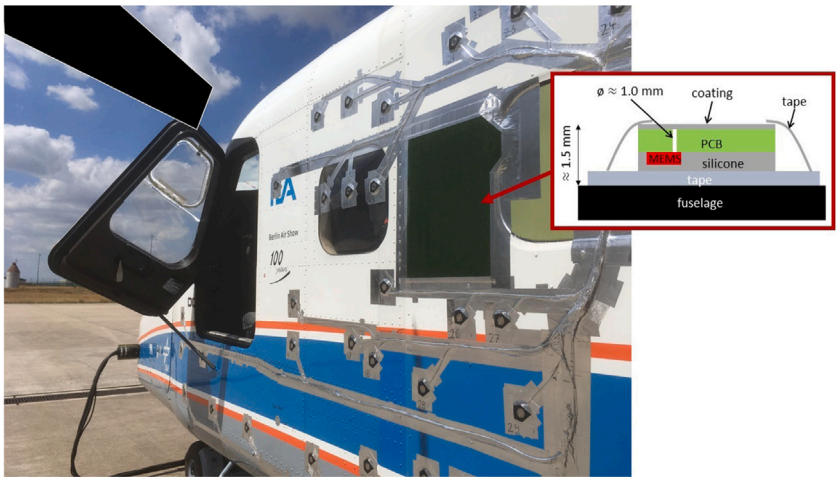

Fig. 6. Photo of the propeller aircraft with the MEMS microphone array mounted on the fuselage and a sketch depicting the MEMS microphone array mounting.

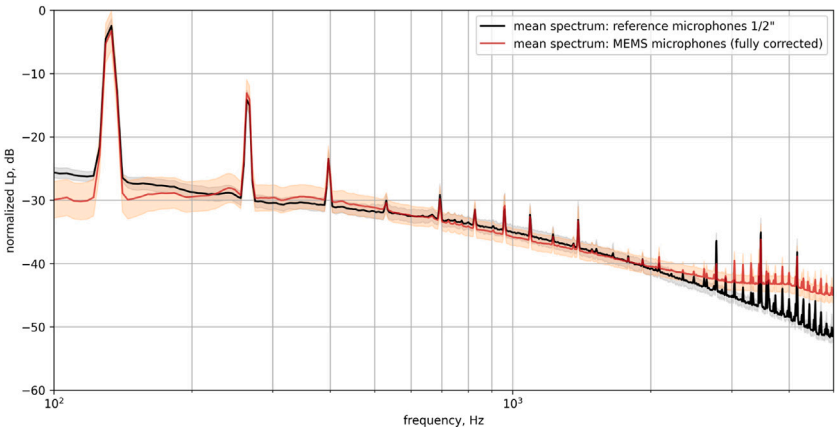

Fig. 7. Comparison of the mean spectra of the MEMS microphones and the reference microphones with standard deviation.

shape of the signal. Above 2 kHz the reference microphone exhibits a stronger drop in signal compared to the MEMS microphone. This drop in signal amplitude at higher frequencies is due to the surface integration of the larger reference microphones.

The study indicated that MEMS microphones are an inexpensive alternative to conventional microphones with increased potential for spatially high-resolved measurements even at challenging experimental conditions during flight tests.

Written by: Thomas Ahlefeldt: thomas.ahlefeldt@dlr.de, DLR, Germany.

2.4. Automatic source localization and spectra generation from sparse beamforming maps

Beamforming is an imaging tool for the investigation of aeroacoustic phenomena and results in high dimensional maps, see Fig. 8, that are broken down to spectra by integrating spatial Regions Of Interest (ROI). However, the ROI are typically designed by hand to achieve satisfying results, which is a slow and iterative process. We present two methods [17] that enable the automated identification of aeroacoustic sources in sparse beamforming maps and the extraction of their corresponding spectra to overcome this challenge. The first relies on the spatial normal distribution of broadband sources in sparse beamforming maps and is similar to an iterative Gaussian Mixture approach. The second uses hierarchical clustering [18] to identify sources in the space-frequency domain. Both methods are robust to statistical noise and predict the existence, location, and spatial probability estimation for sources based on which ROI are automatically determined. The methods are evaluated on two scaled airframe half-model wind-tunnel measurements and on a generic monopole source to provide a quantitative error metric. Fig. 9 shows ROI that result from the iterative Gaussian fitting and Fig. 10 shows the corresponding flap side edge (source no. 13) and its corresponding spectrum, the colour displays the spectrum confidence estimation. This confidence indicates the reliability of the spectra at a given frequency. Both methods show very precise source location estimations with angular errors $\epsilon_\phi \approx 0.4°$, and reconstruct the corresponding spectra with a frequency averaged error of $\epsilon_L \approx 2$ dB in the generic dataset.

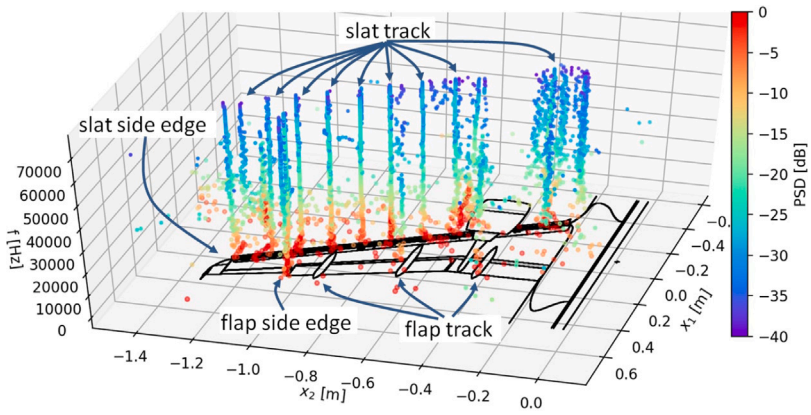

Fig. 8. Sparse CLEAN-SC result on 2D spatial plane using conventional beamforming, the z-axis displays the frequency. The colour represents the normalized PSD in decibel.

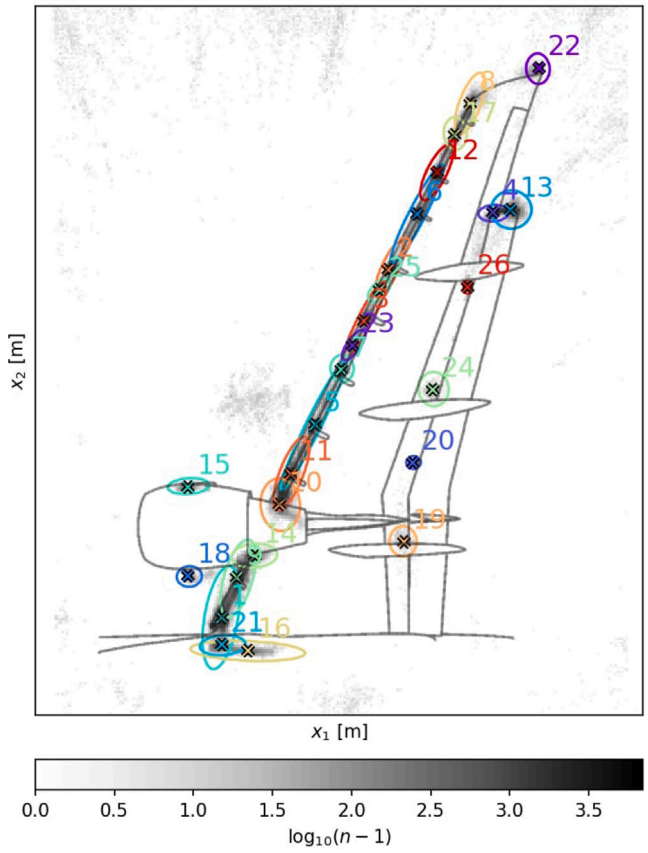

Fig. 9. ROI from the Gaussian fitting result. The ROI numbers correspond to the order of found sources via the maxima in the CLEAN-SC occurrence-histogram, which is displayed with the underlying black/white-map. The ellipses around the ROI represent the normalized Gaussian at $1-3\sigma$.

Written by: A.Goudarzi: armin.goudarzi@dlr.de, C.Spehr, DLR, Germany, S.Herbold, TU Clausthal, Germany.

2.5. Comparative assessment of aircraft system noise simulation tools

In 2012, DLR has initiated an international working group in the area of overall aircraft noise prediction between NASA, ONERA, and DLR. The main goal of the group was to compare their simulation tools and to establish common ground in that area. Two

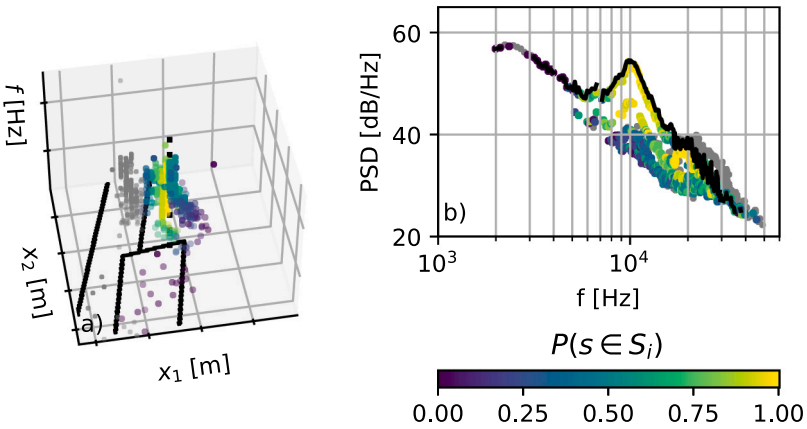

Fig. 10. (*a*) shows the CLEAN-SC results at the flap side edge. (*b*) shows the same points without the x_i-information. Each point is a CLEAN-SC result. The colour represents the probability of belonging to the source ROI $P(s \in S_j)$, grey points were rejected as noise or assigned to another source. The black line represents the integrated spectrum from all source-parts that were assigned to the ROI.

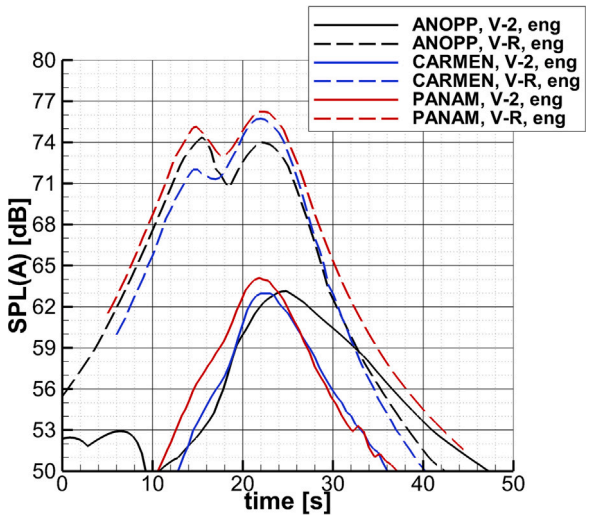

Fig. 11. SPL(A) time-history of engine noise contribution predicted by NASA, ONERA, and DLR.

conceptual aircraft designs have been provided by DLR as an input for a dedicated simulation benchmark test. The input data was comprised of aircraft and engine design, engine performance data, and selected flight procedures. Noise emission spectra for defined operating conditions and immission levels along the flight procedures were predicted within the benchmark activity. The two aircraft, i.e., a conventional tube-and-wing transport aircraft "V-R" and a low-noise concept with engines mounted above the wing-fuselage-junction "V-2", are therefore assessed with NASA's ANOPP, ONERA's Carmen, and DLR's PANAM software. Agreement of the predicted results is good among the three tools, i.e., a 3-−4 dB deviation in maximum A-weighted sound pressure level for the conventional aircraft [19] and up to 4 dB for the low-noise design associated with significant engine noise shielding [20]. In conclusion, the prediction results highlight and confirm the significant noise reduction potential due to shielding for the unconventional aircraft architecture over the conventional under-wing engine installation [21]. For example, see the A-weighted level time-history of the engine noise contribution for both vehicles as predicted by each software in Fig. 11. The results from ANSWr are understood as a first and positive step towards reliable and comprehensive assessment of overall aircraft noise simulation tools. Based on the ANSWr prediction results, the simulated flyover events of both aircraft were also made audible [22].

Written by: L. Bertsch (lothar.bertsch@dlr.de), DLR, Germany, L. Sanders, M. Lorteau, I. Legriffon, ONERA, France, R.H. Thomas, J.C. June, I.A. Clark, NASA, USA.

2.6. Acoustic phase-gradient metasurfaces in aeronautics

Metamaterials might be one of the breakthrough technologies needed from the aeronautic industry to achieve the more and more challenging targets set by the international authorities, specially about noise emissions. However, the direct simulation of

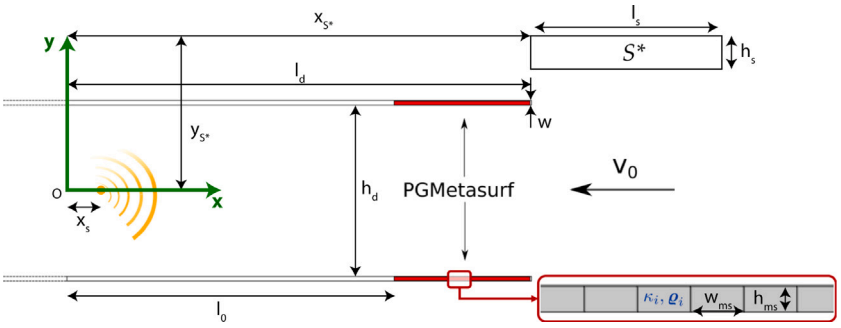

Fig. 12. Sketch of the 2D duct geometry, including the detail of the elementary cells of PGMS based on discrete metafluid and the rectangular subdomain S used to define the objective function in the optimization process.

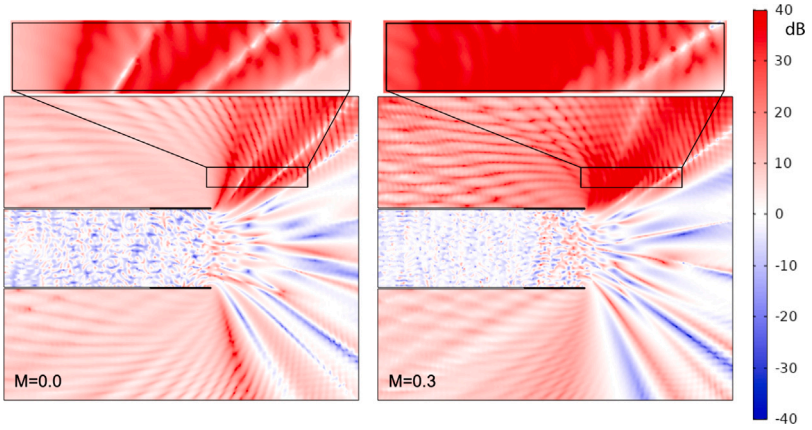

Fig. 13. Delta SPL between sound hard-wall and metafluid lining for $M = 0.0$ and for a uniform flow at $M = 0.3$.

metamaterials and metasurfaces in the aeroacoustic context can be computationally very expensive, even when involved geometries are not particularly complex, limiting the possibility to include metamaterial effects into multidisciplinary design processes for applications of aeronautical interest. A link between Transformation Acoustics (TA) [23] and Generalized Snell's Law, two widely used metamaterial models, has been demonstrated analytically [24]. This theoretical connection allows to consider a phase delay as an acoustic mirage obtainable with an equivalent metafluid, avoiding the burden of modelling specific microstructures in numerical simulations. It also opens new ways to pract ically realize Phase-Gradient Metasurfaces (PGMSs): all the concepts able to change the effective density and speed of sound of a domain, e.g. pentamode materials which already have been demonstrated to be effective in realizing TA concepts, can be adopted for this purpose. Taking advantage of the proposed framework, a simulation-based optimization procedure has been used to address the conceptual design of phase-graded metasurfaces for the acoustic lining of a 2D duct in the presence of a simple uniform flow aimed at reducing the sound pressure level inside an arbitrarily selected region (see Fig. 12). It has been found that the optimized PMGSs introduce an extra degree of freedom in the design of acoustic treatments, in this case exploited to obtain significant changes of the acoustic directivity and a substantial reduction to the noise radiated in the selected region, without modifying the geometry of the duct (see Fig. 13).

Written by: Giorgio Palma (giorgio.palma@uniroma3.it) and L. Burghignoli, Università Roma Tre, Italy.

2.7. New results and applications of pridmore-brown modes

A study is made [25] of acoustic modes in lined ducts with isentropic inviscid transversely non-uniform (i.e. sheared) mean flow and sound speed. As the corresponding eigenvalue problem is called 'Pridmore-Brown equation', these modes are commonly called 'Pridmore-Brown modes'.

Next to some high and low frequency approximations, a numerical solution is presented, utilizing the following (weak) version (1) of the equation, saying that for any test function φ where $p(\mathbf{x}, t) = \hat{p}(y, z)\exp(\mathrm{i}\omega t - \mathrm{i}\kappa x)$ and $\Omega = (\omega - \kappa u_0)/c_0$.

A collection of results is presented, among which the effects of transverse turning points, leading to the occurrence of modes insensitive to the wall impedance (Fig. 14).

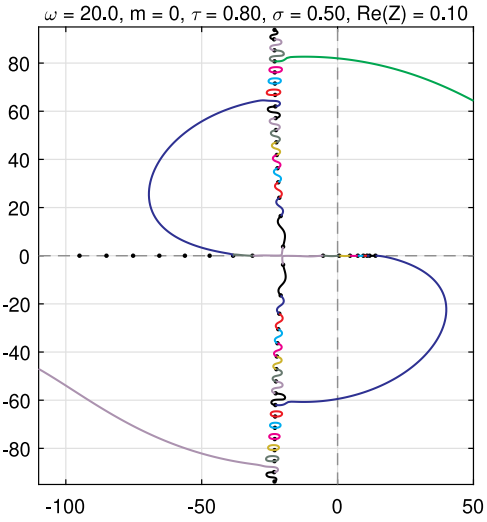

Fig. 14. Complex wave numbers κ for $\omega = 20$ and $u_0 = 0.8 - 0.5r^2$. Tracing for varying $\mathrm{Im}(Z)$ and fixed $\mathrm{Re}(Z) = 0.1$. Note the four surface waves and the practically unaffected cut-on upstream modes.

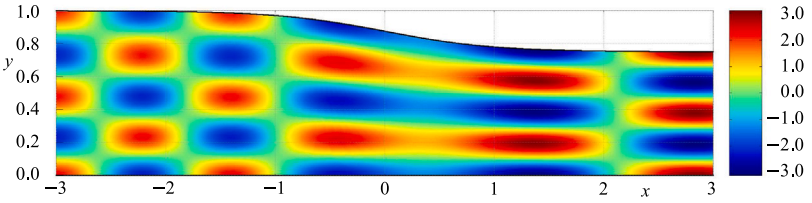

Fig. 15. Pressure field snapshot for right-running mode of order 5 and $\omega = 15$ in converging duct with linearly sheared mean flow.

For slowly varying two-dimensional ducts with a systematically approximated shear flow [26], a slowly varying modes solution of WKB type $p(\mathbf{x}, t) = \Psi(X, y)\, \mathrm{e}^{\mathrm{i}\omega t - \mathrm{i}\int^X \kappa(\varepsilon z)\,\mathrm{d}z}$, $X = \varepsilon x$, is derived, with an incomplete (for general mean flow) and a complete (for linear shear flow) adiabatic invariant of the following form (2).

The occurrence of a complete adiabatic invariant (which is an approximately conserved quantity) is unexpected, because acoustics in sheared flow have in general no conserved energy. By the adiabatic invariant, and apart from the required numerical solution of the Pridmore-Brown equation, the WKB approximation is then virtually available in explicit form (Fig. 15).

$$\int_{\partial\mathcal{A}} \frac{\rho_0 c_0^2}{\mathrm{i}\omega Z}\hat{p}\varphi\,\mathrm{d}\ell + \iint_{\mathcal{A}}\left[-\frac{1}{\Omega^2}\boldsymbol{\nabla}\hat{p}\cdot\boldsymbol{\nabla}\varphi + \left(1-\frac{\kappa^2}{\Omega^2}\right)\hat{p}\varphi\right]\mathrm{d}S = 0, \tag{1}$$

$$\frac{\mathrm{d}}{\mathrm{d}X}\left[\int_g^h \frac{1}{\rho_0\Omega^3 c_0^3}\left(\omega\kappa\Psi^2 + u_0\Psi_y^2\right)\mathrm{d}y\right] = \int_g^h \frac{\kappa u_0 \Psi\Psi_y}{\Omega^4 c_0^4}\left(\frac{u_{0y}}{\rho_0}\right)_X \mathrm{d}y. \tag{2}$$

Written by Sjoerd Rienstra: s.w.rienstra@tue.nl, Eindhoven University of Technology, The Netherlands.

2.8. Acoustic and hydrodynamic instabilities of the flow through a circular aperture in a plate

Plates with orifices are widely adopted in numerous industrial applications, e.g., silencers or fuel injectors. Unfortunately, the analysis of the system dynamics is often oversimplified. In particular, simplified approaches are not able to predict the occurrence of acoustic instabilities and they do not consider energy dissipation processes. A series of articles [27,28] explores the occurrence of acoustic instabilities in a fluid flow through a hole-tone configuration. In light of the limitations listed above, the authors use the full Navier–Stokes equations, and its linearized counterpart, to obtain the reference flow states and analyse the evolution of the perturbations, following the approach described in [29]. The linearized Navier–Stokes equations (LNSE) turned out to correctly describe the spatial amplification of the perturbations and the resulting impedance. These studies revealed the importance of proper treatment of the far-field boundary conditions in truncated domains to resolve the flow field. A novel non-reflecting boundary condition denoted as complex mapping technique [30,31] was introduced to overcome the numerical difficulties created by the strong spatial amplification of the fluctuations. Such a technique was demonstrated to be far more efficient than buffer-layer regions to prevent the appearance of reflected acoustic waves and non-local effects of the incompressible Navier–Stokes equations, see

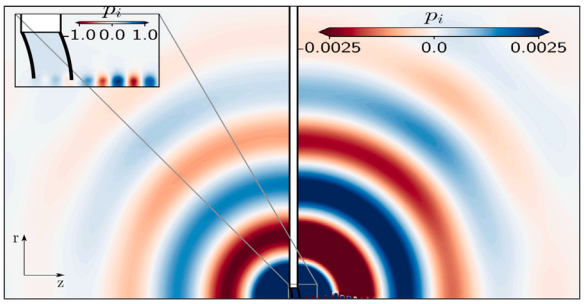

Fig. 16. Pressure p issued from global stability for the hole-tone configuration at $Re = 1600$ and $M = 0.05$ Second mode of instability. The main figure displays the radiation or the acoustic field whereas the zoomed region shows the spatially hydrodynamic mode.

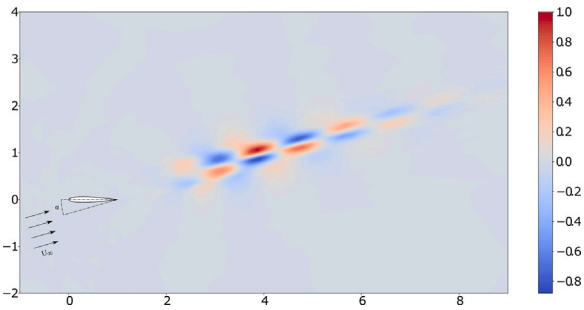

Fig. 17. Streamwise velocity u_x of the most unstable mode at $Re = 1000$, $M = 10^{-1}$ and $\alpha = 16°$.

Figs. 16, 17. Regarding the case of a circular aperture in a thick plate [28], the authors investigated the flow dynamics in both the forced and unforced problem. Two types of acoustics instabilities were identified, pure hydrodynamic instability and conditional instability (Class II and Class III aerodynamic whistles). In future works, the authors will explore the effect of compressibility on either type of instability and the effect on the radiation pattern.

Written by Javier Sierra Ausin: javier.sierra@imft.fr and F. Giannetti Università degli studi di Salerno, Italy, and D. Fabre, Institut des Mécaniques des Fluides, France, and V. Citro, Università degli studi di Salerno, Italy.

2.9. Structural response of stiffened plates in similitude under a turbulent boundary layer excitation

In structural dynamics, similitude laws have been applied to many different configurations [32,33]. Among these, few test-articles analyse stiffened plates or shells. The analyses of these last structures are usually based on the similitude laws for analogous thin, homogeneous and isotropic structural domains and the stiffeners are modelled through a “smeared” approach. In addition, very few papers study the forced vibrations of scaled orthotropic domains by distributed and stochastic loads. This research activity extends the applicability of some similitude laws, developed for thin flat plates under a turbulent boundary layer (TBL) load, to ribbed plates forced by the same wall pressure fluctuations [34]. In particular, the present analysis, concerning the structural response of stiffened plates, does not pursue a general formulation for all possible ribbed configurations, and is focused on a specific TBL model. The methodological approach starts from a specific structural configuration and tries to design an experimental set-up (structural domain and flow conditions) considering and highlighting some elements of feasibility. The proposed approach leads to a distorted similitude and a simple approach to circumvent the distortion effects is proposed. A comparison between the results of two different (in material and dimension) plates, S0 and M1, derived for a different asymptotic speed and using the above-discussed approach is reported in Fig. 18. These results confirm the degree of accuracy that can be achieved with the re-modulation of the results of a scaled configuration, with a small discrepancy that could be not relevant if it is compared with the usual range of uncertainties of experimental data. Moreover, they show that the similitude relationship for the cross-spectral density functions, developed for thin flat plates, can be used for the design of an experimental set-up involving stiffened plates.

Written by Francesco Franco: francof@unina,it, G. Petrone and S. De Rosa, Department of Industrial Engineering, University of Naples Federico II, Italy, and A. Berry and O. Robin, Department of Mechanical Engineering, University of Sherbrooke, Canada, and E. Ciappi, CNR-INSEAN, Italian National Maritime Research Centre, Italy.

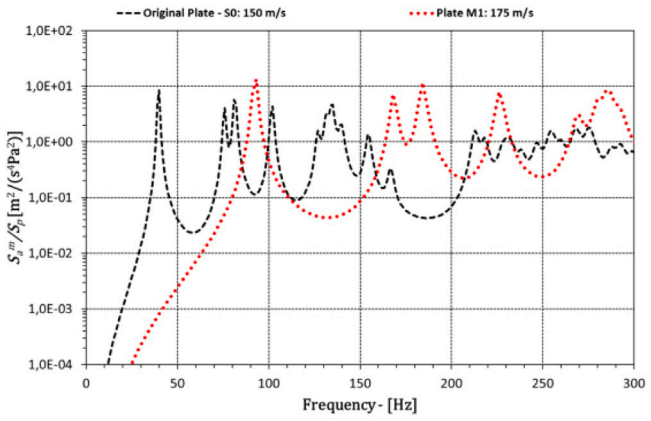

(a) Unscaled results.

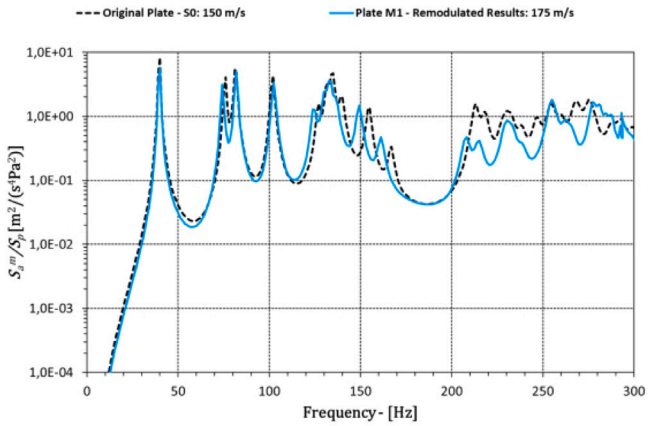

(b) Scaled results– Frequency interpolated results.

Fig. 18. Scaling of vibration response of model plate M1 to original plate S0.

2.10. Weighted data spaces for correlation-based array imaging in experimental aeroacoustics

This contribution presents a concept of data weighting for correlation-based source aeroacoustic imaging methods in frequency domain as detailed in [35]. Each weighting is characterized by its weighting matrix W and defines a corresponding data space with a norm that depends on W. On each data space we can define an associated Beamforming functional. Furthermore, many well-known Beamforming methods (e.g. Conventional Beamforming, Robust Adaptive Beamforming) can be classified in this framework by an explicit choice of W. In particular, we consider an approach motivated by generalized least squares [36] – weighting with the covariances of the correlation data. These statistical quantities are fourth-order moments of the pressure data and can be efficiently estimated from the raw data by Isserlis' theorem [37]. A theoretical analysis reveals that the Beamforming functional that is associated with the full covariance matrix of the correlation data has the lowest variance among all Beamformers from the described class. Numerical computations on synthetic and experimental data (benchmark data from [38]) show that this weighting can help to improve the resolution and dynamic range of Beamforming methods (see Figs. 19 and 20). Moreover, the concept of weighted data norms can be transferred to other source imaging methods such as DAMAS-NNLS. We would like to emphasize that the focus of this article is the introduction of the weighting concept and the use of higher statistical moments of the data, rather than the study of specific imaging methods. The covariances of the correlation data provide useful information on the probability distribution of the measurement error. Therefore, they can be employed for uncertainty quantification of any evaluation method based on correlation data, not necessarily only for source power imaging methods.

Written by H.-G. Raumer: hans-georg.raumer@dlr.de and C. Spehr, DLR, Germany, and T. Hohage, University of Göttingen and Max Planck Institute for Solar System Research, Germany, and D. Ernst, DLR, Germany.

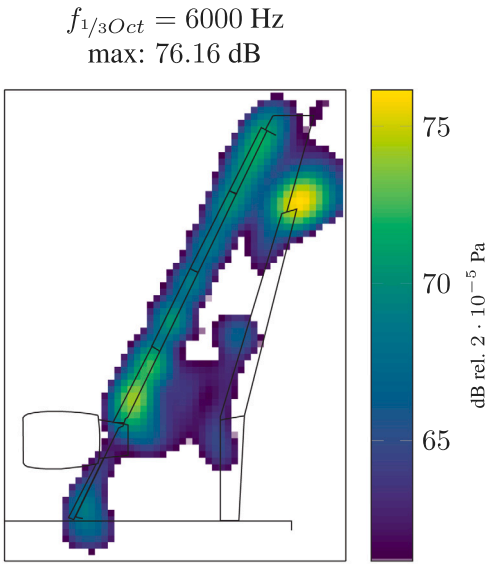

Fig. 19. Conventional Beamforming.

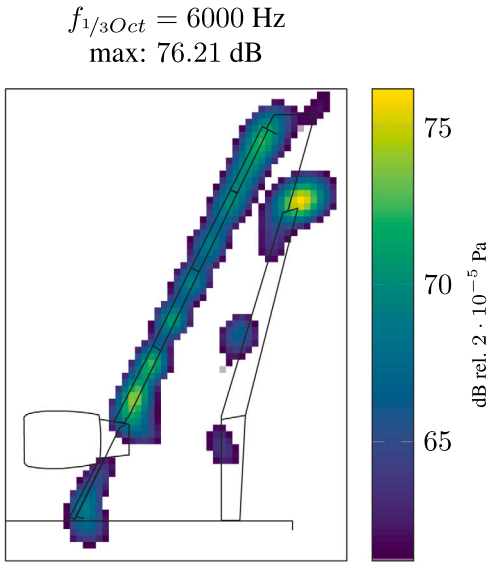

Fig. 20. Weighted Beamforming with the covariance matrix of the correlation data.

2.11. Aeroacoustics simulations of the EAA benchmark case of an axial fan

Future power units of cars (the electric motor, battery, fuel cell) generate little noise during operation. Consequently, the noise of auxiliary units (cooling fan of a battery unit, the turbocharger of fuel cells [39]) becomes an essential task of the developing process. Since performing robust measurements are costly and time-consuming, the presented validated simulation workflow enhances development and research [40].

Within this finished research project, we investigated the individual steps of the hybrid aeroacoustic workflow in detail. Based on existing benchmark data for low-pressure axial fans [41], the perturbed convective wave equation (PCWE) and the Ffowcs Williams and Hawkings analogy Farassat's 1 A (FWH) are analysed. We performed a mesh convergence study and altered the turbulence modelling approach (visualization see Fig. 21). The detached eddy simulation model and a grid of 23.4million cells delivered the most accurate sound radiation (see Fig. 22). The validation of the results allows us to conclude that the fluctuating flow pressure is the relevant flow-convergence criteria, motivated by the fact that it is the dominant source term both for PCWE and FWH.

Furthermore, we showed the robustness of the developed grid interpolation techniques [42] using the Richardson extrapolation. Considering the short duct, we found that for frequencies below 700 Hz, FWH and PCWE deliver a comparable accuracy of sound

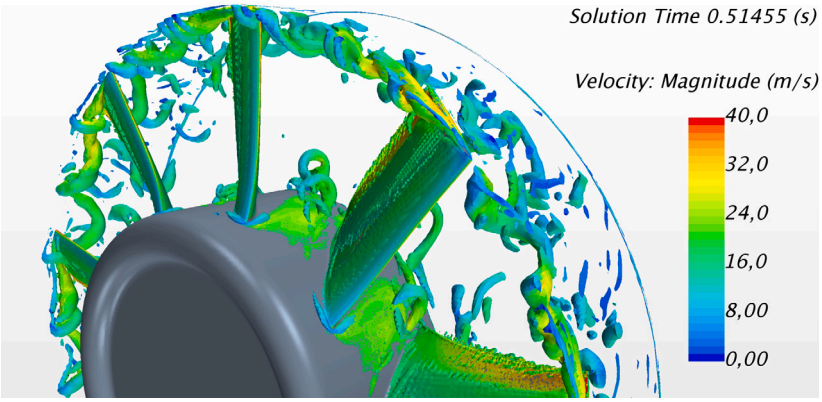

Fig. 21. Q-criterion at instantaneous time, which is showing the turbulent structures of the tip flow.

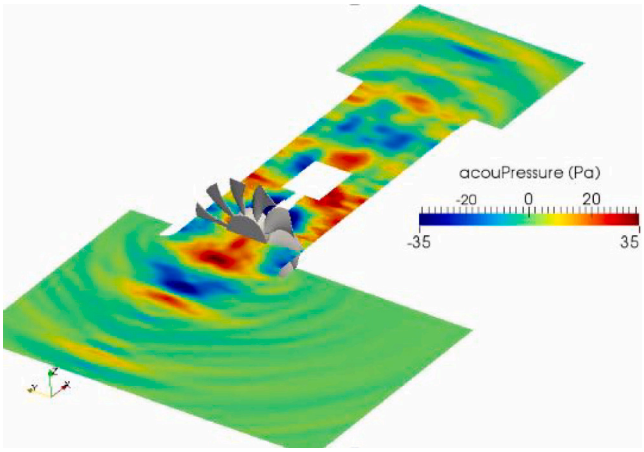

Fig. 22. Sound propagation visualization.

prediction [40]. However, for sources at a higher frequency, the directivity of the propagation matters (which the PCWE accounts for). Since most industrial applications have complicated geometries, including in-duct systems, the PCWE (discretized by the finite element method) is preferable.

Written by: S. Schoder: stefan.schoder@tugraz.at, A. Wurzinger, C. Freidhager, M. Kaltenbacher, IGTE, TU Graz, Austria

2.12. An acoustic relaxation term for damping and forcing of waves

The question of damping or forcing of waves is an important topic in Computational Aero-Acoustics (CAA). In this contribution, an Acoustic Relaxation Term (ART) is presented that is able to control acoustic modes in linear and nonlinear perturbation equations while leaving other modes untouched [43]. This ART is based on the difference between the resolved dilatation and the imposed target dilation, with dilatation being the divergence of the fluctuating velocity field. If the target field is set to zero, the ART acts as a damping term. As opposed to this, waves are excited for a non-zero target dilation. The ART can be seen as the acoustic variant of the previously investigated eddy relaxation term introduced by Ewert at al. [44] and further investigated in Akkermans et al. [45]. Among others, the ART damping characteristics are shown to be favourably frequency selective, i.e., the ART is able to remove undesired oscillations while leaving the hydrodynamics untouched. Note that the ART acts on resolved scales and thereby relies on the accuracy of the numerical scheme (see [43]). The damping characteristic of the ART is illustrated with a benchmark case. It consists of an oscillating energy source (located at origin) inside a 2D jet, which generates acoustic waves that are refracted by the jet's shear-layer (see, e.g., [46]). The turbulent instabilities excited by the periodic energy injection yield problems for CAA methods based on non-viscous linear equations. Fig. 23a) presents the fluctuating pressure contours for $\sigma = 0$ (i.e., no damping), showing the acoustic waves propagating upward and the strong hydrodynamic structures convecting in the downstream direction. Fig. 23b) presents the same, for the case with damping. The comparison clearly shows that the hydrodynamics is maintained whereas the acoustic wave pattern emitted from the source is successfully removed by the ART. Similar behaviour is shown in Fig. 23c) for the

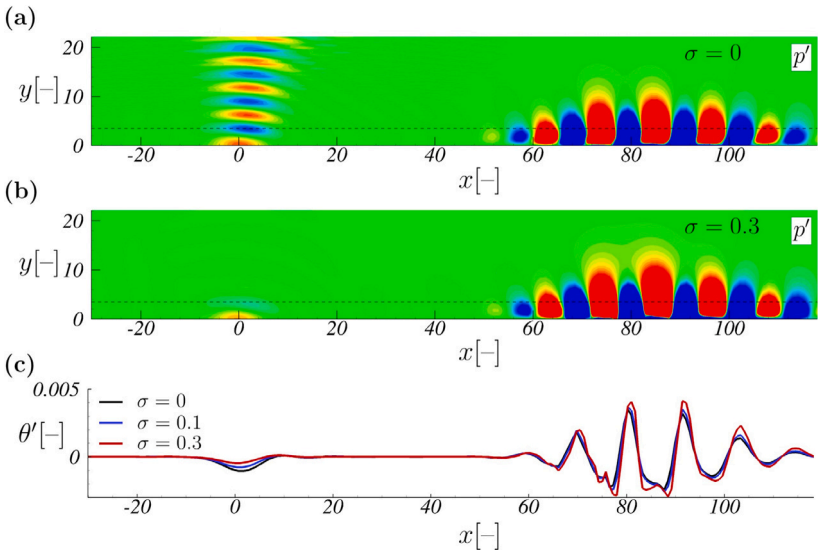

Fig. 23. Contour plot of instantaneous pressure fluctuations p' due to a harmonic energy source, which is located at the origin, for (a) no damping $\sigma = 0$, (b) non-zero damping $\sigma = 0.3$, and (c) variation of the fluctuating dilatation θ' in the 2-D unstable jet along a horizontal line at $y = 3.5$ for different values of damping σ. Note that the damping is only applied in the area where $y < 10$ (dashed line).

dilatation θ' extracted at $y = 3.5$. For the strongest damping, the hydrodynamic disturbances are slightly increased as this particular σ value acts at its upper stability limit.

P. Bernicke: p.bernicke@tu-braunschweig.de, TU Braunschweig, Germany, R.A.D. Akkermans, Hamburg University of Applied Sciences, Germany, R. Ewert, J. Dierke, DLR, Germany

2.13. Sound quality assessment of novel aircraft concepts

Literature suggests that psychoacoustic metrics (PM), which are deeply based on the human auditory system, may provide a better objective quantification of short-term annoyance to aircraft noise than the Effective Perceived Noise Level (EPNL) [47,48]. Aiming at the sound quality assessment of novel aircraft concepts, Ref. [49] presents a comprehensive methodology based on (1) computational predictions of aircraft noise immission using the DLR tool PANAM [50,51] and (2) a sound quality analysis tool (see Fig. 24). The feasibility of the methodology is proven by a case study. Therein, the noise immissions of a novel medium-range aircraft design (denominated V-2) with enhanced fan-noise shielding properties (due to the positioning of the engines above the fuselage) are assessed in terms of the PM loudness, sharpness, and tonality. Moreover, the methodology is steered towards comm unity noise assessment, where the impact on short-term annoyance brought by the novel aircraft is compared to a reference A319-like aircraft (denominated V-R). The assessment is based on the modified psychoacoustic annoyance model ($\mathrm{PA}_{\mathrm{mod}}$) proposed by More [47]. The results (see Fig. 25) show that the fan-noise shielding vehicle architecture under consideration is beneficial for the short-term annoyance mainly in the area directly below the flight trajectory. For areas adjacent to the flight trajectory, an increase of the short-term annoyance is observed, which is mainly due to the lateral directivity of the V-2 aircraft engine noise. Future work will focus on automated sound quality evaluation within large conceptual aircraft studies, aiming at (1) assessing possible improvements on current aircraft configurations, and (2) investigating novel low-annoyance aircraft designs.

Written by G. F. Greco: g.felix-greco@tu-braunschweig.de, TU Braunschweig, Germany, and L. Bertsch, DLR, Germany, and T. P. Ring and S. C. Langer, TU Braunschweig, Germany.

2.14. Computation of adjoint Green's functions using the flow reversal theorem

The adjoint method offers a sensor-based description of sound propagation, and the most general form of the reciprocity principle that is valid for an arbitrarily mean flow. A good approximation of linearized Euler's equations is moreover proposed, which preserve the acoustic energy and prevents from the possible coupling with hydrodynamic modes. The implementation of the technique is illustrated and the valuable assets of considering a simplified self-adjoint wave operator are highlighted. In particular, the reciprocal solution can be computed with the handy flow reversal theorem [52]. This study considers sound propagation over a strongly sheared and stratified parallel flow for which Lilley's wave equation offers an exact description of the acoustics. Fig. 26 presents the fluctuating pressure for an emblematic quadrupole source solved with Lilley's equation. Propagation effects and sound source directivity are intertwined. Fig. 27 shows the solution to Lilley's adjoint equation for a pointwise sensor set out of the flow. This

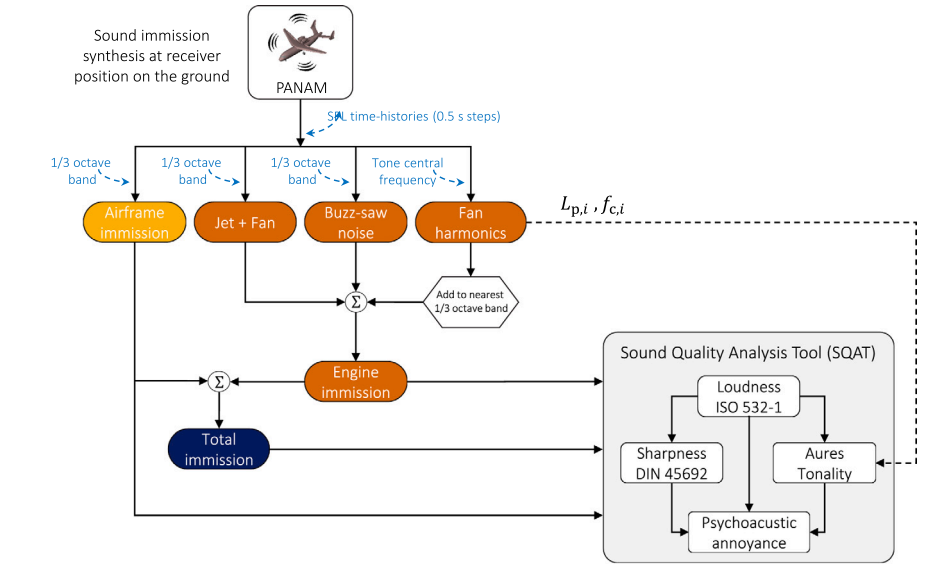

Fig. 24. Sound quality analysis tool: schematic representation of the input data flow and available psychoacoustic metrics.

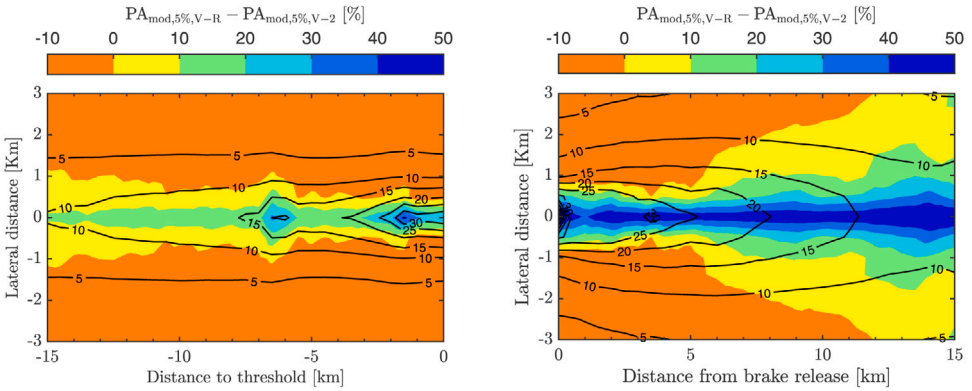

Fig. 25. Short-term annoyance predictions for the overall aircraft noise immissions: contours of modified psychoacoustic annoyance (5% percentile values) for (1) the reference aircraft (solid black lines), and (2) reduction of the V-2 vehicle with respect to the reference aircraft (coloured contours), i.e., negative reduction values implies that the V-2 aircraft promotes higher short-term annoyance than the reference aircraft.

adjoint Green's function accounts for all acoustic propagation effects towards the sensor, and only for the latter. It is noted that a very reasonable description of the propagation effects could be obtained with Pierce's wave equation that is self-adjoint. A procedure to solve adjoint Green's functions for this wave equation with the commercial finite element solver *Actran TM* is then presented [53]. The adjoint method is indeed extensively used in statistical jet noise modelling and the emblematic mixing noise model of is reformulated here for Pierce's wave equation.

Written by Étienne Spieser: etienne.spieser@ec-lyon.fr and C. Bailly, Fluid Mechanics and Acoustics Laboratory (LMFA), France.

2.15. A tunnel-shaped array of MEMS microphones for aeroacoustic measurements in an open test-section wind-tunnel

In order to study the aeroacoustic radiation of obstacles presenting three-dimensional (3D) geometries, acoustic arrays surrounding the wind-tunnel test-section are needed. Such arrays require a high number of microphones (typically, several hundred), which is made possible nowadays by the use of new generation microphones. In this work, the antenna system MegaMicros (designed at Institut d'Alembert), gathering a large number of digital MEMS (Micro ElectroMechanical Systems) microphones (up to 1024), was set up in the open test-section anechoic wind-tunnel BETI at Institut PPRIME [54]. The acoustic antenna is made of 4 planar sub-arrays of 256 channels each, forming a tunnel around the test-section. Acoustic measurements were conducted using three sub-arrays to study the aeroacoustic radiation of one single and two parallel wall-mounted aerofoils [55] (Fig. 28). Such acoustic sources require that their dipolar nature should be taken into account. A 3D volumetric implementation of the beamforming technique was

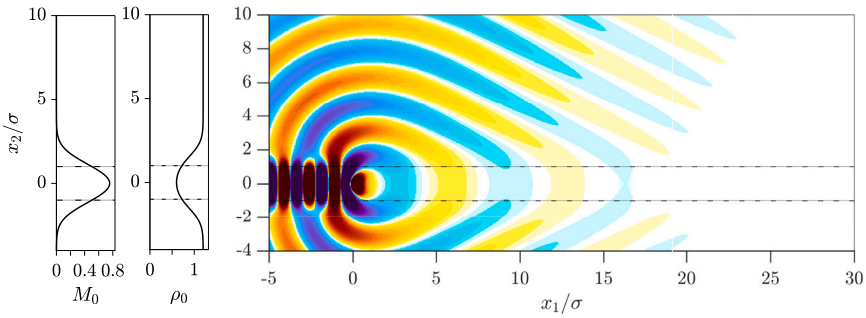

Fig. 26. Mach number M_0 and density ρ_0 profiles of the parallel mean flow considered and snapshot of the fluctuating pressure produced by a quadrupole source and solved with Lilley's wave equation. Dashed lines represent the position of maximal shearing ($x_2/\sigma = 1$).

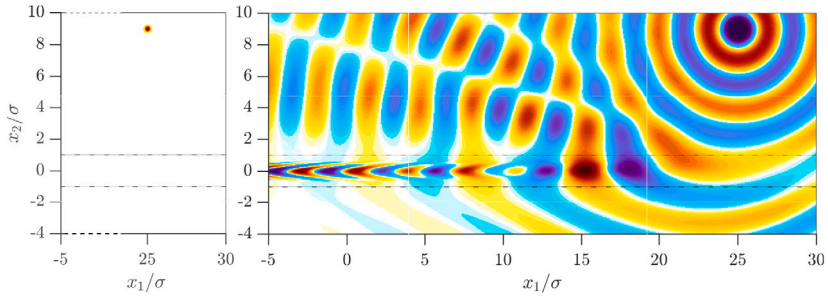

Fig. 27. Adjoint point source set at the observer location and solution to adjoint Lilley's equation for the frequency and the mean flow considered.

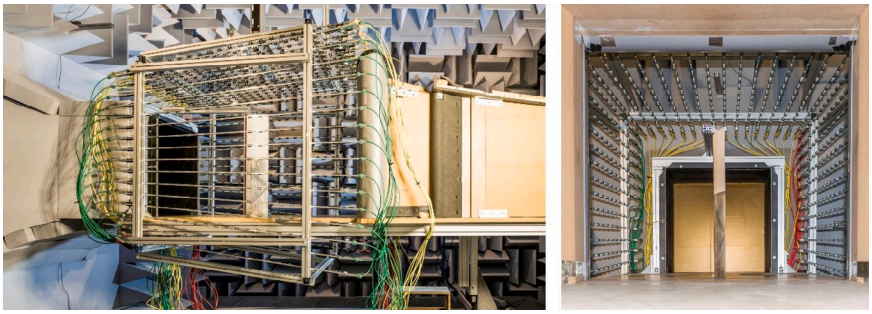

Fig. 28. Left: general view of the tunnel-shaped array in the anechoic wind-tunnel (here, 3 planar sub-arrays of 256 microphones each) right: view from the wind-tunnel collector with a wall-mounted NACA 0012 aerofoil in the test-section.

used under this assumption, associated to proper shear flow corrections. The CLEAN-SC method had to be applied as a post-treatment technique to discard the numerous side lobes present in the 3D sound maps (example on Fig. 29). The different sound sources (trailing edge noise, tip noise, junction noise) were successfully identified using the sound maps. The tunnel-shaped array associated to a robust 3D array processing is a promising tool for studying sound emission from geometries presenting strong 3D characteristics.

Written by Vincent Valeau: vincent.valeau@univ-poitiers.fr, Y. Zhou, D. Marx and C. Prax, Institut PPRIME, CNRS-Université de Poitiers-ENSMA, France, and P. Challande, J. Marchal, R. Marchiano and F. Ollivier, Sorbonne Université, CNRS, Institut Jean Le Rond d'Alembert, France.

2.16. Aeroelastic effects on wave propagation and sound transmission of plates and shells

Modal approaches are often preferred to the wave-based ones for the evaluation of instability conditions in classical non-lifting aeroelasticity of plates and shells. In [56], within a wave-based finite element framework, sub- and super-sonic aerodynamic models are introduced to analyse the effect of self-excited aerodynamic loading terms on the dispersive characteristics of structural waves. The method is validated by using a specific literature test-case (see Fig. 30) and is applicable both on isotropic and multi-layered flat and curved structures. The sound transmission is also computed under sub- and super-sonic turbulent boundary layer excitations:

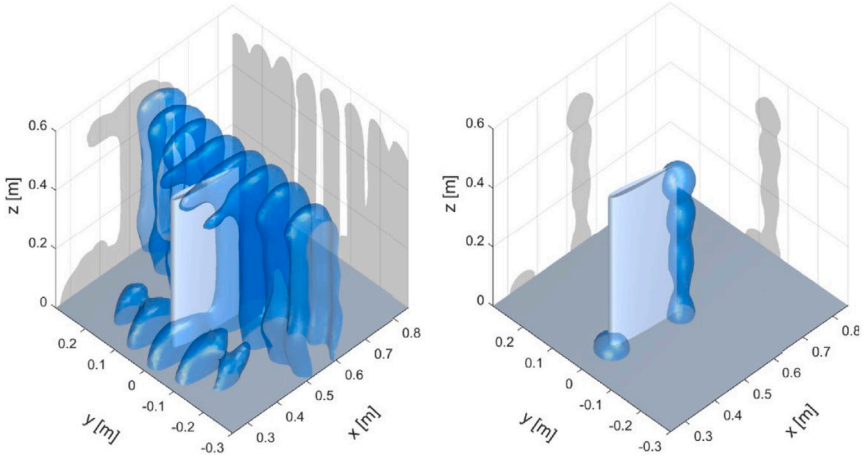

Fig. 29. Sound maps for a wall-mounted finite aerofoil at incoming velocity 40 m/s and angle of attack 10°, at the third-octave band of nominal midband frequency 2.5 kHz. Left: 3D dipolar beamforming right: CLEAN-SC. The 3D isosurface in each sound map is plotted at 9 dB below the maximum value of the sound map.
Source: Taken from [55].

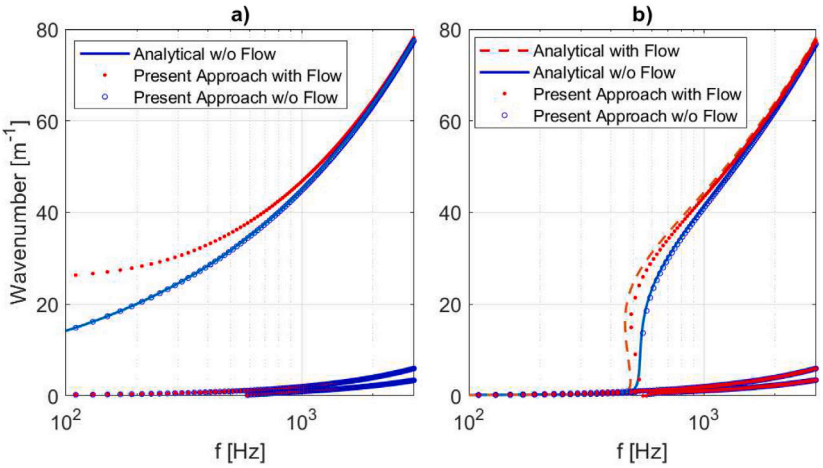

Fig. 30. Dispersion curves for an aluminium shell (2 mm-thick, 1.5 m curvature) with a one-sided flow at Mach 2.5: (a) Axial Waves (b) Circumferential Waves. Analytical model: Ref. [57].

the effect of including or neglecting the aeroelastic coupling is discussed and observed in terms of acoustic indicators as the sound transmission loss. An example is given for a flat and curved panel at Mach 1.5 using the Robertson TBL model shown in Fig. 31.

Written by: Fabrizio Errico (fabrizio.errico@unina.it), F. Franco, S. De Rosa and G. Petrone "Federico II", Italy and M. Ichchou, Ecole Centrale de Lyon, France.

2.17. First models for structural energy transmission decoupling in the high frequency regime under aerodynamic excitation

Turbulent Boundary Layer (TBL) excitation over a structure is one of the most relevant sources of structural vibration and noise in high-speed transportation systems. Wind tunnel facilities are the best way to analyse such systems. In the wind tunnel facility, a test structure is analysed to measure its vibration response to aerodynamic excitation. A support is often required to fix the structure and it is mandatory that this support does not influence the vibration energy to be measured. With this objective, a quick method to estimate the amount of energy decoupling between the structure and the support (Fig. 32(a)), is investigated. Initially a simple structure is examined and then a complex one, by using simplified models for the Turbulent Boundary Layer (TBL) excitation (specifically, the Equivalent Rain-on-the-roof excitation [58]) with a Statistical Energy Analysis (SEA) model [59] for the structure used for the development of the methodology with a particular attention to the calculation of the transmission coefficients and Coupling Loss Factors (CLFs) [60]. The Power Spectral Density (PSD) velocity response of the support structure and test panel are plotted in Fig. 33(a) while the vibration velocity gap ($\Delta v2$), calculated between the test panel PSD response and the PSD mean value

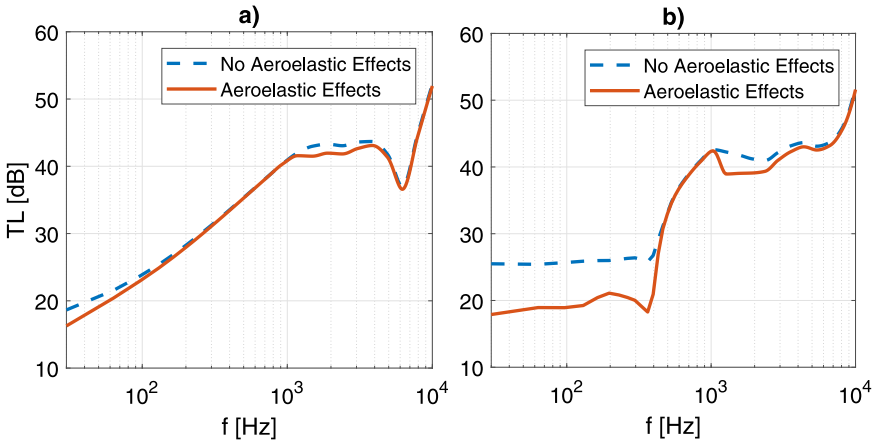

Fig. 31. Sound transmission under a supersonic turbulent boundary layer load (Mach 1.35): (a) Flat Panel (0.5×0.3 m^2) (b) Curved Panel (0.5×0.3 m^2, 2 m curvature).

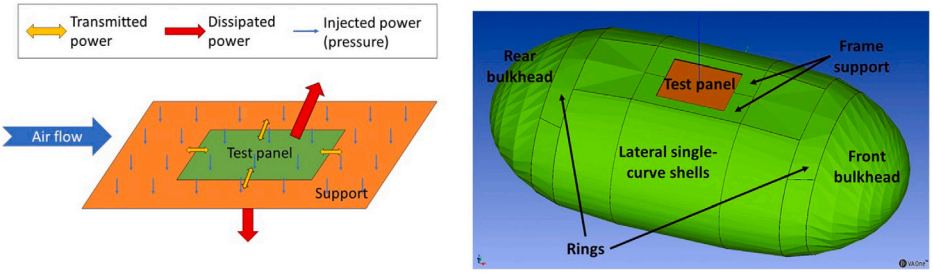

(a) Representation of a support-test panel system based on the Sherbrooke test section setup.

(b) SEA model of a complex structure support

Fig. 32. Setup and model for vibration test.

of all elements of the support, is reported in Fig. 33(b). It can be seen that the $\Delta v2$ value is around 20 dB, which means that there is a good level of energy decoupling between the test article and support. The design process [60] aims to facilitate the choice of material, geometrical size and damping. The method can be applied for any kind of structure because it is based on generic SEA formulations which are valid for any system description.

Written by:G. Mazzeo, M.N. Ichchou, O. Bareille, Ecole Centrale de Lyon, France, G. Petrone, (giuseppe.petrone@unina.it), S. De Rosa, F. Franco, University of Napoli Federico II, Italy

2.18. Numerical investigations about the sound transmission loss of a fuselage panel section with embedded periodic foams

The inclusion of vibroacoustic treatments at early stage of product development through the use of poro-elastic media with periodic inclusions [61,62], which exhibit proper dynamic filtering effects, is a powerful strategy for the achievement of lightweight sound packages and represents a convenient solution for manufacturing aspects. This can have different applications in transportation (aerospace, automotive, railway) engineering fields, where weight, space and vibroacoustic comfort are still critical challenges. Investigation of the sound transmission loss of a typical fuselage panel section (Fig. 34(a)), as well as to propose solutions based on the inclusion of a periodic pattern inside its foam core (Fig. 34(b)), which aim at passively improving the acoustic performance in a mid-high range of frequencies is performed [63]. In detail, the effect of several periodic patterns (different radius of the inclusions and number of unit cells along the thickness) are investigated. Results, in terms of sound TL, are presented for a fixed number of unit cells along the thickness and varying radii of the inclusions (Fig. 35(a)), and another with fixed radius of the inclusions and varying number of unit cells along the thickness (Fig. 34(b)). As expected, in both cases the meta-core shows a performance peak, related to periodicity effects, when half of the wavelength k is equal to periodicity dimension d. It should be noted that it may be challenging to obtain performance peaks at low frequencies, when only a limited thickness is available (as it is in the case of a fuselage bay section). Therefore, it is fundamental to realize that the acoustic approach based on meta-cores presented herein may conceptually be scaled also for low-frequency applications, but only when the total available thickness is sufficiently high.

Written by F. Franco, francof@unina.it, G. Petrone, S. De Rosa, D. Magliacano, University of Napoli Federico II, Italy

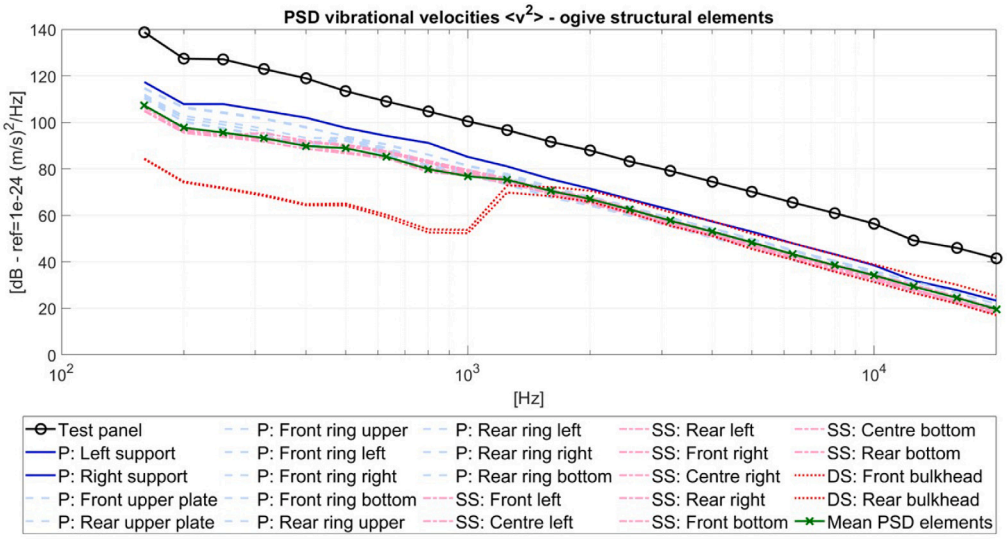

(a) Complex structure support and test panel PSD velocities

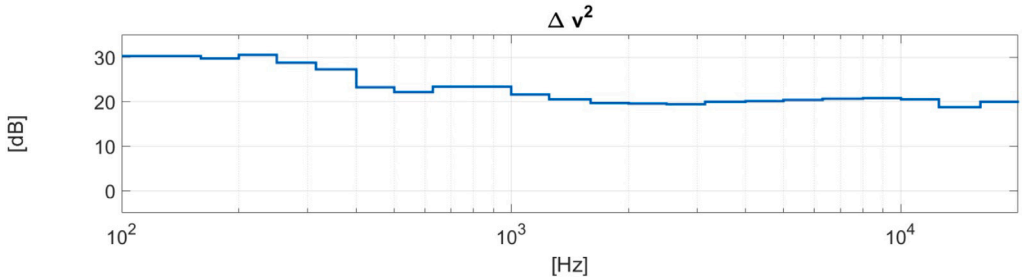

(b) Vibration velocity level gap $\Delta v2$ between test panel PSD and support elements PSD mean value

Fig. 33. Results of vibration tests.

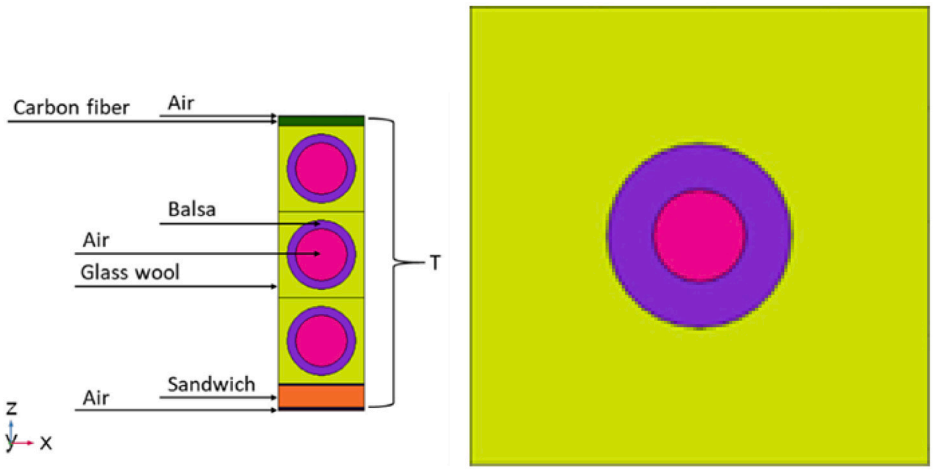

(a) Layering sequence of an acoustic package

(b) Meta-core unit cell

Fig. 34. Schematics.

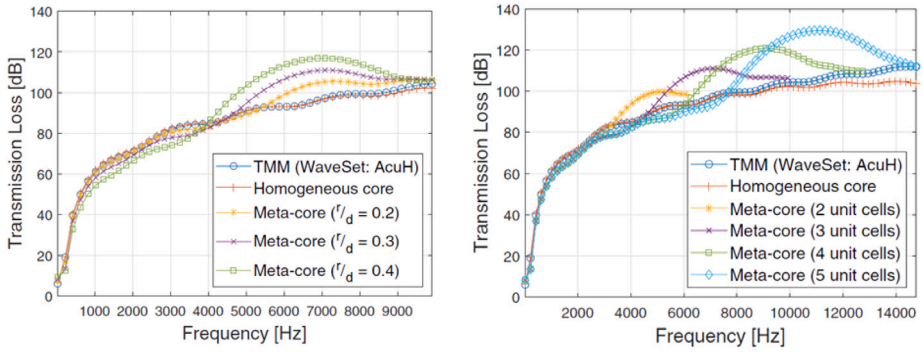

(a) Transmission loss study with a fixed number of unit cells along the thickness and varying radii of the inclusions.

(b) Transmission loss study with fixed radius of the inclusions and varying the number of unit cells along the thickness.

Fig. 35. Transmission loss.

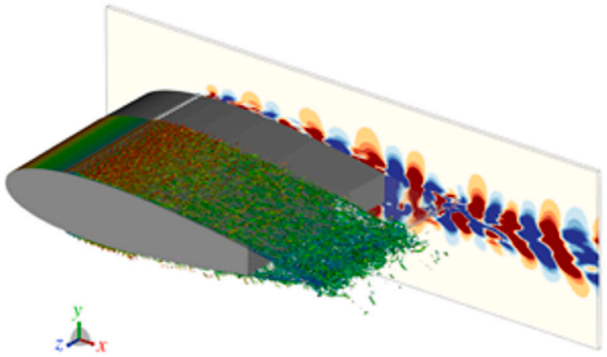

Fig. 36. High fidelity numerical simulations of a porous trailing edge for noise reduction [64].

3. Airframe noise

3.1. On the design and application of porous material for trailing edge noise scattering

Porous materials can be used to mitigate noise scattering caused by a turbulent boundary layer [64] or a grazing acoustic wave [65] scattering at the trailing edge of an aerofoil. Through a combination of experiments [66] carried out in the A-tunnel at TU Delft [67] and high fidelity numerical simulations with the lattice Boltzmann method, see Fig. 36 [64], two major noise reduction mechanisms have been identified: (1) mitigation of the pressure jump at the trailing edge (also known as pressure release process) and (2) destructive interference between the acoustic waves scattered over the entire porous medium. Both numerical and experimental results have shown that the first mechanism is dominant very close to the trailing edge of the aerofoil (5 % of the chord for a NACA0018) for conventional porous foams and perforated trailing edges. This mechanism is more relevant in the region where there is the interaction between the aerodynamic fluctuations from both sides of the aerofoil, see Fig. 37. The second mechanism is caused by the fact that the thickness of the porous material varies in the streamwise direction, thus causing a streamwise-varying impedance that allows local scattering of the acoustic wave. This is visible in acoustic beamforming maps where the location where the maximum of the scattering occurs moves upstream of the trailing edge. The same mechanisms allow noise reduction when the porous materials are used to mitigate jet installation noise [65].

F. Avallone, f.avallone@tudelft.nl, D. Ragni, D. Casalino, C. Teruna, L. Rego, A. Rubio Carpio Delft University of Technology, The Netherlands

3.2. Experimental studies on trailing edge noise reduction using active flow control methods

Recent studies at the University of Bristol considered active noise control methods to reduce trailing edge noise. A detailed set of wind tunnel experiments were considered using flow injection and flow suction on a flat plate upstream a sharp trailing edge, see Fig. 38. A set of flow control severity rates (σ) and flow control angles (α) were considered. After analysing data from flush-mounted microphones and hot-wire anemometry, it was found that both flow suction [68] and flow injection [69] can efficiently

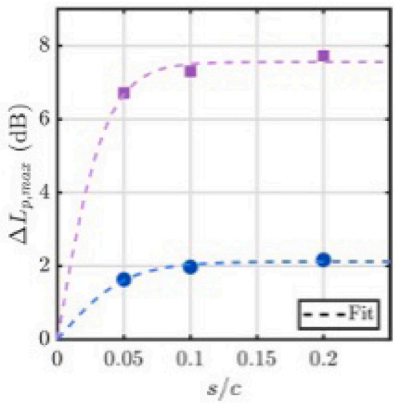

Fig. 37. Maximum noise reduction as a function of the streamwise extent of the porous medium. Two perforated trailing edges with permeability equal to (purple) 31×10^{-10} m^2 and (blue) 5×10^{-10} m^2. (For interpretation of the references to colour in this figure legend, the reader is referred to the web version of this article.)
Source: From [66].

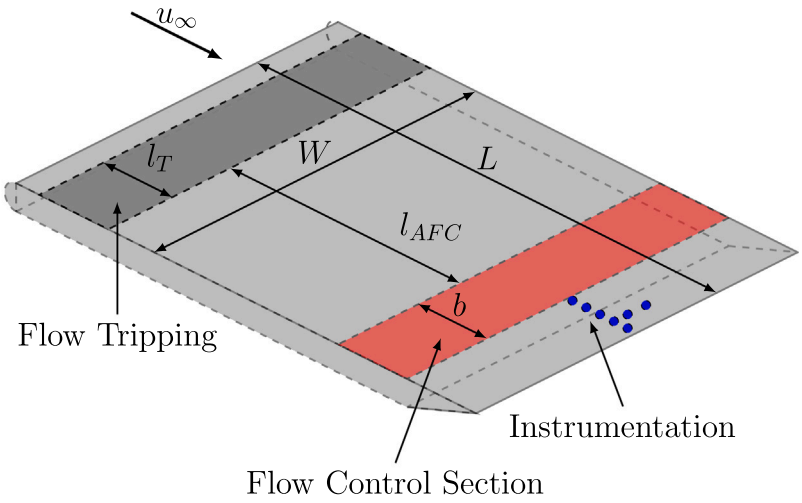

Fig. 38. The schematics of the flat plate test rig used for the flow control studies.

reduce trailing edge noise. Flow suction was found to reduce the flow energy content in the turbulent boundary layer over its entire height, with the most significant reduction observed in the logarithmic region of the boundary layer. The boundary layer responds to flow suction with an increased shear below the logarithmic layer. The flow frequency–energy content was linked with these observations, namely, a drop in the flow energy content was found at mid frequencies, associated with a thinner logarithmic layer, while an increase at high-frequencies was linked with the increased shear at the immediate vicinity of the wall. From an aeroacoustic point of view, the surface pressure fluctuations behaved similar to the velocity spectra indicating a drop at mid frequencies and increase at high frequencies, see Fig. 39. Another contribution of flow suction to trailing edge noise reduction was the decrease in the spanwise length scales of turbulent structures.

The boundary layer was found to be more sensitive to flow injection than flow suction, namely, different flow regions were identified depending on the injection rate applied. At low injection rates, a shear layer developed and remained in the close vicinity of the wall increasing the surface pressure fluctuations in a broadband manner, particularly at low frequencies. As the blowing rate increased, the flow control displaced the shear layer away from the wall. First, an incipient separation was triggered followed by a complete boundary layer detachment at high injection rates. While the shear layer increased the low-frequency aeroacoustic noise, its efficacy of enhancing low-frequency surface pressure fluctuations dropped with increasing wall distance, while the low momentum flow beneath the shear layer decreased the surface pressure fluctuations at the mid- and high-frequencies, see Fig. 40. Overall, flow control with a small incipient separation was found to provide the best combined aeroacoustic and aerodynamic performance.

Written by Máté Szőke: m.szoke@vt.edu, M. Azarpeyvand and D. Fiscaletti, University of Bristol, Bristol, UK.

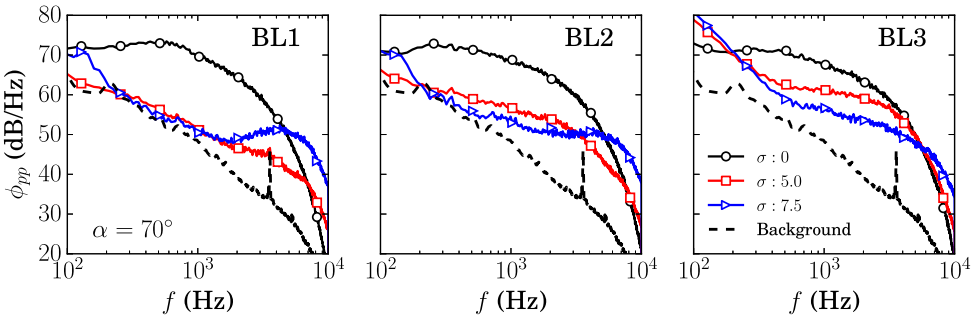

Fig. 39. Power spectral density, ϕ_{pp} (dB/Hz, re. 20 μPa/$\sqrt{\text{Hz}}$), of the surface pressure fluctuations at flow suction angle $\alpha = 70°$ at locations downstream of the flow control section (BL1, BL2, BL3).

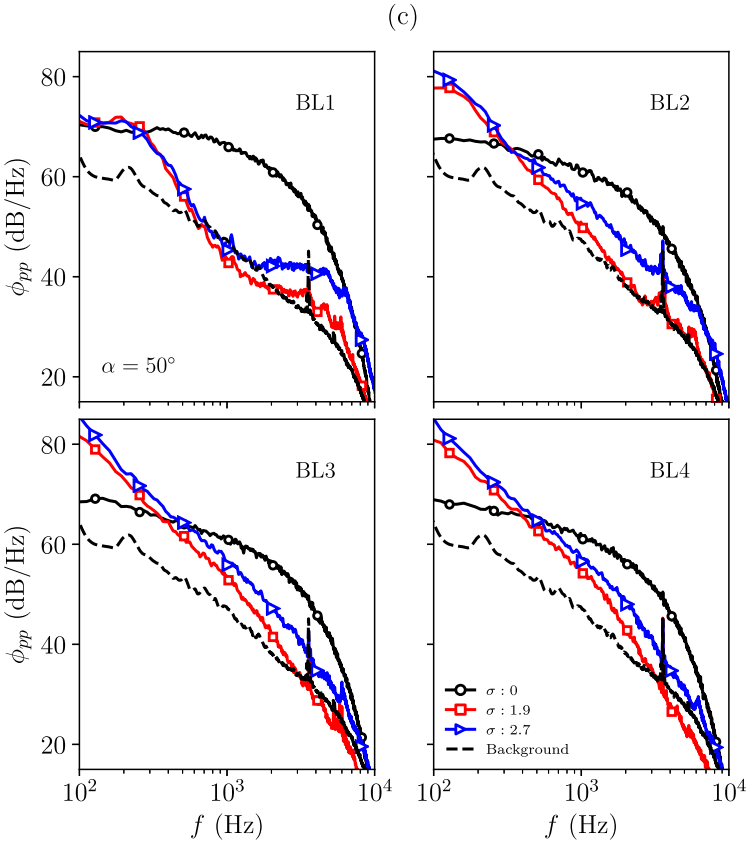

Fig. 40. Power spectral density, ϕ_{pp} (dB/Hz, re. 20 μPa/$\sqrt{\text{Hz}}$), of the surface pressure fluctuations at flow injection angle $\alpha = 50°$ at locations downstream of the flow control section (BL1, BL2, BL3, BL4).

3.3. Evaluation of low-noise technologies applied to a full-scale nose landing gear using three-dimensional acoustic source mapping

Due to their complexity, the search for efficient low noise treatments to reduce landing gear noise continues, as is documented in the review paper of Zhao and Bennett [70]. The European Clean Sky-funded project ALLEGRA (Advanced low noise Main and Nose Landing Gears for Regional Aircraft, coordinator: Gareth J. Bennett, https://cordis.europa.eu/project/id/308225/reporting) assessed the performance of several realistic low-noise technologies (LNTs) applied to a detailed full-scale nose landing gear (NLG) model tested in the Pininfarina aeroacoustic wind tunnel (Turin, Italy) [71–74]. Four individual LNTs were investigated, namely a ramp door spoiler, a solid wheel axle fairing, wheel hub caps, and multiple perforated fairings [75]. Combinations and small variations of some of these LNTs were also evaluated. The use of multiple planar microphone arrays allowed for the application of 2D and 3D acoustic imaging algorithms to evaluate the location and strength of the noise sources within the NLG system in different emission directions for each configuration. The deconvolution method enhanced high-resolution CLEAN-SC (EHR-CLEAN-SC) was

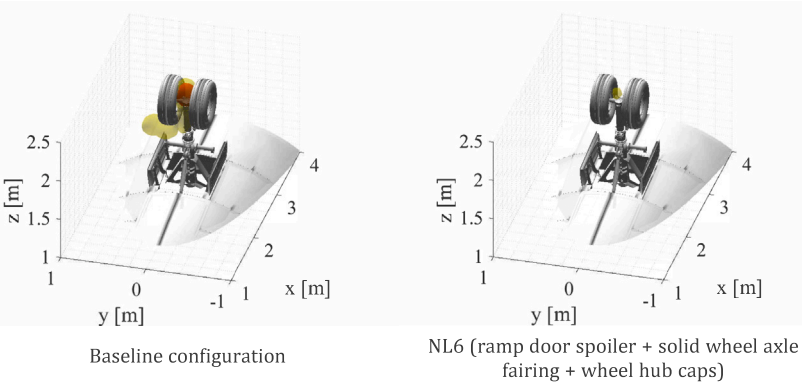

Fig. 41. Three-dimensional EHR-CLEAN-SC source maps for the one-third-octave-band centred at 1250 Hz and a flow velocity of 50 m/s. (left) Reference baseline case, (right) Combined case NL6 (ramp door spoiler + solid wheel axle fairing + wheel hub caps). The values shown are visualized as isocontours 3 dB (in red) and 6 dB (in yellow) below the peak value [72]. (For interpretation of the references to colour in this figure legend, the reader is referred to the web version of this article.)

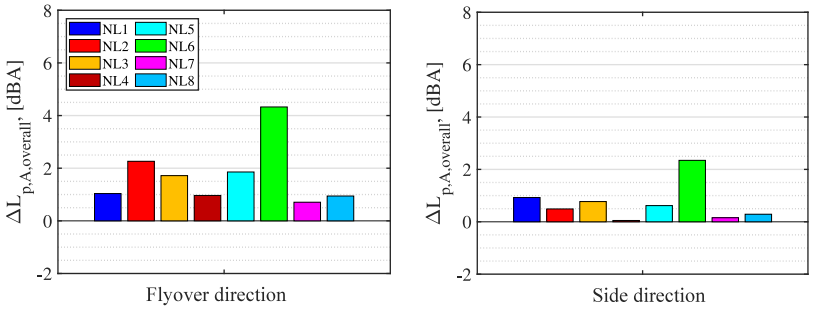

Fig. 42. Reduction of the overall A-weighted sound pressure level in the frequency range between 200 Hz and 4 kHz with respect to the baseline provided by each LNT in (left) the flyover direction and (right) side direction for a flow velocity of 60 m/s. (NL1: ramp door spoiler NL2: solid wheel axle fairing NL3: wheel hub caps NL4: multiple perforated fairings applied to the lower arm, the steering pinions, and the wheel axle NL5: NL2 + NL3 + NL4 NL6: NL1 + NL2 + NL3 NL7: NL4 with alternative porous material and NL8: NL4 only applied to the wheel axle). [75].

employed in a 3D scan grid, [76], see Fig. 41. This approach was proven useful for determining the precise location of the noise sources compared to the 2D source maps. The wheel axle, the inner wheel hubs, the steering pinions and the torque link were identified as the noisiest NLG elements. Overall, all the frequency spectra measured were broadband without any dominant tonal signature [72]. The solid wheel axle fairing was the most effective individual LNT, and it improved its performance when applied in combination with the ramp door spoiler and wheel hub caps, reaching overall A-weighted noise reductions of more than 4 dBA in the frequency range between 200 Hz and 4 kHz, see Fig. 42. In general, all LNTs showed a better performance in the flyover direction than in the side direction.

Written by Roberto Merino-Martinez: r.merinomartinez@tudelft.nl, Delft University of Technology, the Netherlands, and J. Kennedy and Gareth J. Bennett, Trinity College Dublin, the University of Dublin, Ireland.

3.4. On the role of turbulence distortion on leading-edge noise reduction by means of porosity

The noise emitted by an aerofoil interacting with incident turbulence can be reduced using porous materials [77,78]. However, despite the numerous studies, the physical mechanisms associated with this noise mitigation strategy remain unclear.

Recent investigations have been carried out at VKI on a porous NACA-0024 profile fitted with melamine foam and subjected to the turbulence shed by an upstream cylindrical rod. Results have shown that the attenuation in the distortion experienced by the vortical structures on the porous surface plays an important role in the corresponding noise abatement [78].

In particular, the upwash component of the root-mean-square of the turbulent velocity is found to be reduced in a porous aerofoil configuration in contrast to a solid one, resulting in a significant decrease of the turbulent kinetic energy in the stagnation region (see Fig. 43). Moreover, the power spectral density of the incident velocity fluctuations measured at a point close to the leading edge exhibits mitigation in the low-frequency range (see Fig. 44), which can be associated with large-scale structures. The present trend is in agreement with the results of the far-field acoustic spectra, where a noise reduction of up to 2 dB is observed in a similar frequency range (see Fig. 45). These results support a scenario in which the attenuation of the distortion of incident turbulence constitutes one of the plausible explanations for the noise mitigation that can be achieved with a porous treatment of the aerofoil.

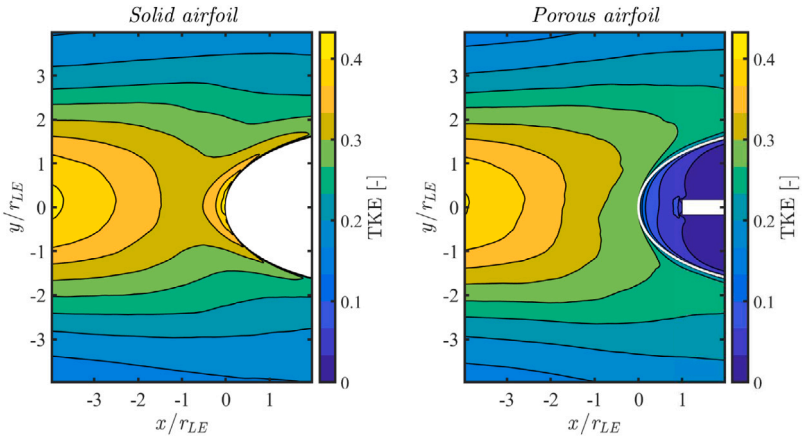

Fig. 43. Turbulent kinetic energy for a solid (on the left) and porous (on the right) aerofoil configuration in the stagnation region computed with large-eddy simulations and made dimensionless by the free-stream velocity, $U_\infty = 30$ ms^{-1}.

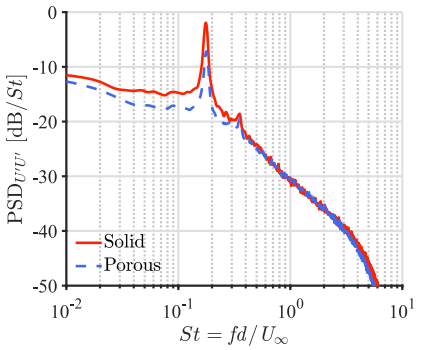

Fig. 44. Power spectral density of the incident-velocity fluctuations for a solid and porous aerofoil configurations measured at a location close to the leading edge. The reference is 1 m^{2}s^{-1}.

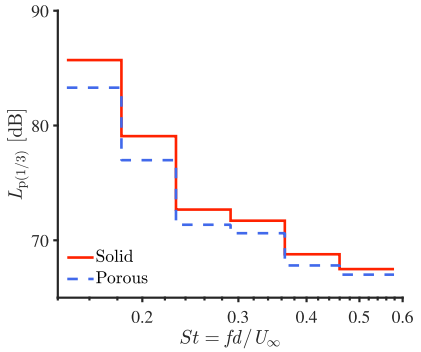

Fig. 45. Generalized inverse beamforming [79] results exhibiting the integrated sound pressure levels for a solid and porous aerofoil configurations expressed in one-third octave bands.

The above research benefited from the support of the European Commission's Framework Program "Horizon 2020", through the Marie Skłodowska-Curie Innovative Training Networks (ITN) "SmartAnswer – Smart mitigation of flow-induced acoustic radiation and transmission" grant agreement No. 722401, to the present research project.

Written by Riccardo Zamponi: riccardo.zamponi@vki.ac.be and C. Schram, von Karman Institute for Fluid Dynamics, Belgium.

3.5. An overset-LES study of trailing edge noise reduction mechanisms of porous material on a lifting aerofoil

Airframe noise is a significant contributor to the overall aircraft noise during the landing phase, and hence its reduction is imperative. Application of porous materials to mitigate this flow induced airframe noise is an emerging passive noise reduction

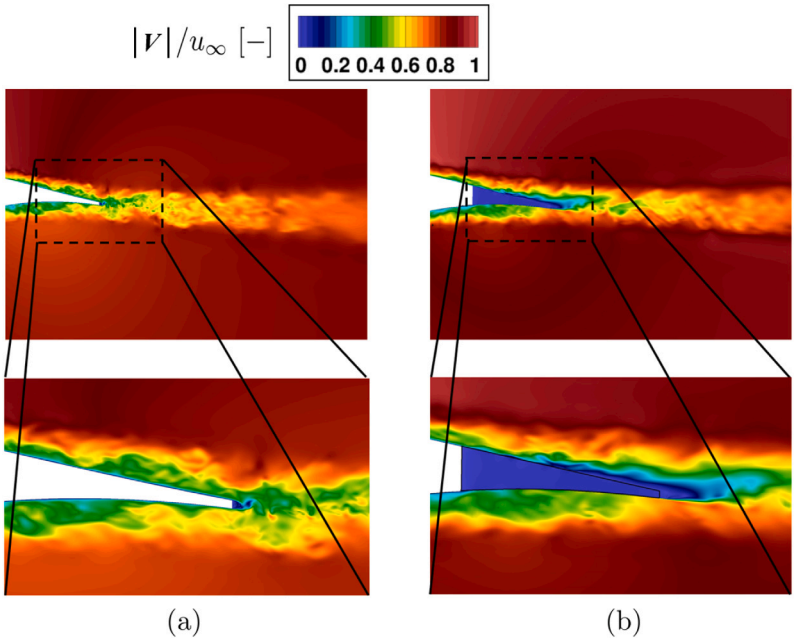

Fig. 46. Instantaneous flow field around (a) the solid trailing-edge and (b) the porous trailing-edge. The contours represent the magnitude of the instantaneous velocity vector. Note that the porous material is applied to the rear 10% of the aerofoil.

strategy. However, its noise reduction mechanism under various flow conditions are not fully known. In the current contribution, a densely packed porous material is applied to the blunt trailing edge of a lifting aerofoil to investigate the underlying noise reduction mechanisms [80]. Overset-LES is performed where the porous material is modelled by a volume-averaged approach. This volume-averaged model leads to a linear Darcy term and a non-linear Forchheimer term in the momentum equations. Additional terms related to porosity gradients are zero as in the current study only porous material with constant material properties are considered [81].

A qualitative comparison of the instantaneous flow field around the solid and porous trailing edges is shown in Fig. 46. The application of porous material results in the elimination of periodic vortex shedding from the blunt trailing edge due to the absence of a distinct trailing edge, thereby mitigating the tonal noise generation mechanism (see Fig. 46(b)). Furthermore, the presence of porous material results in a slow-down of the convective eddies traversing over the trailing-edge (see Fig. 47) which is a major cause of noise reductions as the far-field pressure perturbations depend strongly on this mean convective velocity ($p'^2 \propto \overline{U_c}^5$). This slow-down effect is further enhanced in the adverse pressure gradient boundary layer on the suction side as compared to the negative pressure gradient boundary layer on the pressure side (cf. Figs. 47(a) and 47(b)). In the current study, the two major noise reduction mechanisms due to the application of porous material were identified based as i) the breakdown of the span-wise coherence of surface pressure carrying eddies, and (ii) a drastic reduction of mean convective velocity of the pressure carrying eddies [80]. A noise reduction of up to 5 dB in the upstream-radiation direction is found.

V.B. Ananthan: v.bharadwaj-ananthan@tu-braunschweig.de, P. Bernicke, TU Braunschweig, Germany, R.A.D. Akkermans, Hamburg University of Applied Sciences, Germany, T. Hu, P. Liu, Beihang University, China.

3.6. Shape optimization for aeolian tone

Considering that there have been no aeroacoustic equivalent of head loss tables or Nusselt's number formulas to apply to typical configurations, this project addressed the question of what we could tell to designers about what will happen in the acoustic field if they change the geometry of the system. Several investigations have been combined including numerical [82–84], theoretical [85] and experimental [86] approaches. The numerical study culminates in shape optimizations [82,84] for cylinder noise in the 2D, laminar regime, whose results could be used to refine the design space of parametric studies and to investigate noise generation process by comparing extreme behaviours.

The optimizer relies on an analytical formula for the acoustic power of the aeolian tone, which needs the Strouhal number and the RMS fluctuation of the lift and drag coefficient of the bluff body as inputs. These quantities are obtained from the numerical solution of the unsteady Navier–Stokes equations, using an immersed boundary method so that the grid is the same for thousands of geometries.

At a given aspect ratio (AR) of the sectional breadth to the blocking height, up to 16 dB difference was noticed between the loudest and the most silent shapes, as shown in Fig. 48. Fig. 49 (left) illustrates how general is the take home message that they

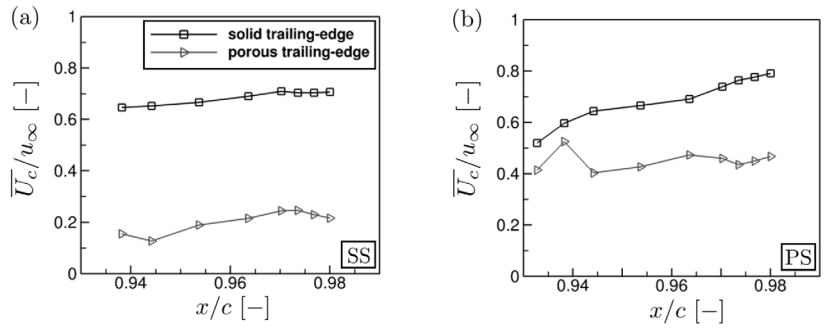

Fig. 47. Mean convective velocity of the stream-wise traversing eddies for solid and porous trailing edges along, (a) suction side, (b) pressure side. The mean convective velocities are computed from the spatio-temporal cross correlations of the unsteady pressure field over the trailing-edge.

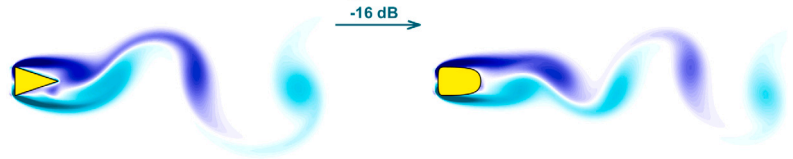

Fig. 48. Optimal shapes for aeolian tone: vorticity fields in the laminar flow over 2D bodies. The left geometry radiates 45 times more acoustic power per unit length.

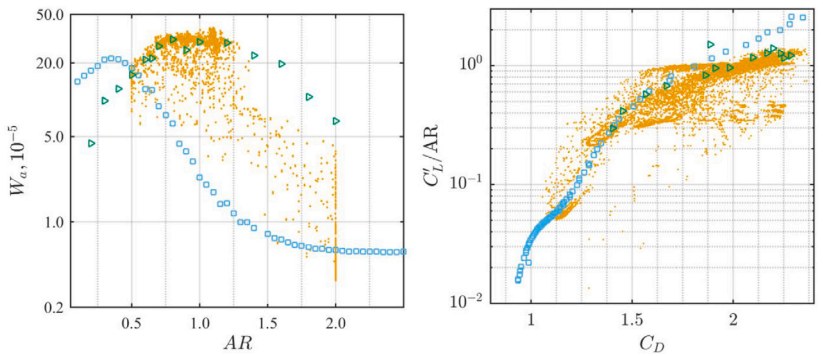

Fig. 49. Acoustic power as a function of the body aspect ratio (left) and lift fluctuation normalized by lifting surface compared to mean drag (right): dots include all the geometries evaluated for the optimizations, while square and triangle markers are for rectangles and back-pointing triangles, respectively.

look respectively like a backward pointing triangle and a rectangle, while the aspect ratio as a universal influence on noise. Finally a global correlation is noticed in Fig. 49 (right) between the mean drag and the pressure fluctuation on the lifting surface. This could allow the prediction of aeroacoustic outputs from only mean flow properties. Even if the latter miss flow history, they still contain information about 3D dynamics as well as couplings between inertia, pressure and friction.

Written by Florent Margnat: florent.margnat@univ-poitiers.fr, Pprime Institute, CNRS, Université de Poitiers, ISAE-ENSMA, France.

3.7. Aeroacoustic investigation of a circulation-controlled high-lift flap by overset-LES

Circulation controlled wings use the Coanda effect to delay or even completely avoid flow separation, e.g., the strongly deflected flow on a wing's flap. Hence, it offers the potential of drastically increasing the lift coefficient. The Coanda effect can be realized by injecting momentum tangential to the wing's surface through a blowing slot (see Fig. 50a). However, such a Coanda-jet equipped flap might significantly contribute to the airframe noise. In this contribution, we report on the outcomes of Overset-LES computations carried out on such a Coanda-jet equipped DLRF16 wing with extended flap [87]. See Ref. [88] for a description of the Overset-LES method. The Q-criterion (coloured by velocity magnitude) is presented in Fig. 50b. The effect of the Coanda-jet can be appreciated as the flow remains attached over almost the complete flap (a small separation is present near the trailing edge). Furthermore, a significant acceleration over the highly curved part of the flap is apparent, followed by a strong deceleration between the flap's curvature and its trailing edge. This simulation allows to identify the different sound sources present on such a jet blown flap: i)

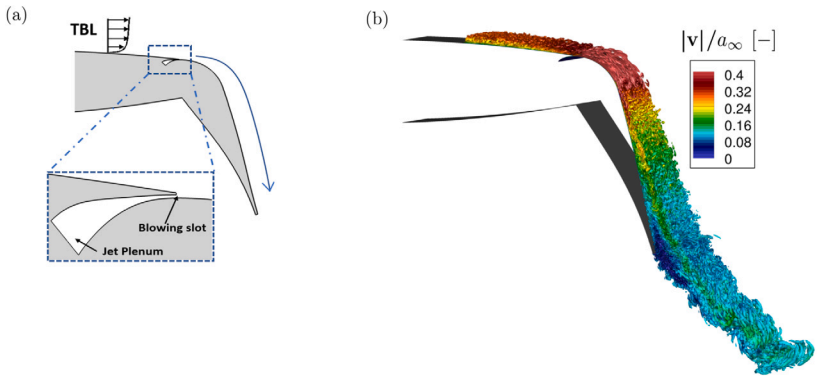

Fig. 50. (a) Schematic of Coanda effect applied just upstream of high-lift device (note that only the flap region is shown). Inset shows details of the Coanda jet blowing slot. (b) Visualization of turbulent structures by Q-criterion (Q = 20) coloured with non-dimensional velocity magnitude. Note that flap deflection angle is 65 degrees.

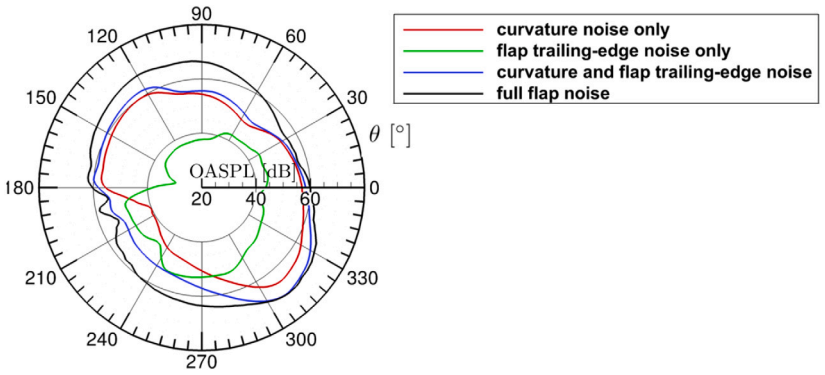

Fig. 51. Directivity of the far-field OASPL (based on frequencies between 500 and 20.000 Hz) for different sound source contributions (green line: flap trailing edge, red line: curvature noise, blue line: curvature and flap trailing edge noise, black line: full flap noise). OASPL is rescaled to 1 m distance. (For interpretation of the references to colour in this figure legend, the reader is referred to the web version of this article.)

curvature noise, ii) flap trailing-edge noise, and (iii) Coanda-jet mixing noise (except for flap-kink noise as the pressure side is not forced). The directivity of these different sound sources are shown in Fig. 51 together with that from the complete flap (the latter denoted by full flap noise). It is noteworthy that the curvature noise is more significant than the flap's trailing-edge noise alone, except for some angles where the re is significant shielding of the curvature noise by the wing's geometry itself. Noise reduction measures should therefore be focused on reducing curvature noise instead of the flap's trailing-edge noise. One interesting aspect of Fig. 51 is that the OASPL of the full flap is larger than that of the curvature and trailing-edge noise together. The current investigation therefore suggests an additional, previously not recognized sound source at play, resulting from the strong flow deceleration at the region between the curvature and the flap's trailing edge (cf. Fig. 50b).

R.A.D.Akkermans: rinie.akkermans(@)haw-hamburg.de, Hamburg University of Applied Sciences, Germany, V.B. Ananthan, P. Bernicke, TU Braunschweig, Germany

3.8. Trailing edge noise control using passive self-oscillating flexible flaplets

The aerodynamic noise generated at the trailing edge of aerofoils is a major contribution to airframe noise. As a possible noise reduction strategy, the use of flexible trailing edge flaplets (see Fig. 52) was investigated in a joint research project between City, University of London and Brandenburg University of Technology (BTU). Following Particle Image Velocimetry (PIV) measurements on an aerofoil equipped with such flaplets that revealed a stabilizing effect on the boundary layer [89], a detailed experimental study on the noise reducing effect of these flaplets attached to a NACA 0012 aerofoil was performed in the aeroacoustic open jet wind tunnel at BTU [90,91]. In this work, the effect of flaplet geometry (length, width and spacing) on the noise generation, the aerodynamic performance and the wake turbulence was examined by means of microphone array and single microphone measurements as well as force measurements, surface flow visualization and Constant Temperature Anemometry (CTA) measurements. In the presence of a laminar boundary layer, the freely oscillating motion of the flaplets can lock-in with the regular vortex shedding, thereby detracting energy and reducing tonal far-field noise at low and medium frequencies. The range of the

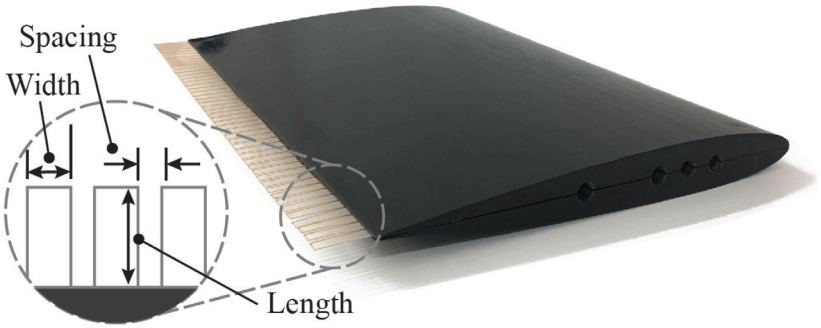

Fig. 52. Photograph of a NACA 0012 aerofoil with flexible trailing edge flaplets.

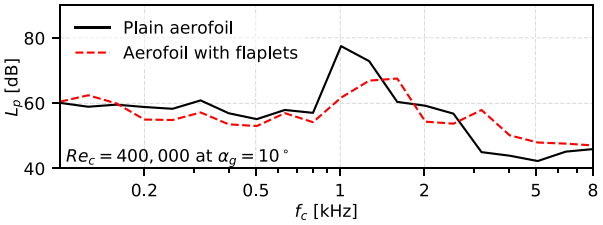

Fig. 53. Single microphone one-third octave band far field sound pressure level spectra measured at a chord-based Reynolds number of $Re_C = 4,00,000$.

noise reduction depends on the flaplet geometry and material. At high frequencies the flaplets were found to lead to a slight noise increase, Fig. 53. When the boundary layer is not laminar but turbulent, the flaplets were still found to be beneficial regarding the overall noise reduction [92].

Written by Thomas F. Geyer: thomas.geyer@b-tu.de, Brandenburg University of Technology, Cottbus, Germany, and E. Talboys, City University London, UK.

3.9. Aeroacoustic mechanisms of porous-edge treatments for trailing-edge noise mitigation.

Recent studies carried out at Delft University of Technology aim at identifying the role of permeability for mitigating turbulent boundary layer trailing-edge (TBL-TE) noise [93] and jet-installation noise (JIN) [65,94]. The high-fidelity lattice-Boltzmann solver SIMULIA PowerFLOW has been employed in these investigations. The first study considers a fully resolved porous TE insert, based on a diamond-shaped structure, that replaces the TE part of an aerofoil (see Fig. 54). It has been confirmed that the pressure-release process, i.e. mitigation of the pressure mismatch at the TE, is the major physical mechanism contributing to noise reduction. The destructive interference between acoustic waves scattered along the streamwise extent of the porous insert also plays a secondary role. The pressure-release process is dominant at locations where the entrance length of the porous material, i.e. the depth of the material where unsteady hydrodynamic velocity and pressure fluctuations dominate, is larger than the local TE thickness [66]. Porous inserts have been also applied for JIN reduction, at the TE of a flat plate located in the near field of a jet. Porous TE inserts significantly reduce the scattering efficiency at the TE, leading to a noticeable noise reduction in the frequency range where JIN is measured. Moreover, the dominant noise source location is shifted upstream from the TE tip to the solid-porous junction, as shown by the beamforming images (Fig. 55). Currently, proof-of-concepts are being prepared to demonstrate the application of porous treatment in more realistic configurations. These include the numerical study on the usage of poro-serrated stators in a full-scale turbofan fan stage, and an experimental study involving a half-span airframe at the German–Dutch Wind Tunnels (DNW).

Written by: C. Teruna: c.teruna@tudelft.nl, L. Rego, D. Ragni, F. Avallone, Delft University of Technology, Netherlands.

4. Fan and jet noise

4.1. Low-speed turbofan aerodynamic and acoustic prediction with an isothermal lattice Boltzmann method

The objective of this study [95] was to assess the capability of the isothermal lattice Boltzmann method (LBM) to correctly capture aerodynamic and acoustic features from a low-speed turbofan. The evaluation has been done on the Advanced Noise Control Fan model developed by NASA Glenn Research Center [96] and an extensive comparison of the measured and computed aerodynamic results has been presented for the first time on this configuration. The trends are well captured, but quantitative discrepancies are observed for some variables, leading to lower fan performance values in the simulations. This last point was also observed in the

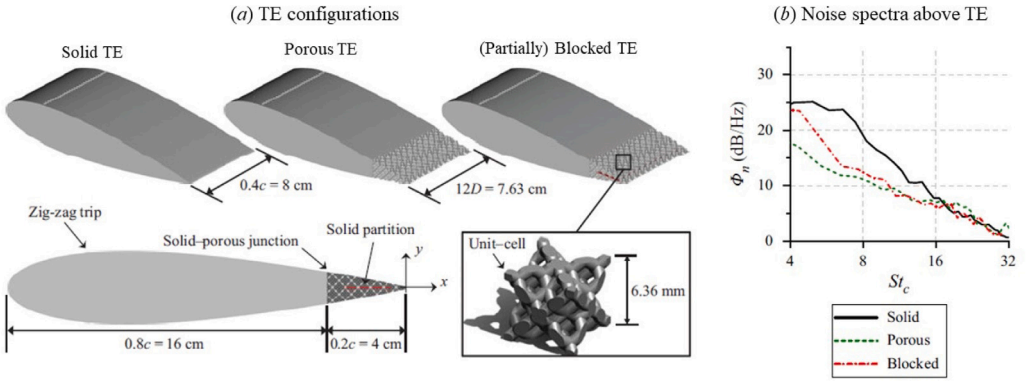

Fig. 54. (a) The test configuration using a NACA 0018 aerofoil with replaceable TE inserts and (b) farfield noise spectra directly above the tip of the TE inserts.

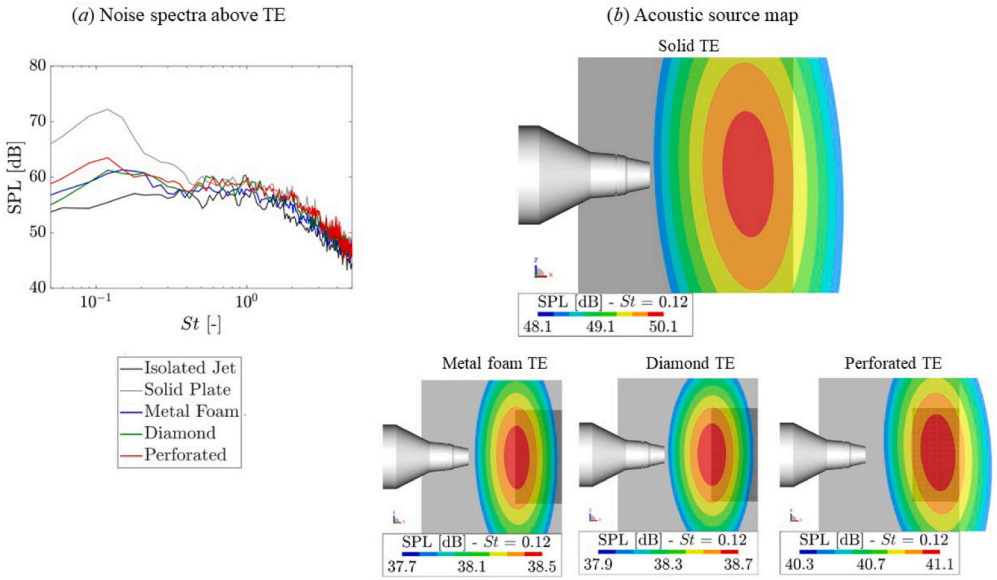

Fig. 55. (a) Farfield noise spectra directly above the tip of the flat plate with different TE types and (b) the acoustic source map obtained using a conventional beamforming technique.

previous related studies, but remained unexplained. By validating in parallel the LBM aerodynamic results with a Reynolds-averaged Navier–Stokes simulation provided by the database, a likely uncertainty of the absolute values of some variables in the experimental mean flow data has been shown (a result of the intent that experimental data were not acquired with absolute levels as an objective). Direct in-duct and far-field acoustic results were also investigated, taking advantage of the low-dissipative characteristics of the LBM (as illustrated in Fig. 56). A good agreement with the measurements in terms of broadband noise is obtained, but the low frequencies tend to be overestimated (see Fig. 57). For the tonal noise, if the expected acoustic modes are recovered, quantitative differences are observed. Predictions based on a hybrid method, where the acoustic sources computed by the LBM are propagated analytically using Goldstein's analogy, have also been made and compare well with the direct predictions, thus proving the correct propagation of acoustic waves by the solver. The authors of this study would like to thank D. Sutliff from NASA Glenn Research Centre for (1) providing the geometry and the experimental results of the Advanced Noise Control Fan and (2) his help in the interpretation of the experimental data.

Written by: M. Daroukh (majd.daroukh@onera.fr), T. Le Garrec and C. Polacsek, Onera, France.

4.2. Novel broadband acoustic liners for aero-engine applications

Engine duct acoustic panels are known to provide a significant contribution to the reduction of radiated noise for aircraft nacelles. They are installed typically in the engine inlet, bypass, and core ducts. Their deployment must be balanced by weight and drag concerns, and by the geometric limitations imposed by high-bypass-ratio engines. Next generation Ultra-High Bypass Ratio (UHBR)

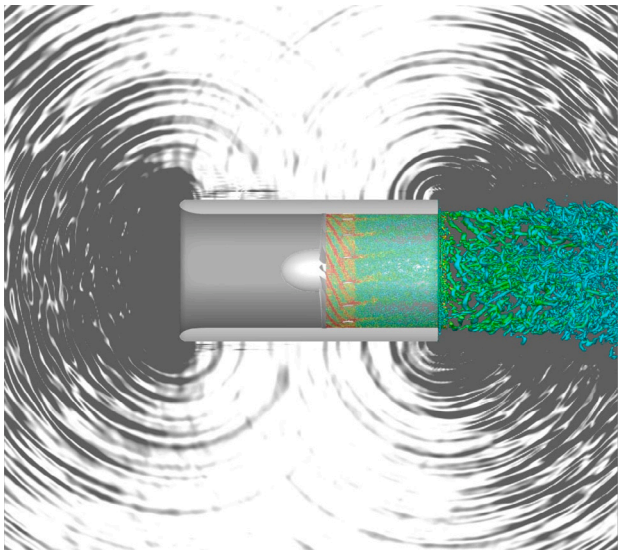

Fig. 56. Contour map of density gradient magnitude extracted from the LBM simulation (fine mesh) and showing the radiation of the acoustic waves generated by the rotor–stator interaction.

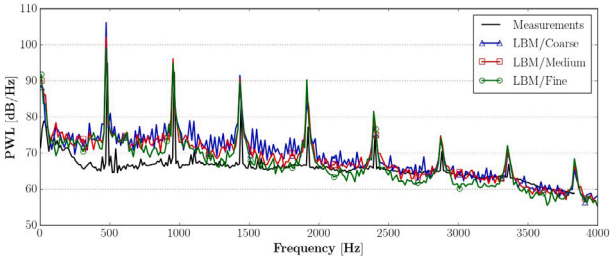

Fig. 57. Comparison of the upstream acoustic power between the measurements and the LBM simulations (with coarse, medium and fine meshes).

turbofan engines will impose several step changes in engine architecture from a noise perspective. The engine fan source spectrum will be broadened, with a dramatic reduction in the frequency of the fan tones, whilst broadband noise will remain significant at higher frequencies. Next generation nacelles will also have a reduced lined length-to-diameter ratio, in order to reduce weight. Hence, acoustic liners must be more efficient just to maintain the status quo from a noise perspective.

In the EU-H2020 project, ARTEM (Aircraft noise Reduction Technologies and related Environmental iMpact, coordinator Karsten Knobloch, Karsten.Knobloch@dlr.de) the primary goal is to develop, manufacture, and validate, novel broadband acoustic liners which can provide efficient low-frequency attenuation within a limited space envelope. Rolls-Royce Deutschland (RRD) was closely involved in shaping the specifications for liner attenuation and in undertaking initial design investigations. The liner designs should be optimized to provide maximum broadband attenuation across different operating conditions for next generation engine platforms.

As shown in Fig. 58, particular emphasis was put on the design of the liner cavity, with complex internal structures designed to realize an improved match to the optimum impedance spectrum for the Netherlands Aerospace Centre (Royal NLR) flow duct facility. Emphasis was placed on achieving maximum insertion loss at representative sound pressure levels, for grazing incidence of multi-modal sound in the presence of flow [97]. The ISVR work involved numerical impedance modelling of novel cavity concepts, using the COMSOL FEM code [98]. Small scale test samples for no-flow normal impedance tests were also 3-D printed, and tested at the ISVR using the Rolls-Royce portable impedance tube. The high SPL normal incidence acoustic impedance measurements provided a check of the impedance modelling, manufacturing quality, and on the influence of the design tolerances [97].

Large scale panels of two novel liner concepts, a Slanted Septum Core (SSC) and a Multiple FOlded CAvity Liner (MultiFOCAL), were manufactured and tested in the NLR flow duct facility. Consequently, the grazing flow simulations in this work reflected the NLR test set-up. NLR tests were performed for range of Mach numbers from 0 to 0.7, for both upstream and downstream propagation, to assess the influence of flow on liner attenuation. Detailed analysis of the NLR test data was undertaken at the ISVR, with COMSOL simulations also accounting for the influence of boundary-layer refraction.

The COMSOL model of the lined duct was validated using pre-existing data [97]. As shown in Fig. 59, the predicted insertion loss results for the novel liners have shown that both concepts provide significant attenuation improvements at lower frequencies, when compared with an optimized SDOF perforate liner at the Mach 0.3 (downstream propagation) design point, while maintaining

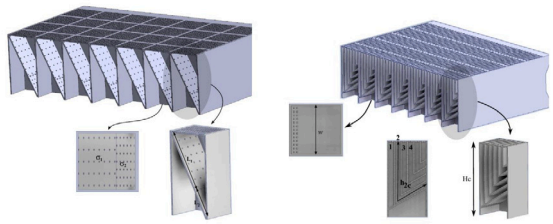

(a) Slanted Septum Core with variable open area

(b) MultiFOCAL Panel

Fig. 58. Schematics of the Slanted Septum Core (SSC) and the MultiFOCAL liner concepts.

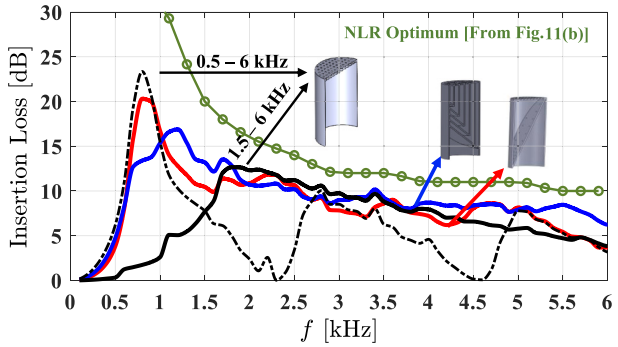

Fig. 59. Predicted insertion loss of the Slanted Septum Core (SSC) and the MultiFOCAL liner concepts.

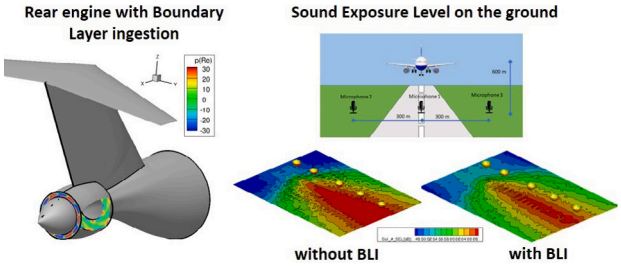

Fig. 60. Acoustic effect on the airport runway of BLI rear engine properly designed using computational mid-fidelity procedure.

similar levels of attenuation at higher frequencies. Future studies will look at the development of full-scale manufacturing processes for the novel designs.

Written by: Suresh Palani (sp4n13@soton.ac.uk), Paul Murray, Alan McAlpine, ISVR, University of Southampton, United Kingdom, Christoph Richter, Rolls-Royce Deutschland Ltd & Co KG, Germany, Daisuke Sasaki, Department of Aeronautics, Kanazawa Institute of Technology, Japan.

4.3. Aeroacoustics assessment of an hybrid aircraft configuration with rear-mounted boundary layer ingested engine

The European Commission established the 2050 goals in terms of reduction, among the others, of 65% noise impact of aircraft. Hybrid propulsion configuration can achieve this target, this work focused on the evaluation of the noise performances of a rear-mounted boundary layer ingestion [99] (BLI) engine at ground level (airport runway).

A fast simulation chain provided mid-fidelity acoustic results involving a Computational Fluid Dynamics approach to give input to Computational Aero-Acoustics methods [100]. It is possible to evaluate the far-field propagation of noise, including the acoustic masking contribution and the engine-aircraft integration, see Fig. 60. The procedure for the calculation of aircraft noise in the vicinity of airports is compliant with the regulation standard provided by SAE-International [101]. This work illustrates the importance of taking into account the design of the engine-fuselage integration in the early phases of aircraft project for an effective noise reduction at ground level.

Written by:Francesco Petrosino (f.petrosino@cira.it), Mattia Barbarino, CIRA, Italy, Martin Staggat, DLR, Germany

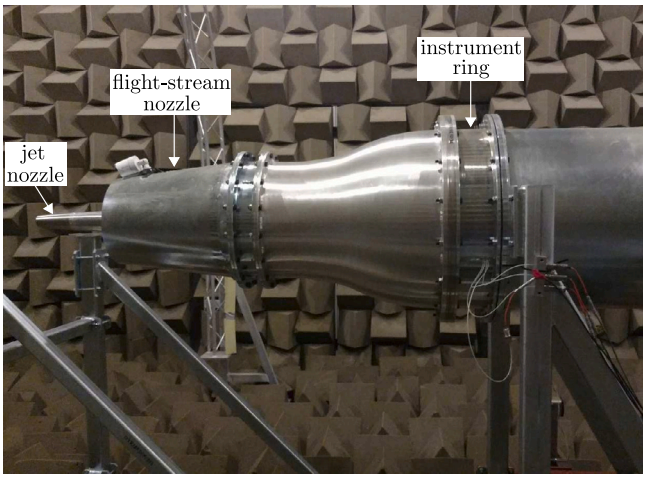

Fig. 61. The new Flight Jet Rig in the Doak Laboratory at the University of Southampton.

4.4. Experimental investigation into the turbulence flowfield of in-flight round jets

The jet exhausted from turbofan engines remains a dominant noise source of modern commercial aircraft at the sideline certification location. During takeoff, the exhausted jet is stretched due to the airspeed between the aircraft and ambient airflow. As well as reducing the magnitude of jet mixing noise, this stretching also lead to a modification of the jet installation noise compared with the static case. A new flight-jet rig was designed, built and commissioned at the University of Southampton (see Fig. 61). Scarce amounts of experimental data exist regarding the unsteady flowfield of in-flight jets. Thus, a detailed analysis of the turbulence statistics of isolated and installed jets was carried out in the Doak Laboratory [102–104]. Insight into the modelling of single-point and two-point statistics of a subsonic round jet ($0.2 \leq M_j \leq 0.8$) has been provided. Forward flight effects are simulated up to a speed of 100 m/s, which is representative of a modern commercial aircraft during take-off. The data suggests that the degree to which the jet stretches with increasing flight velocity can be discerned with the knowledge of the decay of the mean velocity field downstream of the end of the jet's potential core, see Fig. 62. This stretching factor can then be used to predict the changes in the static jet turbulence statistics for the in-flight case. Empirical models for the in-flight jet's shear stresses, cross-correlations, and power spectral density functions are computed and compared with those derived for the static jet case. The two-point statistics has the same self-similar parameters as the single-point functions, Fig. 63. The statistical models presented in the paper can be used for the prediction of in-flight jet mixing noise and the final database is currently being used to inform the development of in-flight jet-surface interaction noise methodologies.

Written by Anderson Proenca: a.proenca@soton.ac.uk, J. Lawrence and R. Self, Institute of Sound and Vibration Research, University of Southampton, UK.

4.5. Wall pressure fluctuations induced by a single stream jet over a semi-finite plate

The reduction of aircraft noise and fuel consumption is a key issue for manufacturers in the design of modern aircraft engines. In order to pinpoint a compromise between thrust and fuel consumption, the current tendency is to increase the engine bypass ratio, a solution that, as an indirect benefit, leads to a reduction of the overall noise [105] due to the lower exhaust velocity. The drawback of this configuration is the very large size of the nacelle diameter, which results in the engine being placed very close to the wing in order to maintain the same ground clearance. In this context, wall pressure fluctuations induced by the jet over an infinite flat plate or a wing have been extensively investigated in [106,107] for the prediction of the vibro-acoustic response of the aircraft surfaces.

The statistical analysis of jet-induced wall pressure fluctuations is also the subject of the highlighted work [108] where the stream issued by a highly compressible subsonic jet flow convects across a semi-infinite plate, see Fig. 64(a). The main novelty proposed therein is the parametric study carried out in terms of the axial distance between the nozzle exit plane and the trailing edge, an issue that has never been investigated before even though it is of interest for realistic jet-wing installation architectures. The analyses in the Fourier and physical domains shows the relevant influence of the parameter L_{TE}/D. The region upstream of the jet exhaust is characterized by the presence of upstream travelling waves whose trace has been identified both in the auto-spectra and cross-correlations. In this region the statistics are almost Gaussian and the OASPL is relatively low. Downstream and for increasing $L_{TE} = D$, the flow rapidly evolves towards a quasi developed state and the statistical properties become similar to those commonly observed in turbulent boundary layers, details see Figs. 64(b–d).

Written by Stefano Meloni: stefano.meloni@uniroma3.it, Università Roma Tre, Italy, and J. Lawrence, A. Proenca, R. Self, University of Southampton, UK., and R. Camussi, Università Roma Tre, Italy.

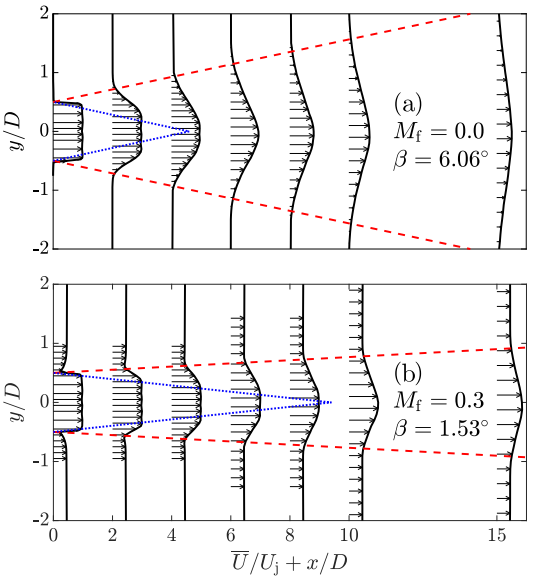

Fig. 62. Mean axial velocity distribution showing the change in the spreading rate of the jet with flight velocity.

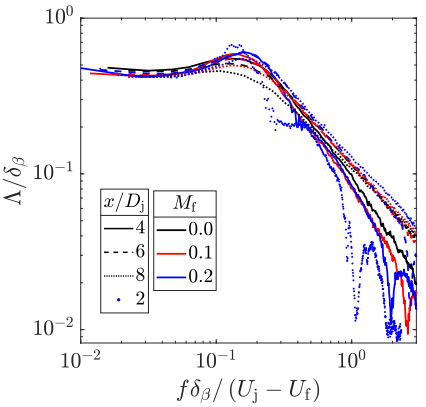

Fig. 63. Frequency-dependent length-scales obtained from two-point statistical models.

4.6. Aeroacoustic design and broadband noise predictions of a fan stage with serrated outlet guide vanes

In the framework of the TurboNoiseBB European project, an advanced aeroacoustic design methodology for Outlet Guide Vanes (OGVs) with leading edge (LE) serrations has been proposed by ONERA [109]. This work includes details on broadband noise and aerodynamic performance of a fan stage using state-of-the-art numerical simulations. The serrated-LE OGV corresponds to a modified stator from a scale-model of an aero-engine fan stage tested at the AneCom AeroTest's facility (Germany). Sinusoidal LE patterns with varying amplitude and wavelength along the span were designed in collaboration with Safran Aircraft Engines. The geometry of the LE serrations was adjusted to account for the local turbulence characteristics provided by Reynolds-Averaged Navier–Stokes (RANS) calculations. Optimal design parameters were found by using simple design rules that are discussed in [109]. Serrated-LE OGV designs (see Fig. 65) were down-selected through a numerical assessment of aerodynamic performances in accordance with industrial specifications, including aerodynamic criteria on the loss coefficient and isentropic efficiency. Broadband noise simulations were performed using a Computational AeroAcoustic (CAA) code that solves the linearized Euler equations with a synthetic turbulence model. Additionally, the acoustic response of the serrated-LE aerofoils was also estimated using an analytical model based on the Wiener–Hopf (WH) technique. Numerical predictions at approach conditions were compared to available measurements (for the baseline case with straight LE) and to analytical Amiet-based and WH predictions. Overall, a good agreement was found for the sound power spectrum in the bypass duct from experimental, numerical and analytical results. The acoustic benefit at the design point of the low-noise OGV with spanwise-varying wavelengths was assessed by CAA and WH methods (see Fig. 66), which suggests

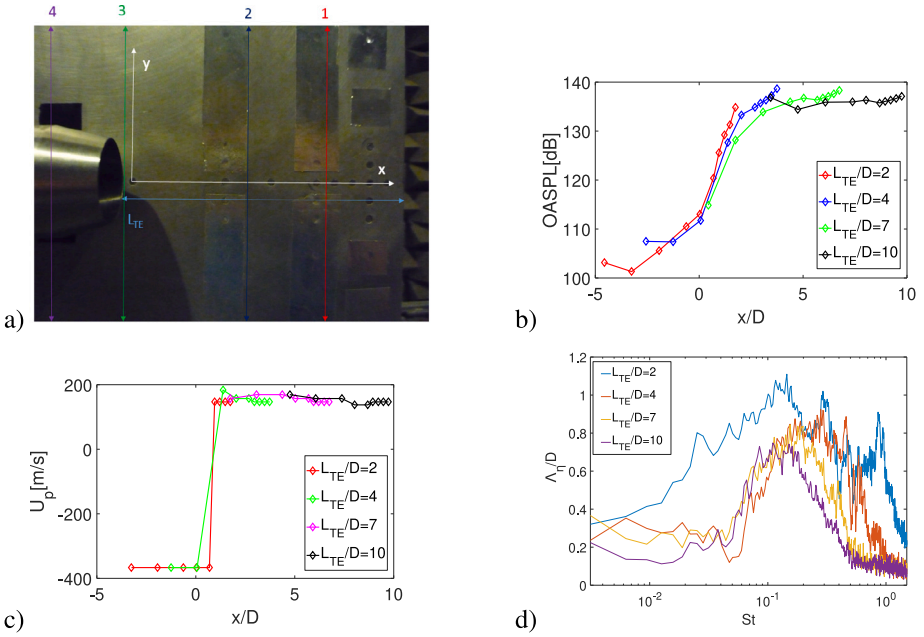

Fig. 64. (a) Experimental setup. Coloured lines show the different nozzle exhaust positions from the TE: (1) $L_{TE}/D = 2$ in red line (2) $L_{TE}/D = 4$ in blue line (3) $L_{TE}/D = 7$ in green line (4) $L_{TE}/D = 10$ in purple line (b) OASPL stream-wise evolution (c) Axial evolution of the phase velocity (d) Span-wise integral coherence lengths. (For interpretation of the references to colour in this figure legend, the reader is referred to the web version of this article.)

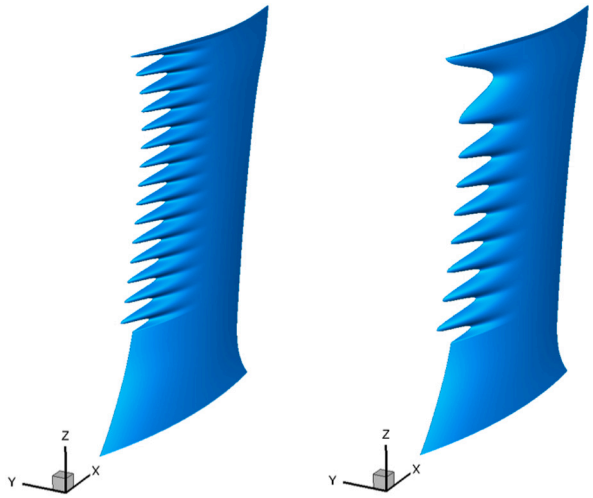

Fig. 65. Low-noise OGV designs using locally distributed serrations along the span with constant (left) and spanwise-varying (right) wavelengths.

a noise reduction between 2.5 dB and 3.5 dB on the overall sound power level. This work has received funding from the European Union's Horizon H2020 TurboNoiseBB program under grant agreement No 690714.

Written by C. Polacsek: cyril.polacsek@onera.fr, M. Buszyk and R. Barrier, ONERA, France, and F. Gea-Aguilera, Safran Aircraft Engines, France.

4.7. Influence of swept blades on low-order acoustic prediction for axial fans

VKI is pursuing research for a better understanding, modelling, and eventually mitigation of the noise emitted by low-speed axial fans used for automotive engine cooling. A low-order sound-prediction methodology has been developed considering the blade sweep-angle effect on the acoustic predictions of the turbulence-impingement and the trailing-edge noise-generating

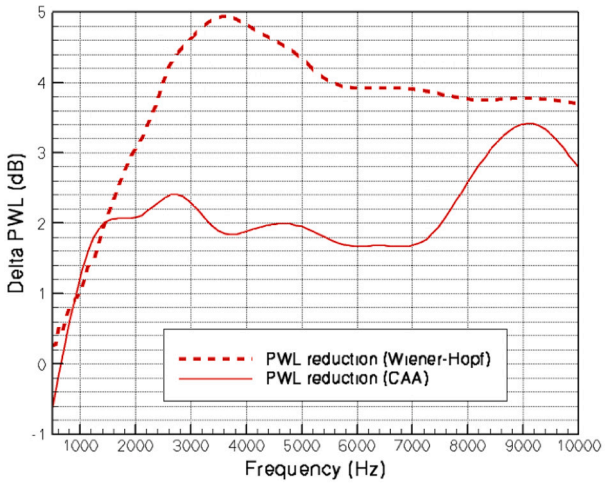

Fig. 66. Noise reduction from the low-noise OGV (with spanwise-varying wavelengths) assessed by the CAA and WH methodologies.

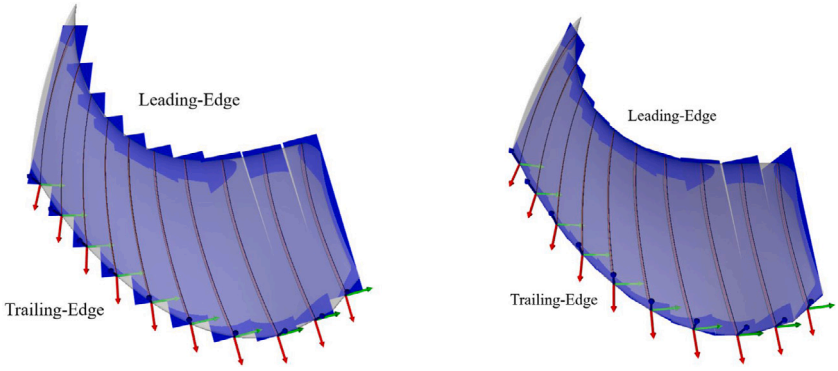

Fig. 67. With a parallelogram representation of the blade strips implemented in Amiet's theory, the noise emitted by the blade turbulent boundary layer at the trailing edge is more accurately modelled. A similar improvement has been brought to the leading-edge noise model.

mechanisms [110]. The prediction method implemented in the VKI in-house aeroacoustic solver BATMAN is based on a semi-analytical framework following Amiet's theory, via a strip decomposition of the blade modified to include the blade forward curvature (Fig. 67). The predicted results were compared with far-field sound measurements obtained in the ALCOVES anechoic laboratory of the VKI [111]. It was shown that the effect of the sweep angle is to globally reduce the emitted noise by the fan and to change the sound distribution of the sources along the blade span (Fig. 68). Furthermore, not accounting for the sweep angle can yield wrong conclusions on the dominating noise-generating mechanisms, between turbulence-interaction noise and trailing-edge noise. The above research benefited from the support of the European Commission's Framework Program "Horizon 2020", through the Marie Skłodowska-Curie Innovative Training Networks (ITN) "SmartAnswer – Smart mitigation of flow-induced acoustic radiation and transmission", grant agreement No. 722401 to the present research project.

Written by Alessandro Zarri: alessandro.zarri@vki.ac.be, and J. Christophe, von Karman Institute for Fluid Dynamics, Belgium, and S. Moreau, Université de Sherbrooke, Canada, and C. Schram, von Karman Institute for Fluid Dynamics, Belgium.

4.8. Active control of jet-plate interaction noise for excited jets by plasma actuators

Controlling of jet-wing interaction noise by plasma actuators is investigated in Ref. [112]. The low-frequency part of the jet installation noise is considered as produced by the diffraction of instability wave packets developing in the jet shear layer. Thus, the main idea of noise control comes to the attempt to reduce the amplitude of these wave packets near the wing trailing edge. A simplified jet-plate configuration is studied experimentally for jet Mach numbers ranging from 0.4 to 0.6 (Fig. 69). To avoid additional complications related to the control of stochastic signals in the first step, the jet is excited by a loudspeaker at a frequency corresponding to Strouhal number 0.6 (similar approach for uninstalled jet was considered in [113]). Acoustic forcing generates axisymmetric instability wave in the jet shear layer, which is the object of control. The control action is implemented by a high-frequency dielectric barrier discharge (HF DBD) plasma actuator with a ring-like electrode mounted inside the nozzle near the exit.

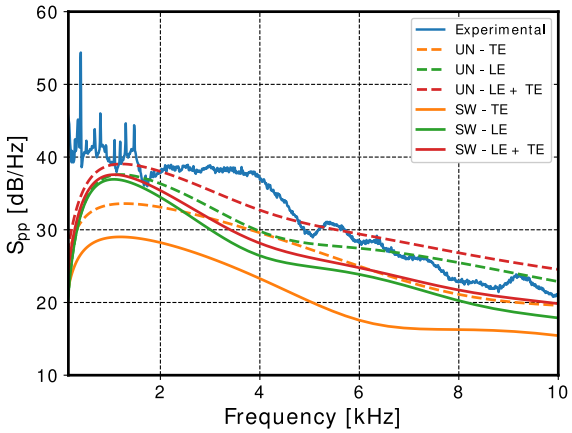

Fig. 68. Comparison between the fan measured acoustic field and the semi-analytical prediction including the trailing-edge (TE) and leading-edge (LE) noise mechanisms, accounting (SW) or not (UN) for the blade sweep.

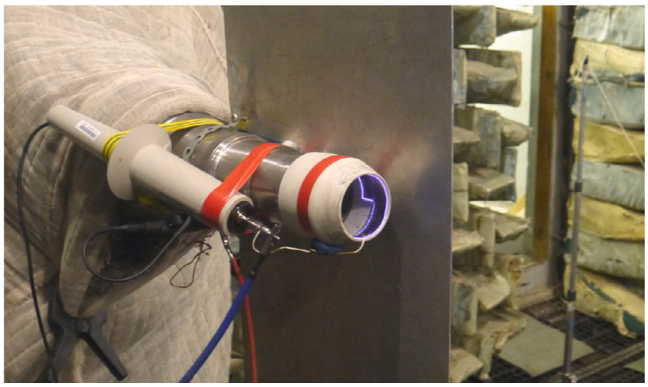

Fig. 69. Experimental setup for installation noise control.

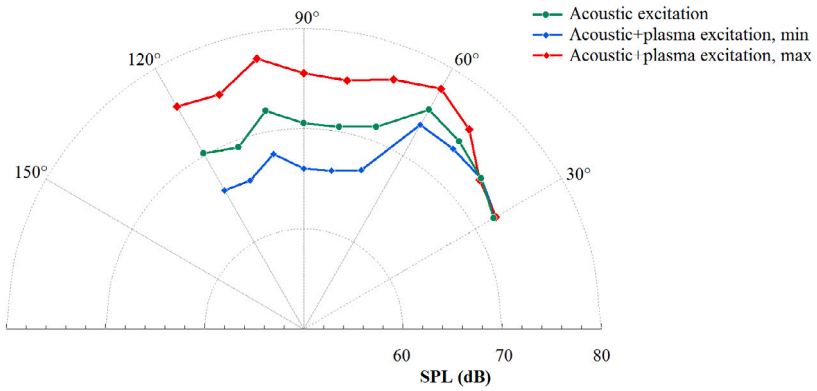

Fig. 70. Directivity of installed jet noise at the forcing frequency (Strouhal number $St = 0.6$) for the reference acoustic excitation (green) and simultaneous acoustic and plasma excitations at phase shifts corresponding to the maximum installation noise reduction (blue) and amplification (red). (For interpretation of the references to colour in this figure legend, the reader is referred to the web version of this article.)

It is demonstrated that installation noise can be significantly suppressed if the plasma actuator generates instability wave with the amplitude equal to that of the excited by the loudspeaker, but in antiphase to it, and vice versa, if these instability waves are in phase, installation noise increases by about 6 dB (Fig. 70). The obtained results support the idea that low-frequency jet-wing installation noise can be controlled in a linear framework. These results are quite promising and show the potential of such a technique for

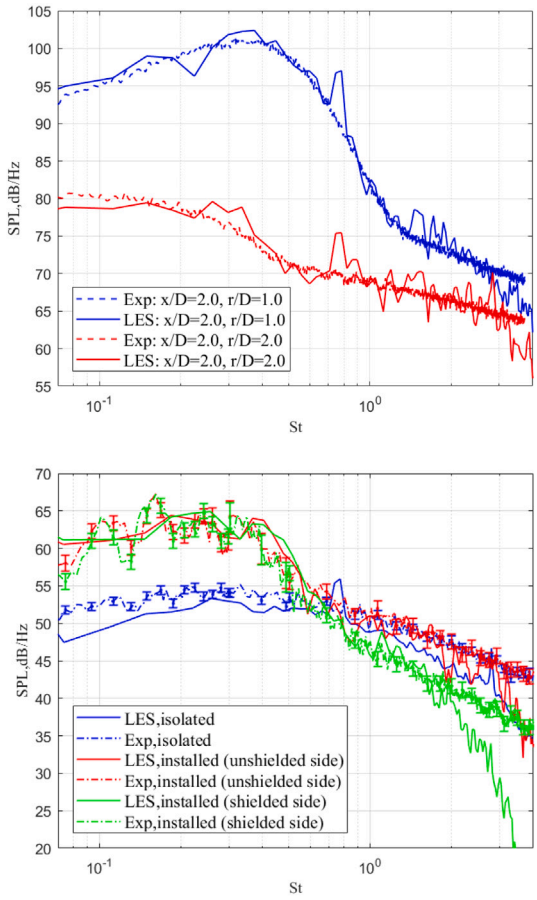

Fig. 71. Near-field (above) and far-field (below) pressure spectra of isolated and installed jets.

installation noise mitigation. Implementation of this concept for unexcited jets of practical interest will be the next step of the research.

Written by V. Kopiev: vkopiev@mktsagi.ru and G. Faranosov, TsAGI, Russia.

4.9. LES study of an installed jet flow and noise with detailed experimental validation

Extra noise is generated at low frequencies when a jet is installed near a solid surface. This becomes one of the primary noise sources for future aircraft configurations with close engine-airframe integration, such as ultra-high-bypass-ratio engine powered aircraft and NASA's low boom supersonic aircraft. Large-eddy simulation (LES) was performed on a generic installed jet configuration — a high-speed turbulent round jet installed below a horizontal flat plate and also on an isolated jet to provide time-accurate turbulent flow data for fundamental study of installation noise generation [114]. The far-field sound was predicted by surface integration over the near-field LES data following the Ffowcs Williams–Hawkings (FW–H) equation. The flow and acoustics predicted by LES were compared in great detail with experimental measurements using hot-wire anemometry [115], unsteady surface pressure sensors, and far-field microphones [116]. Good agreement has been achieved on flow statistics, space–time velocity correlations, and both near-field and far-field spectra (see Fig. 71). The peak in the far-field noise spectra, due to the installation, is well captured by the simulation. This installation noise is generated by a new source introduced near the plate trailing edge (TE). This is generated by scattering the 'silent' hydrodynamic waves into 'audible' acoustics (see Fig. 72). The wavenumber decomposition along the plate surface centre line distinguishes the energy distributions between the propagating acoustic and evanescent hydrodynamic waves near the TE (see Fig. 73). This well-validated LES data will be a great asset for understanding installed jet noise generation mechanisms and informing low-order noise model development.

Written by: Zhong-Nan Wang University of Birmingham, UK. Z.N.Wang@bham.ac.uk, A. Proenca, J. Lawrence, P. G. Tucker, R. Self

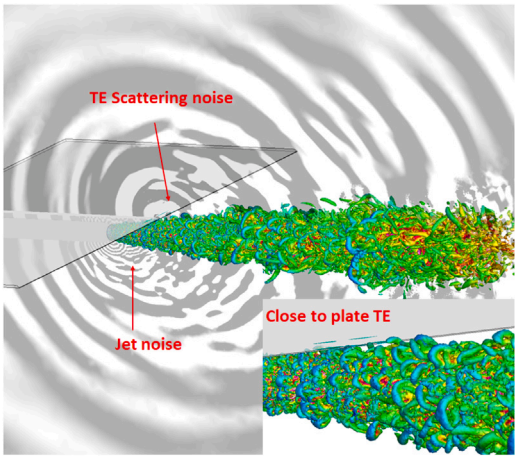

Fig. 72. Flow structures (Q-criterion isosurfaces coloured by axial velocity) and acoustics (time derivative of pressure as background contour) in installed jets from the LES.

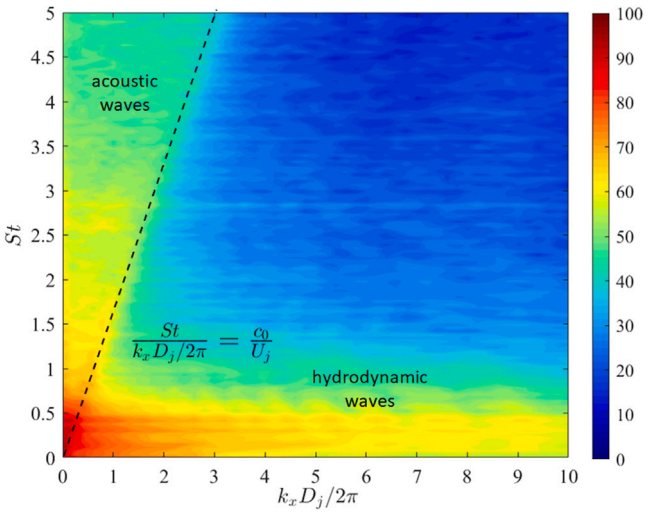

Fig. 73. Wavenumber spectra of surface pressure underneath the plate along the centre line.

5. Aircraft interior noise

5.1. Coherence and coherence lengths of wall pressure fluctuations

The wall pressure coherence for zero and adverse pressure gradient (ZPG and APG) boundary layer flows was measured on a flat plate model with pinhole-mounted pressure sensors. The Reynolds number dependence of the streamwise coherence decay for ZPG flows is found to be related to the ratio of the friction velocity and the free-stream velocity [117]. A relation between the decay coefficient and the Reynolds number is established based on the measured coherence along with results of other published datasets. Furthermore, results of the off-axis coherence show that the Smol'yakov and Tkachenko model [118], with an elliptical combination of the streamwise and spanwise coherence, has an accurate prediction in both frequency and spatial domains, whereas the Corcos model [119] underpredicts the off-axis coherence, see Fig. 74.

The coherence lengths, calculated based on the coherence, show a significant Reynolds number dependence in the streamwise direction and at low frequencies for both streamwise and spanwise directions, see Fig. 75. A coherence length model for ZPG boundary layers, taking the Reynolds number effect into account, is proposed based on the coherence length spectra [117]. As example, Figs. 76 and 77 show the prediction of the coherence lengths for a wind tunnel test with a low Reynolds number [117] and a flight test with cruise conditions [120]. In comparison with the other published models, the present model achieves a considerable improvement of the prediction accuracy for boundary layer flows, covering a large range of Reynolds numbers. Furthermore, the results of the coherence lengths for APG boundary layers show that the APG reduces the streamwise coherence length throughout

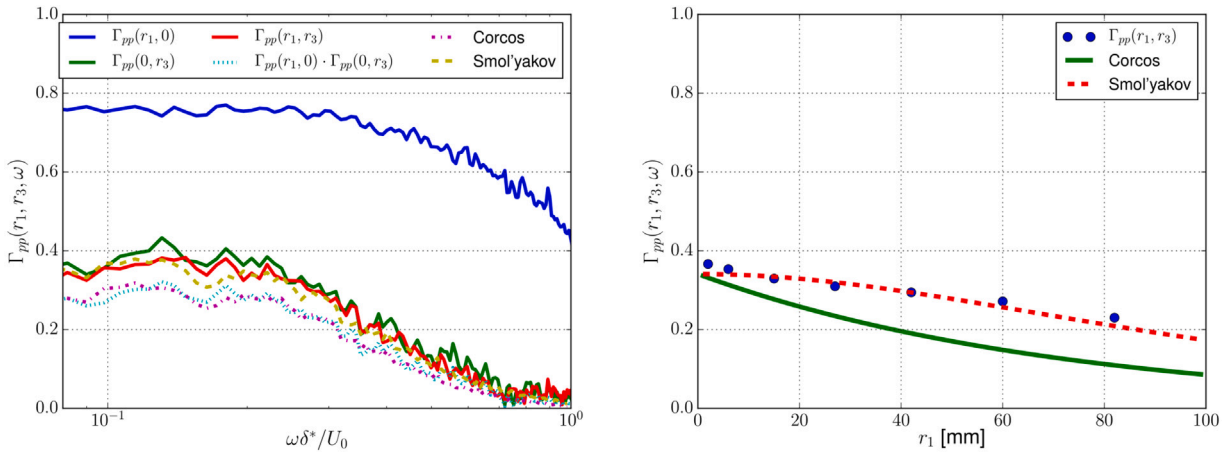

Fig. 74. Comparison of the measured and calculated off-axis coherence with $r_3 = 12$ mm for ZPG with $U_0 = 58.7$ m/s and $Re_\theta = 8685$ (left) $r_1 = 15$ mm (right) $\omega\delta^*/U_0 = 0.21$.

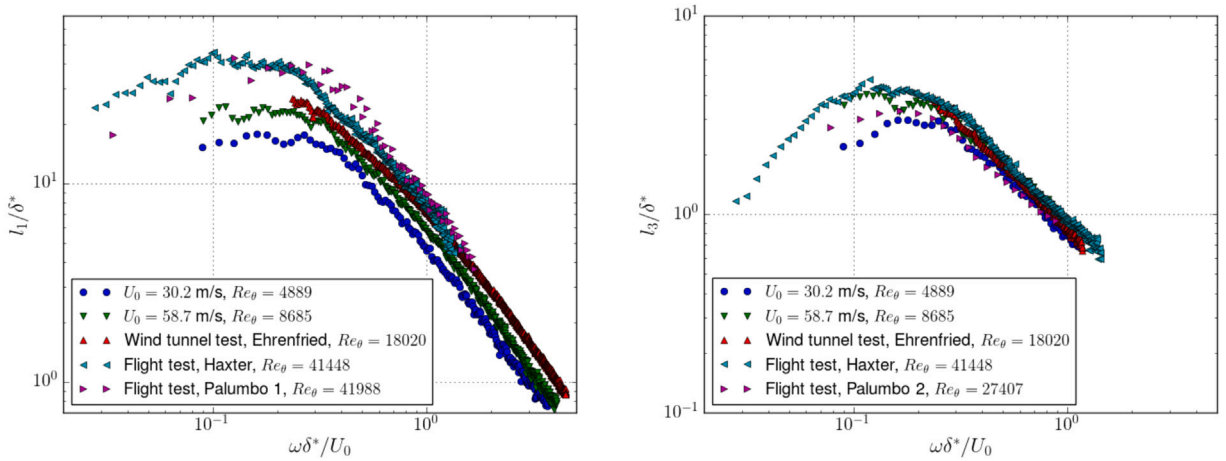

Fig. 75. Comparison of scaled coherence length spectra (left) streamwise direction (right) spanwise direction.

the whole frequency range, but increases the spanwise coherence length mostly at lower frequencies, leading to a steeper spectral drop at high frequencies.

Written by: Nan Hu (nan.hu@dlr.de) DLR, Germany

5.2. Wall pressure fluctuations on a full-scale cockpit model

A wind tunnel investigation of the wall pressure fluctuations has been conducted on a full-scale model of a business jet front part [121]. Given the difficulties faced when characterizing the wavenumber–frequency spectra of such fluctuations [122], a great care was put in the design of the bespoke antennas, consisting of 40 MEMS microphones, non-uniformly distributed on a cross pattern [123]. These thin antennas, placed at key locations of the fuselage as shown in Fig. 78, provided repeatable and homogeneous data.

Classical models, such as Goody's, did not match the measured frequency spectra. Coherence exhibited an exponential decay for any given frequency, but the associated decay rate's frequency dependence also deviated from the prediction of Corcos' or associated models. The wavenumber–frequency spectra showed well defined convection ridges, from which the convective wavenumber or the associated velocity could be computed. Furthermore, they enabled the spectral filtering and extraction of acoustic content, generated by an external source, from the wall pressure field itself. As illustrated in Fig. 79, the acoustic components were indeed clearly differentiated from the convective ridge, and it was thus possible to filter out one of the two. At moderate speed, an excellent match was found between the reconstructed spectrum and that measured with only acoustic waves and no flow.

A companion study focused on fuselage vibrations and interior noise radiation, with measurements also conducted during the same campaign. Specific panels that micmicked the vibrational behaviour of the true fuselage were instrumented and the interior

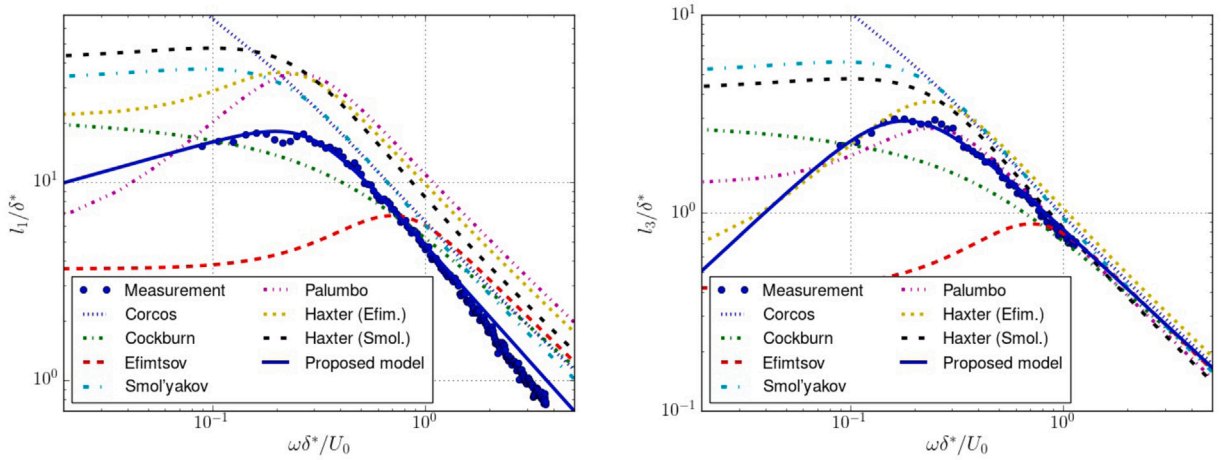

Fig. 76. Prediction of coherence lengths for a wind tunnel test case with $U_0 = 30.2$ m/s and $Re_\theta = 4889$ (left) streamwise direction (right) spanwise direction.

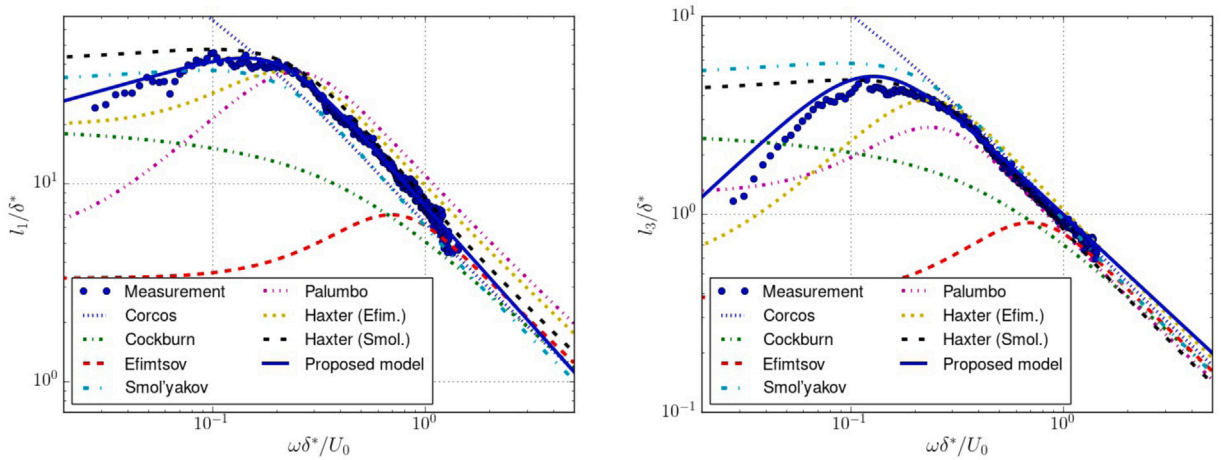

Fig. 77. Prediction of coherence lengths for a flight test case with $U_0 = 250$ m/s and $Re_\theta = 41448$ (left) streamwise direction (right) spanwise direction.

noise was measured. A RANS simulation was performed and checked against experimental data, to provide input to a vibrational model. The computed cabin noise radiation power was within 2 – 5 dB of the measured one, for the studied frequency range. While further analysis will provide more detailed information, this is an encouraging first step. Project: Canoble, Coordinator: Romain Leneveu, Vibratec.

Written by: Simon L. Prigent: simon.prigent@ec-lyon.fr, Édouard Salze, Emmanuel Jondeau and Christophe Bailly, École Centrale de Lyon, France, and Romain Leneveu, Vibratec, France.

6. Miscellaneous topics

6.1. Acoustic metamaterial for broadband noise attenuation

Equivalent circuit analysis is a powerful tool for analysing acoustic systems where a lumped element model is valid. These equivalent circuits allow an overall impedance of the structure to be estimated which facilitates predictions of the reflectivity, transmissibility and/or absorptivity of the system. However, more complex acoustic systems require non-planar equivalent circuits which are much more challenging to simplify to a single overall impedance value using traditional Kirchoff's Law simplifications. A two-point impedance method [124] is developed using graph theory which allows the impedance of a circuit to be estimated without simplification [125]. The graph theory method is applied to a type of acoustic absorber structure named SeMSA (Segmented Membrane Sound Absorber) which had previously been developed as low-frequency super-absorber [126]. This method allows the SeMSA analysis to be expanded to multi-sector designs with a wider parameter space, see Fig. 82. A local optimization routine is applied to the graph theory impedance estimation to maximize acoustic absorption of the SeMSA under consideration of absorber

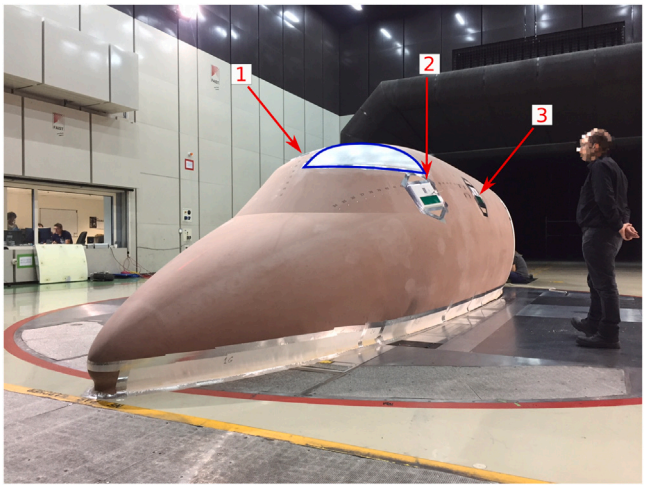

Fig. 78. Mock-up installed in the wind tunnel with the location of the three wall pressure antennas and one of three vibrational panels (delimited in blue). (For interpretation of the references to colour in this figure legend, the reader is referred to the web version of this article.)

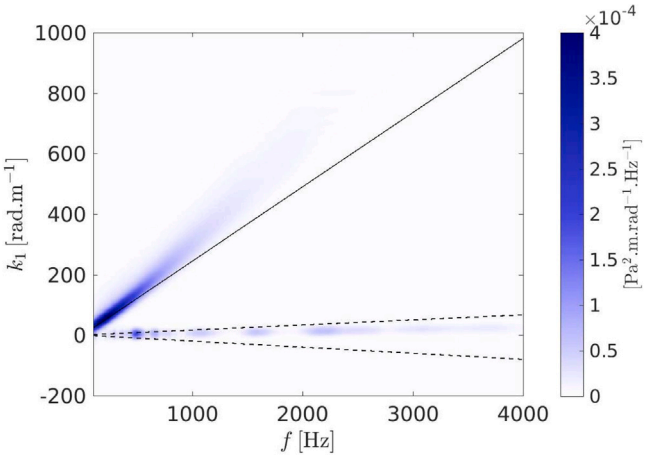

Fig. 79. Wave number–frequency spectra at 30 m.s^{-1}, with acoustic source on. For reference : (solid line) $k_c = 2\pi f/(0.8 \times U_e)$ and (dashed line) bounds of the acoustic ellipse.

depth, causal optimality and the targeted noise spectra. Analytical predictions are validated using numerical simulations. The optimized multi-sector absorber demonstrates 70.5% white noise absorption in the 20–4500 Hz frequency range with an absorber depth of 16 mm and is just 0.5 mm from the theoretical minimum depth to achieve this absorption response, see Fig. 80. The method can also be applied to micro-perforated panel type liners and can be used to target specific narrow band noise as well as broadband noise, Fig. 81.

Written by: Gareth J. Bennett (gareth.bennett@tcd.ie), Trinity College Dublin, Ireland

6.2. Acoustics of micro-slit plates

Micro-Perforated Plates (MPP) are plates with perforations of the order of the Stokes viscous boundary layer. For audio-frequencies applications, this is a few tenths of a millimeter. For porosities of a few percent, the transfer resistance approaches the characteristic impedance of air. A Micro-perforate plate backed by a suitable cavity provides an effective and lightweight alternative solution to porous material. Literature on Micro-perforates focuses on circular perforations. However, equivalent acoustical properties can be obtained by replacing circular perforations with slits. A small number of slits can replace many circular perforations. Despite the limited literature on Micro-Slit Plates (MSP), their application shows promising results [127]. Analytical models combining a parallel flow approximation within the slit with potential flow theory for the end-corrections are proposed for the high Stokes number limit [128]. These models allow the prediction of the effect of rounding of the edges of the slit and the influence of the proximity of the slit to the sidewall of a back cavity. These models are compared to results of numerical

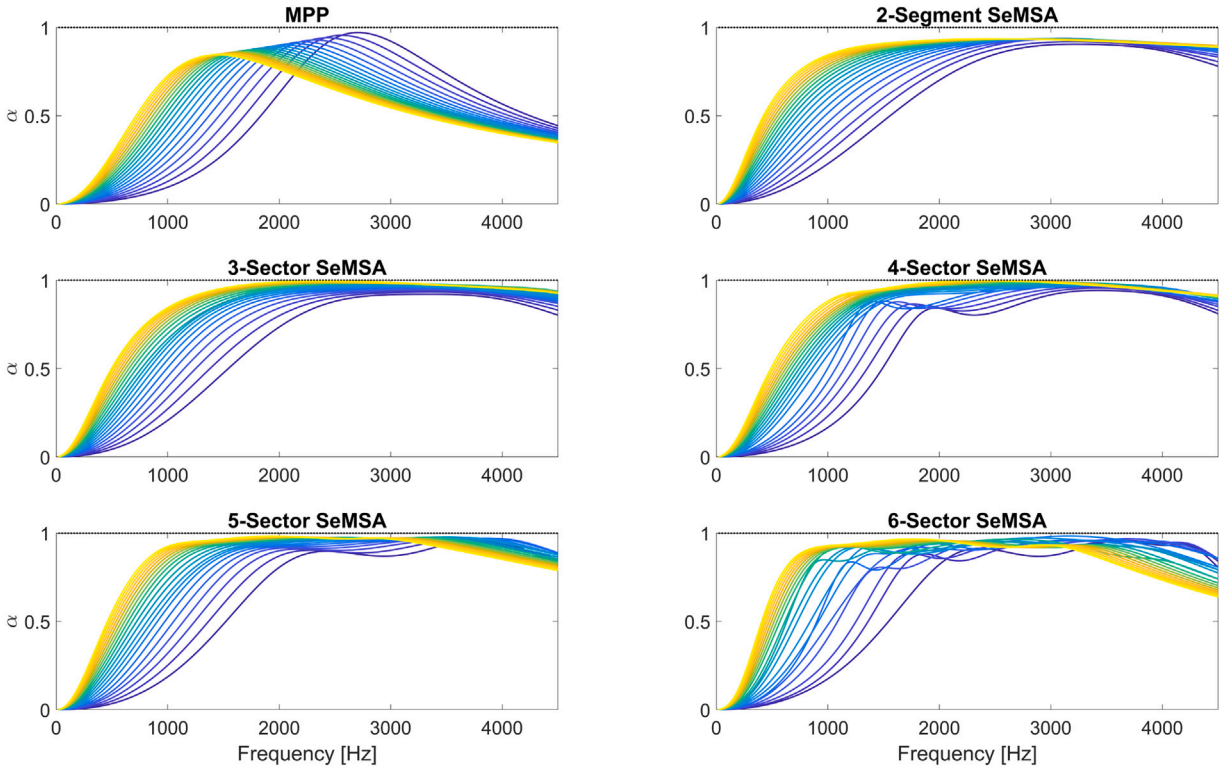

Fig. 80. Absorption spectra for a range of absorber depths from 10 mm (blue) to 50 mm (red). Target spectrum = white noise. Frequency range = 20 Hz–4500 Hz. $R = 40$ mm, MPP=micro-perforated panel. (For interpretation of the references to colour in this figure legend, the reader is referred to the web version of this article.)

solution of the two-dimensional Linearized Navier–Stokes Equations (LNSE) for an incompressible flow. The results are summarized in correlation formulas for the prediction of the transfer impedance at an arbitrary Stokes number. Further research is currently focusing on the non-linear response of MSPs [129].

Written by: Alessia Aulitto : A.Aulitto@tue.nl, A. Hirschberg, I. Lopez-Arteaga, Technische Universiteit Eindhoven, The Netherlands

6.3. Main flow oriented vorticity noise

Entropy inhomogeneities and vorticity patches induce so-called indirect combustion noise when passing through a choked nozzle referred to as entropy noise and vorticity noise, respectively. It was found that vorticity noise depends on the orientation of the vorticity viz., oriented normal or parallel to the axial main flow [130–132]. At the DLR's Engine Acoustics laboratory – using a dedicated experimental setup [131,132] – an experimental investigation of parallel component vorticity noise was performed [131,132]. In the experiment, a time-dependent swirling flow was induced by unsteady tangential injection in a pipe upstream of a choked convergent–divergent nozzle. Theoretical analysis [130,132] found that as the resulting swirling flow passes through the nozzle, the axial stretching of the fluid causes an increase in rotation energy. The steady energy conservation in an isentropic flow (Bernoulli) implies a Mach number higher than unity at the throat and an associated reduction of density. Ergo, the critical axial mass-flow rate (for fixed reservoir pressure and temperature) decreases quadratically with increasing swirl intensity. The acoustic waves radiated downstream of the nozzle are a direct measure for this axial mass-flow rate modulation. Using a semi-empirical model, this sound production mechanism was demonstrated to indeed be quasi steady [132].

Written by: Written by Lionel Hirschberg: l.hirschberg@imperial.ac.uk, Imperial College London, UK., Steven J. Hulshoff, Delft University of Technology, The Netherlands, Friedrich Bake, Bundesanstalt für Materialforschung und -prüfung (BAM), Germany, Karsten Knobloch, Deutsches Zentrum für Luft- und Raumfahrt (DLR), Germany

6.4. Low frequency behaviour of the cremer impedance

The Cremer impedance is a well-known solution for optimum propagational damping of a mode in a duct [133]. It is based on the creation of an exceptional point where two modes merge. For flow ducts the solution is derived based on the Ingard-Myer boundary condition, i.e., continuity of pressure and normal displacement. This leads to the occurrence of a negative real part of the

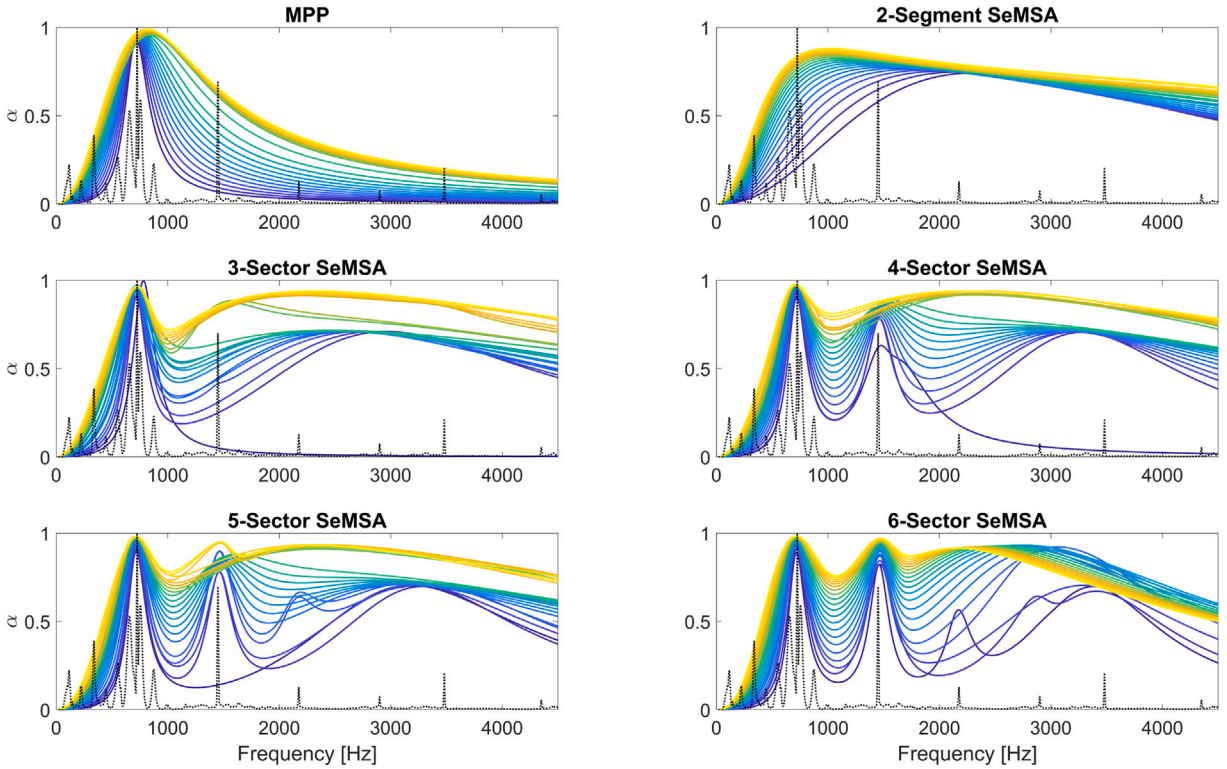

Fig. 81. Absorption spectra for a range of absorber depths from 10 mm (blue) to 50 mm (red). Target spectrum = fan noise. Frequency range = 20 Hz–4500 Hz. $R = 40$ mm, MPP=micro-perforated panel. (For interpretation of the references to colour in this figure legend, the reader is referred to the web version of this article.)

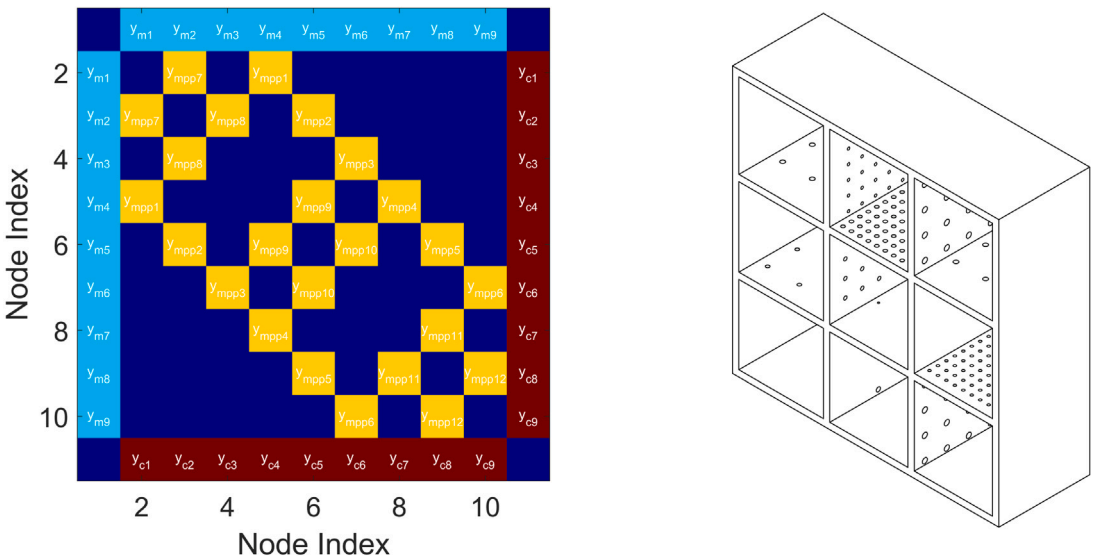

Fig. 82. Adjacency matrix (left) for a 3×3 rectangular grid form of SeMSA (right).

impedance in the low-frequency limit [133,134]. The solution in the upstream direction also breaks down when this happens while the downstream solution still is valid [134]. A relevant question is how dependent these results are on the boundary condition? The question of the correct boundary condition in flow ducts has received considerable attention over the years. For a locally reacting duct wall it is in general not sufficient to describe the boundary condition by just an impedance [135]. Based on the published works one can conclude that the Ingard-Meyer condition is valid in the high-frequency range, where the acoustic boundary layers

are smaller than the flow viscous sub-layer. The proposed models as well as experiments support that at sufficiently low frequencies the classical boundary condition, i.e., continuity of pressure and normal velocity, should be used instead. In a recent paper Åbom and Sack [136] investigated how the wall boundary condition affects the low-frequency behaviour of the Cremer solution. Unlike Ingard-Meyer the classical boundary condition yields a solution with a positive Cremer resistance that merge the 0:th and 1:st mode for both up- and downstream propagating waves. This suggests that for low frequency noise control the best strategy, for optimum damping of the plane wave, is to compute the Cremer impedance based on the classical boundary condition. In particular for applications with upstream propagation, where the Ingard-Meyer solution fails, this is an important result.

Written by: Written by Mats Åbom: matsabom@kth.se, KTH-The Royal Inst. of Technology, Stockholm.

6.5. A high-fidelity aeroacoustic simulation of a VTOL aircraft in an urban air mobility scenario

Despite the growing interest for the Urban Air Mobility market and the explosion of electric vertical take-off and landing (eVTOL) aircraft development, barriers to their commercial feasibility and public acceptance needs still to be addressed, as vehicle performance, safety, emission and noise. Despite the fact that the electric propulsion system is characterized by zero emissions, a safe and well performing eVTOL vehicle can, in any case, pose problems of unacceptable noise levels. Therefore, public acceptance of UAM noise remains one of the major concerns. This work demonstrates the set-up of a comprehensive numerical chain for assessing the noise impact of a VTOL vehicle during its whole operation in a complex urban scenario [137]. The computational procedure consists of an aerodynamic free-wake vortex lattice boundary element method (BEM) for the prediction of the rotor–rotor and rotor–fuselage interactions (Fig. 83), an integral approach based on the Ffowcs Williams and Hawkings (FW–H) equation for the acoustic characterization of the VTOL as noise source (Fig. 83(b)) [138], a fast ray-tracing approach for the acoustic far-field propagation and the assessment of the urban areas noise exposure during its flight operations (Fig. 83(c)) [101], and an Adaptive black-box Fast Multipole Method (AbbFMM) [100], for the accurate prediction of the acoustic scattering phenomena when the vehicle is approaching in proximity of the urban centre, Fig. 83(d).

Written by: M. Barbarino: m.barbarino@cira.it, F. Petrosino, A. Visingardi, CIRA, Italy

6.6. Application of noise certification regulations within conceptual aircraft design

A virtual noise certification process within the conceptual aircraft design phase is realized [139]. This new simulation process as depicted in Fig. 84 is assembled by simulation tools that each have a specific task and represent a relevant discipline, e.g., aircraft flight simulation. Noise certification regulations according to ICAO Annex 16 are assessed, documented, and implemented in order to enable a virtual assessment early within the conceptual design phase of existing and/or novel aircraft concepts. Modifications and future updates to the regulations can readily be investigated with this process. An application of this process to existing aircraft (A319-100 and B747-400) is conducted and a comparison of the predicted certification noise levels shows satisfying agreement with discrepancies in the range of less than 1 EPNdB up to 3.2 EPNdB. Remaining discrepancies can be attributed to specific aspects of the simulation process. All underlying simulation steps are investigated for their influence on the prediction result. It can be demonstrated that the major contributor to these discrepancies can be attributed to the complexity of the EPNL metric if applied based on data from conceptual aircraft design. This finding can be confirmed by comparison of prediction results to data from a flyover noise campaign, i.e., see Fig. 85. In conclusion, the novel process can be applied to realize a virtual noise certification according to the ICAO regulations. At this point, it is recommended, to focus on a comparative assessment rather than evaluation of absolute noise levels due to remaining discrepancies. Such a comparative assessment of novel low-noise aircraft concepts is presented. It can be shown that different technologies and aircraft architectures (described in Ref. [19]) have an advantageous effect to meet even more stringent noise certification limits, e.g., see Fig. 86.

Written by: M. Noeding (michel.noeding@dlr.de), L. Bertsch, DLR, Germany

6.7. Liner impedance eduction under shear grazing flow at a high sound pressure level

The effect of a complex flow on the acoustical behaviour of nacelle liners remains a topical and challenging subject for nacelle liner design. For a classical perforate-over-honeycomb liner, it is usually assumed that the liner impedance is constant along the streamwise direction. However, when the incident sound pressure level (SPL) is high, vortex shedding appears and leads to an increase of the resistance. In a lined duct configuration used to perform an impedance eduction, the SPL may be much higher upstream than downstream of the liner (propagation-wise), it thus seems relevant to take into account the space-dependency of the impedance as a function of the total SPL which decreases along the liner.

In [140], experiments were conducted in a grazing flow duct at ONERA (B2 A). The impedance was then educed with an inverse method adapted to a shear flow using a Discontinuous Galerkin scheme for solving the Linearized Euler Equations in the frequency domain. To take into account the effects of the variation of the SPL, a space-dependent impedance boundary condition was considered in the eduction strategy.

The resistance was defined as an affine function in the streamwise direction. A parameter L_τ was introduced to represent the length of liner over which the resistance is expected to change due to the SPL effect. This affine formulation was shown to be a good compromise between efficiency and ease of implementation.

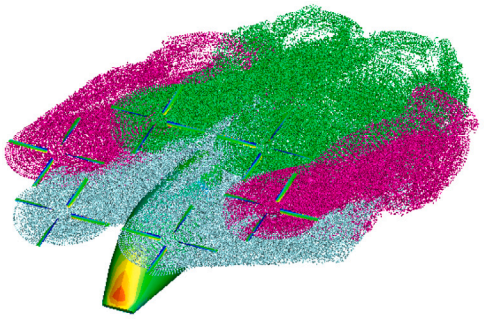

(a) Wake system developed by the VTOL configuration.

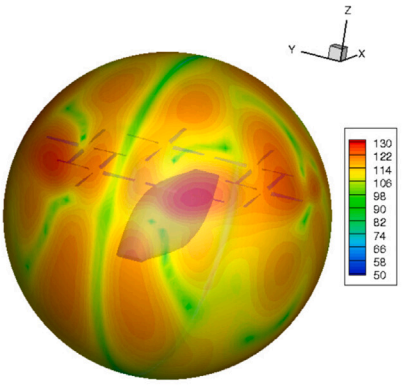

(b) Spherical acoustic source encompassing the VTOL configuration.

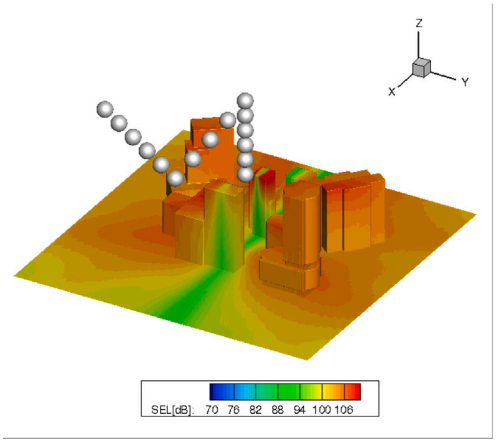

(c) Sound Exposure Level during the VTOL flight operation and computed on the large urban area.

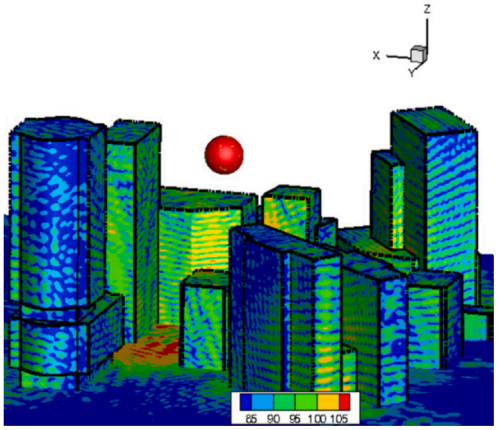

(d) VTOL scattering by the large urban area in terms of SPL, at the 1st BPF.

Fig. 83. VTOL noise in urban air mobility scenario.

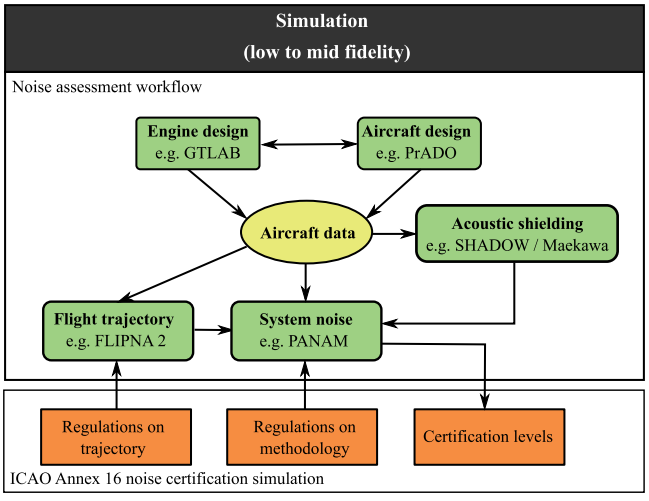

Fig. 84. Simulation process for automated virtual noise certification.

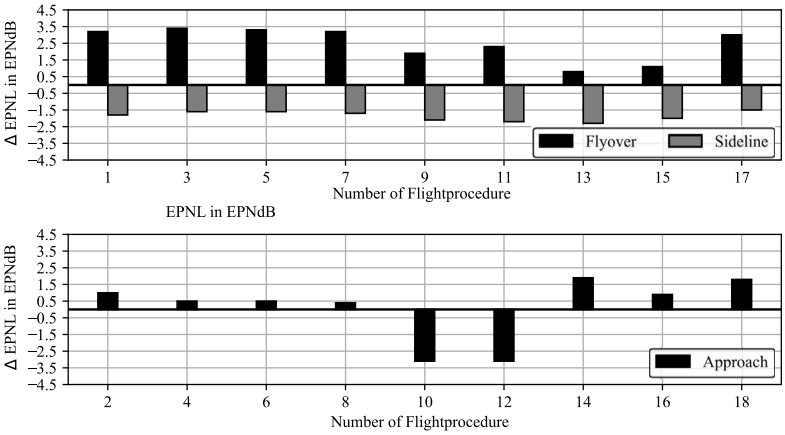

Fig. 85. Comparison of EPNL: measurement vs. simulation.

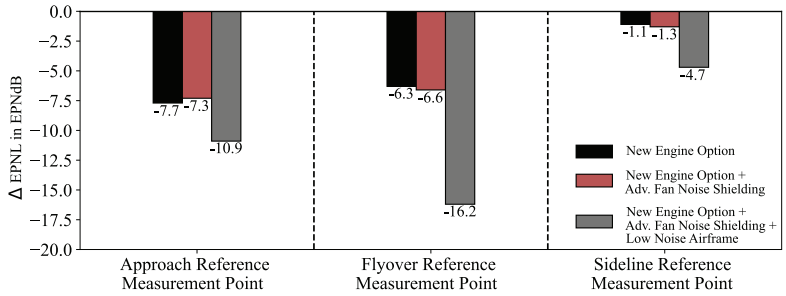

Fig. 86. Certification level deltas for selected technologies and vehicle concepts.

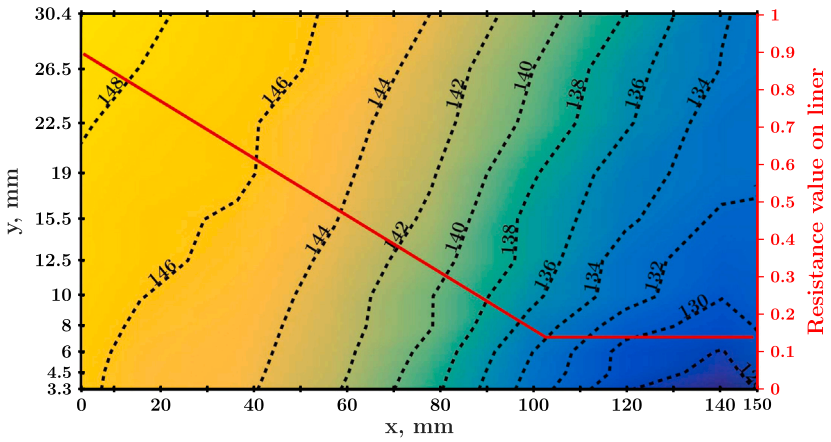

Fig. 87. Educed resistance evolution along the liner (in red) and sound pressure field simulated with the LEE (background colour and isocontours) for $M_b = 0.1$, single tone excitation, $f = 1528$ Hz, incident SPL = 150 dB in the B2 A rig.

Using this new formulation has shown the existence of a SPL threshold value above which the effects of the SPL can be described with a space-dependent expression. Under this threshold, the resistance stays constant (see Fig. 87). This approach allowed then the finer analysis of a multiphysics configurations where thermal effects were taken into account [141].

Written by Victor Lafont: victor.lafont@onera.fr, F. Méry, R. Roncen, F. Simon and E. Piot, ONERA, France.

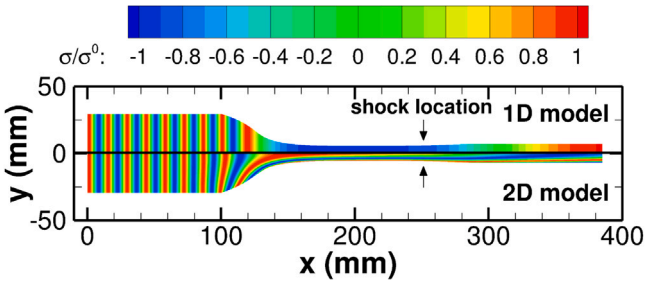

Fig. 88. 1D- and 2D-modelled non-dimensional entropy fluctuation at 1000 Hz.

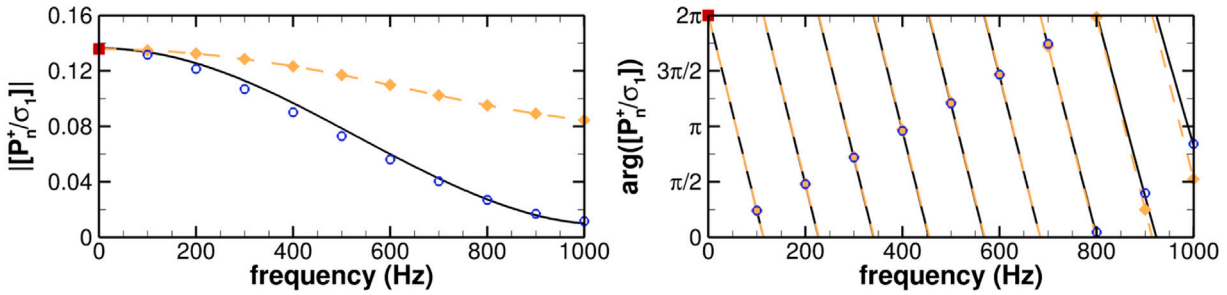

Fig. 89. Modelled and computed entropy noise at nozzle exit. ■ compact solution, ♦– – 1D model, — 2D model, ∘ CAA simulation..

6.8. 2D modelling of entropy noise through supercritical nozzle flows

Entropy noise is produced when temperature fluctuations (entropy spots) are accelerated by the mean flow inside the gas turbine, through a nozzle or a turbine stage for instance. Its prediction is important because it plays a role in community noise as well as on the onset of combustion instabilities. Most of the models available in the literature assume planar perturbations, but it was recently demonstrated numerically that this assumption does not hold for entropy fluctuations : when entropy wavelength becomes comparable to or smaller than the size of the nozzle, radial deformation of the entropy fronts must be accounted for to correctly predict the noise generated, as illustrated in Fig. 88. This radial deformation was included in a 2D model at ONERA for subsonic inviscid nozzle flows [142]. Recently, the model was extended to deal with supercritical configurations, without and with a normal shock in the diffuser [143]. The model assu mes linear perturbations and a harmonic regime, radial acoustic modes are considered to be cut-off for the frequencies of interest and vorticity is neglected so that pressure and velocity fluctuations are purely 1D and of acoustic nature. The specificity of supercritical nozzle flows is accounted for through a Mach number of unity at nozzle throat and the shock, if present, is modelled through dynamic shock relations. Validation of the 2D model is achieved through comparisons with numerical simulations, reproduced in Fig. 89, which outline in addition the failure of 1D model to correctly predict entropy noise. Noise scattering through the nozzle is also investigated. Both 1D and 2D models are found to correctly recover transmitted and reflected acoustic waves, which indicates that 2D mean flow effects are negligible for the propagation of the acoustic waves through the nozzle.

Written by Maxime Huet: maxime.huet@onera.fr, A. Emmanuelli and T. Le Garrec, ONERA, France.

6.9. Noise sources of an unconfined and a confined swirl burner

In this study [144], the sound sources of an unconfined and a confined swirl burner are investigated by a two-step approach. The Reynolds number is $Re_D = 8800$ and the swirl number is $S = 0.73$. First, the conservation equations of a compressible fluid are solved to determine the flow field under reacting and non-reacting conditions. The solution determines the mean flow field and the source terms of the acoustic perturbation equations. The contributions of the various sound sources are analysed by solving the acoustic perturbation equations in a computational aeroacoustics simulation for each of the source terms.

For the unconfined swirl burner, the precessing vortex core of the swirl flow is a dominant sound source in non-reacting flow, whereas in reacting flow the unsteady heat release dominates the sound field. This changes when the burner is confined. A self-excited instability occurs at the quarter-wave mode of the burner and further sources become important to accurately predict the sound pressure amplitude of the limit cycle. The pressure signals of the most significant sources of the confined burner are shown in Fig. 90. The source formulation must comprise the heat release source $q_{e,h}$, the entropy source $q_{e,III}$, and the momentum subsource $q_{m,p}$ to accurately reconstruct the signal of the full source formulation.

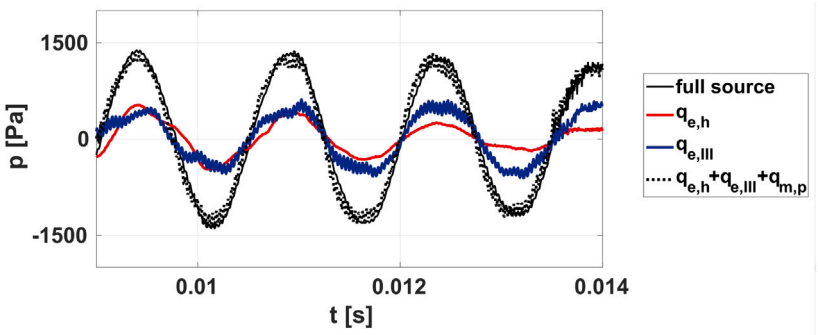

Fig. 90. Pressure signal of the confined swirl flame recorded on the centreline 16D downstream of the injector exit. The signals generated by the full set of sources (solid black line), the heat release source $q_{e,h}$, the entropy source $q_{e,III}$, and a reduced set of sources $q_{e,h} + q_{e,III} + q_{m,p}$ is shown.

Note that for the flames investigated in a previous study [145] the same set of source terms was required for an accurate prediction of the pressure signals. However, the impact of these sources on the sound field is different for the current flame. That is, for the quarter-wave oscillation, which clearly dominates the pressure signal in Fig. 90, the pressure signals by the various source terms show no significant differences in phase. Thus, the heat release source mispredicts the amplitude, but determines the correct phase of the quarter-wave mode oscillation.

S. Herff, AIA RWTH, Aachen, Germany: s.herff@aia.rwth-aachen.de, K. Pausch, JSC, Jülich, Germany, W. Schröder, AIA RWTH, Aachen, Germany

CRediT authorship contribution statement

Attila Balázs Nagy: Writing – review & editing. **Jan Delfs:** Writing – review & editing. **Gareth J. Bennett:** Software to acquire highlight, Writing – original draft, Writing – review & editing, Project administration.

Declaration of competing interest

The authors declare that they have no known competing financial interests or personal relationships that could have appeared to influence the work reported in this paper.

References

[1] C. Poggi, M. Rossetti, G. Bernardini, U. Iemma, C. Andolfi, C. Milano, M. Gennaretti, Surrogate models for predicting noise emission and aerodynamic performance of propellers, Aerosp. Sci. Technol. (2021) 107016.
[2] M. Gennaretti, G. Bernardini, J. Serafini, G. Romani, Rotorcraft comprehensive code assessment for blade-vortex interaction conditions, Aerosp. Sci. Technol. 80 (2018) 232–246.
[3] E. Grande, G. Romani, D. Ragni, F. Avallone, D. Casalino, Aeroacoustic investigation of a propeller operating at low Reynolds numbers, AIAA J. 60 (2) (2021) 860–871.
[4] D. Casalino, G. Edoardo, G. Romani, D. Ragni, F. Avallone, Definition of a benchmark for low Reynolds number propeller aeroacoustics, Aerosp. Sci. Technol. 113 (106707) (2021) 106707.
[5] G. Romani, E. Grande, F. Avallone, D. Ragni, D. Casalino, Performance and noise prediction of low-Reynolds number propellers using the Lattice-Boltzmann method, Aerosp. Sci. Technol. (2021) 107086.
[6] R. Gojon, T. Jardin, H. Parisot-Dupuis, Experimental investigation of low Reynolds number rotor noise, J. Acoust. Soc. Am. 149 (6) (2021) 3813–3829.
[7] H. Parisot-Dupuis, R. Gojon, T. Jardin, Y. Jo, N. Doué, J.-M. Moschetta, Y. Jo, Experiments on UAV rotor noise at low Reynolds and low mach numbers, in: Quiet Drones International E-Symposium on UAV/UAS Noise, Oct. 2020, Paris, 2020.
[8] N. Zawodny, D. Boyd Jr., C. Burley, Acoustic characterization and prediction of representative, small-scale rotary-wing unmanned aircraft system components, in: AHS International Forum 72 May 17-19, 2016 West Palm Beach, Florida, USA, (20160009054) NTRS - NASA Technical Reports Server, 2016, URL https://ntrs.nasa.gov/citations/20160009054.
[9] N. Zawodny, D. Boyd, Investigation of rotor–airframe interaction noise associated with small-scale rotary-wing unmanned aircraft systems, J. Am. Helicopter Soc. 65 (1) (2020) 1–17.
[10] G. Bernardini, F. Centracchio, M. Gennaretti, U. Iemma, C. Pasquali, C. Poggi, M. Rossetti, J. Serafini, Numerical characterisation of the aeroacoustic signature of propeller arrays for distributed electric propulsion, Appl. Sci. 10 (8) (2020) 2643.
[11] G. Bernardini, C. Poggi, M. Gennaretti, C. Testa, Study of velocity-potential integral formulations for sound scattered by moving bodies, AIAA J. 59 (3) (2021) 1008–1019.
[12] M. Gennaretti, G. Bernardini, C. Poggi, C. Testa, Velocity-potential boundary-field integral formulation for sound scattered by moving bodies, AIAA J. 56 (9) (2018) 3547–3557.
[13] K. Taylor, A transformation of the acoustic equation with implications for wind-tunnel and low-speed flight tests, Proc. R. Soc. Lond. Ser. A Math. Phys. Eng. Sci. 363 (1713) (1978) 271–281.
[14] S. Mancini, R.J. Astley, S. Sinayoko, G. Gabard, M. Tournour, An integral formulation for wave propagation on weakly non-uniform potential flows, J. Sound Vib. 385 (2016) 184–201.
[15] C. Yang, P. Zhang, S. Jacob, E. Trigell, M. Åbom, Investigation of extended-tube liners for control of low-frequency duct noise, AIAA J. 59 (2021) 1–16.

[16] T. Ahlefeldt, S. Haxter, C. Spehr, D. Ernst, T. Kleindienst, Road to acquisition: Preparing a MEMS microphone array for measurement of fuselage surface pressure fluctuations, Micromachines 12 (8) (2021) 961.
[17] A. Goudarzi, C. Spehr, S. Herbold, Automatic source localization and spectra generation from sparse beamforming maps, J. Acoust. Soc. Am. 150 (3) (2021) 1866–1882.
[18] R.J.G.B. Campello, D. Moulavi, J. Sander, Density-based clustering based on hierarchical density estimates, in: J. Pei, V.S. Tseng, L. Cao, H. Motoda, G. Xu (Eds.), Advances in Knowledge Discovery and Data Mining, Springer Berlin Heidelberg, Berlin, Heidelberg, 2013, pp. 160–172.
[19] L. Bertsch, R. Thomas, L. Sanders, I. Legriffon, The aircraft noise simulation working group (ANSWr) - tool benchmark and reference aircraft results, in: 25th AIAA/CEAS Aeroacoustics Conference, in: AIAA 2019-2539, AIAA, Delft, Netherlands, 2019.
[20] L. Sanders, R. Thomas, L. Bertsch, I. Legriffon, I. Clark, J. June, M. Lorteau, The aircraft noise simulation working group (ANSWr) – V2 aircraft results, in: 25th AIAA/CEAS Aeroacoustics Conference, in: AIAA 2019-2540, AIAA, Delft, Netherlands, 2019.
[21] L. Bertsch, L. Sanders, R. Thomas, I. Legriffon, J. June, I. Clark, M. Lorteau, Comparative assessment of aircraft system noise simulation, J. Aircr. 58 (4) (2021) 867–884.
[22] S. Rizzi, I. Legriffon, R. Pieren, L. Bertsch, A comparison of aircraft flyover auralizations by the aircraft noise simulation working group, in: AIAA AVIATION 2020 FORUM, in: AIAA 2020-2582, AIAA, online, 2020.
[23] U. Iemma, G. Palma, Design of metacontinua in the aeroacoustic spacetime, Sci. Rep. 10 (2020) 18192.
[24] G. Palma, L. Burghignoli, On the integration of acoustic phase-gradient metasurfaces in aeronautics, Int. J. Aeroacoust. 19 (6–8) (2020) 294–309.
[25] S.W. Rienstra, Numerical and asymptotic solutions of the pridmore-brown equation, AIAA J. 58 (7) (2020) 3001–3018.
[26] S.W. Rienstra, Slowly varying modes in a two-dimensional duct with shear flow and lined walls, J. Fluid Mech. 906, A23 (2021) 1–25, (Open Access).
[27] R. Longobardi, D. Fabre, P. Bonnefis, V. Citro, F. Giannetti, P. Luchini, Studying sound production in the hole-tone configuration using compressible and incompressible global stability analyses, in: M. Braza, K. Hourigan, M. Triantafyllou (Eds.), Advances in Critical Flow Dynamics Involving Moving/Deformable Structures with Design Applications, Series Notes on Numerical Fluid Mechanics and Multidisciplinary Design, Springer International Publishing, 2021, pp. 251–263.
[28] D. Fabre, R. Longobardi, V. Citro, P. Luchini, Acoustic impedance and hydrodynamic instability of the flow through a circular aperture in a thick plate, J. Fluid Mech. 885 (2020) A11.
[29] D. Fabre, V. Citro, D. Ferreira Sabino, P. Bonnefis, J. Sierra, F. Giannetti, M. Pigou, A practical review on linear and nonlinear global approaches to flow instabilities, Appl. Mech. Rev. 70 (6) (2018) 060802.
[30] J. Sierra, D. Fabre, V. Citro, Efficient stability analysis of fluid flows using complex mapping techniques, Comput. Phys. Comm. 251 (2020) 107100.
[31] J. Sierra, V. Citro, D. Fabre, On boundary conditions for compressible flow simulations, in: Fluid-Structure-Sound Interactions and Control, Springer Singapore, 2021, pp. 335–340.
[32] G. Petrone, M. Manfredonia, S.D. Rosa, F. Franco, Structural similitudes of stiffened cylinders, Math. Mech. Solids 24 (2019) 527–541.
[33] A. Berry, O. Robin, F. Franco, S.D. Rosa, G. Petrone, Similitude laws for the sound radiation of flat orthotropic flexural panels, J. Sound Vib. 489 (2020) 115636.
[34] F. Franco, A. Berry, G. Petrone, S. De Rosa, E. Ciappi, O. Robin, Structural response of stiffened plates in similitude under a turbulent boundary layer excitation, J. Fluids Struct. 98 (2020) 103119.
[35] H.-G. Raumer, C. Spehr, T. Hohage, D. Ernst, Weighted data spaces for correlation-based array imaging in experimental aeroacoustics, J. Sound Vib. (2020) 115878.
[36] A. Aitken, IV.—on least squares and linear combination of observations, Proc. Roy. Soc. Edinburgh 55 (1936) 42–48.
[37] L. Isserlis, On certain probable errors and correlation coefficients of multiple frequency distrubutions with skew regression, Biometrika 11 (3) (1916) 185–190.
[38] T. Ahlefeldt, Aeroacoustic measurements of a scaled half-model at high Reynolds numbers, AIAA J. 51 (12) (2013) 2783–2791.
[39] C. Freidhager, P. Maurerlehner, K. Roppert, A. Wurzinger, A. Hauser, M. Heinisch, S. Schoder, M. Kaltenbacher, Simulationen von Strömungsakustik in rotierenden Bauteilen zur Entwicklung von Antriebskonzepten der Autos der Zukunft, E I Elektr. Inf. 138 (2021) 212–218.
[40] S. Schoder, C. Junger, M. Kaltenbacher, Computational aeroacoustics of the EAA benchmark case of an axial fan, Acta Acust. 4 (2020) 17.
[41] M. Hornikx, M. Kaltenbacher, S. Marburg, European acoustics association: Benchmark cases for computational acoustics, 2017.
[42] S. Schoder, A. Wurzinger, C. Junger, M. Weitz, C. Freidhager, K. Roppert, M. Kaltenbacher, Application limits of conservative source interpolation methods using a low mach number hybrid aeroacoustic workflow, J. Theore. Comput. Acoust. 29 (2021) 28.
[43] P. Bernicke, R. Akkermans, R. Ewert, J. Dierke, Acoustic relaxation term for damping and forcing of waves, AIAA J. 58 (2020) 2029–2041.
[44] R. Ewert, J. Dierke, A. Neifeld, M.A. Moghadam, Linear and non-linear perturbation equations with relaxation source terms for forced eddy simulation of aeroacoustic sound generation, in: 20th AIAA/CEAS Aeroacoustics Conference, Atlanta, GA, 16-20 June 2014, 2014, AIAA Paper No. 2014-3053.
[45] R. Akkermans, P. Bernicke, R. Ewert, J. Dierke, Zonal overset-LES with stochastic volume forcing, Int. J. Heat Fluid Flow 70 (2018) 336–347.
[46] A. Agarwal, P.J. Morris, R. Mani, Calculation of sound propagation in nonuniform flows: Suppression of instability waves, AIAA J. 42 (2004) 80–88.
[47] S.R. More, Consideration of Aircraft Noise Annoyance During Conceptual Aircraft Design (Ph.D. thesis), Purdue University, 2010.
[48] A. Vieira, U. Mehmood, R. Merino-Martinez, M. Snellen, D.G. Simons, Variability of sound quality metrics for different aircraft types during landing and take-off, in: 25th AIAA/CEAS Aeroacoustics Conference, in: AIAA 2019-2512, AIAA, Atlanta, Georgia, 2019.
[49] G. Felix Greco, L. Bertsch, T.P. Ring, S.C. Langer, Sound quality assessment of a medium-range aircraft with enhanced fan-noise shielding design, CEAS Aeronaut. J. 12 (2021) 481–493.
[50] L. Bertsch, Noise Prediction within Conceptual Aircraft Design (Ph.D. thesis), Technische Universität Braunschweig, 2013.
[51] L. Bertsch, F. Wolters, W. Heinze, M. Pott-Pollenske, J. Blinstrub, System noise assessment of a tube-and-wing aircraft with geared turbofan engines, AIAA J. Aircr. 56 (2019) 1577–1596.
[52] E. Spieser, C. Bailly, Sound propagation using an adjoint-based method, J. Fluid Mech. 900 (2020) A5.
[53] E. Spieser, G. Bodard, C. Bailly, Jet noise prediction based on a self-adjoint operator, in: E-Forum Acusticum, December 7-11, 2020, pp. 1325–1332.
[54] Y. Zhou, F. Ollivier, P. Challande, R. Marchiano, V. Valeau, D. Marx, C. Prax, Design and use of a three-dimensional array of MEMS microphones for aeroacoustic measurements in wind-tunnels, in: 8th Berlin Beamforming Conference (BeBeC), Mar. 2020, Berlin, Germany, 2020.
[55] Y. Zhou, V. Valeau, J. Marchal, F. Ollivier, R. Marchiano, Three-dimensional imaging of aeroacoustic sources in an anechoic wind-tunnel using a massive array of MEMS microphones, J. Sound Vib. 482 (2020) 115459.
[56] F. Errico, F. Franco, S. De Rosa, G. Petrone, M. Ichchou, Aeroelastic effects on wave propagation and sound transmission of plates and shells, AIAA J. 58 (5) (2020) 2269–2275.
[57] N. Peake, On the behaviour of a fluid-loaded cylindrical shell with mean flow, J. Fluid Mech. 338 (1997) 387–410.
[58] B.H. M. Ichchou, B. Troclet, Equivalent 'rain on the roof' loads for random spatially correlated excitations in the mid-high frequency range, J. Sound Vib. 322 (2009) 926–940.
[59] G. Petrone, G. Melillo, A. Laudiero, S.D. Rosa, A statistical energy analysis (SEA) model of a fuselage section for the prediction of the internal sound pressure level (SPL) at cruise flight conditions, Aerosp. Sci. Technol. 88 (2019) 340–349.
[60] G. Mazzeo, M. Ichchou, G. Petrone, O. Bareille, S. De Rosa, F. Franco, First models for structural energy transmission decoupling in the high frequency regime under aerodynamic excitations, Proc. Inst. Mech. Eng. C 236 (3) (2021) 1307–1321.

[61] J.-P. Groby, A. Wirgin, L. Ryck, W. Lauriks, R. Gilbert, Y. Xu, Acoustic response of a rigid-frame porous medium plate with a periodic set of inclusions, J. Acoust. Soc. Am. 126 (2009) 685–693.

[62] L. Xiong, B. Nennig, Y. Aurégan, W. B., Sound attenuation optimization using metaporous materials tuned on exceptional points, J. Acoust. Soc. Am. 142 (2017) 2288–2297.

[63] D. Magliacano, G. Petrone, F. Franco, S. De Rosa, Numerical investigations about the sound transmission loss of a fuselage panel section with embedded periodic foams, Appl. Acoust. 182 (2021) 108265.

[64] C. Teruna, F. Manegar, F. Avallone, D. Ragni, D. Casalino, T. Carolus, Noise reduction mechanisms of an open-cell metal-foam trailing edge, J. Fluid Mech. 898 (2020) A18.

[65] L. Rego, D. Ragni, F. Avallone, D. Casalino, R. Zamponi, C. Schram, Jet-installation noise reduction with flow-permeable materials, J. Sound Vib. 498 (2021) 115959.

[66] A.R. Carpio, F. Avallone, D. Ragni, M. Snellen, S. van der Zwaag, Quantitative criteria to design optimal permeable trailing edges for noise abatement, J. Sound Vib. 485 (2020) 115596.

[67] R. Merino-Martínez, A. Rubio Carpio, L. Lima Pereira, S. van Herk, F. Avallone, D. Ragni, M. Kotsonis, Aeroacoustic design and characterization of the 3D-printed, open-jet, anechoic wind tunnel of delft university of technology, Appl. Acoust. 170 (2020) 107504.

[68] M. Szőke, D. Fiscaletti, M. Azarpeyvand, Influence of boundary layer flow suction on trailing edge noise generation, J. Sound Vib. 475 (2020) 115276.

[69] M. Szőke, D. Fiscaletti, M. Azarpeyvand, Uniform flow injection into a turbulent boundary layer for trailing edge noise reduction, Phys. Fluids 32 (8) (2020) 085104.

[70] K. Zhao, P. Okolo, E. Neri, P. Chen, J. Kennedy, G.J. Bennett, Noise reduction technologies for aircraft landing gear-A bibliographic review, Prog. Aerosp. Sci. 112 (2019) 100589.

[71] G. Bennett, E. Neri, J. Kennedy, Noise characterization of a full-scale nose landing gear, J. Aircr. 55 (2018) 2476–2490.

[72] R. Merino-Martinez, E. Neri, M. Snellen, J. Kennedy, D.G. Simons, G.J. Bennett, Multi–approach study of nose landing gear noise, J. Aircr. 57 (2020) 517–533.

[73] E. Neri, J. Kennedy, G.J. Bennett, Aeroacoustic source separation on a full scale nose landing gear featuring combinations of low noise technologies, in: Internoise2015: Proceedings of the Internoise 2015/ASME NCAD Meeting, American Society of Mechanical Engineers, San Francisco, CA, USA, 2015, Paper No: NCAD2015–5912.

[74] E. Neri, J. Kennedy, M.D. Giulio, C. O'Reilly, J. Dahan, M. Esposito, M. Bruno, F. Amoroso, A. Bianco, G.J. Bennett, Characterization of low noise technologies applied to a full scale fuselage mounted nose landing gear, in: Internoise2015: Proceedings of the Internoise 2015/ASME NCAD Meeting, American Society of Mechanical Engineers, San Francisco, CA, USA, 2015, Paper No: NCAD2015–5911.

[75] R. Merino-Martinez, J. Kennedy, G.J. Bennett, Experimental study of realistic low–noise technologies applied to a full–scale nose landing gear, Aerosp. Sci. Technol. 113 (2021) 1–20.

[76] S. Luesutthiviboon, A. Malgoezar, R. Merino-Martinez, M. Snellen, P. Sijtsma, D. Simons, Enhanced HR–CLEAN–SC for resolving multiple closely spaced sound sources, International Journal of Aeroacoustics 18 (2019) 392–413.

[77] R. Zamponi, D. Ragni, N. Van de Wyer, C. Schram, Experimental investigation of airfoil turbulence-impingement noise reduction using porous treatment, in: 25th AIAA/CEAS Aeroacoustics Conference, in: AIAA 2019-2649, American Institute of Aeronautics and Astronautics, Delft, The Netherlands, 2019.

[78] R. Zamponi, S. Satcunanathan, S. Moreau, D. Ragni, M. Meinke, W. Schröder, C. Schram, On the role of turbulence distortion on leading-edge noise reduction by means of porosity, J. Sound Vib. 485 (2020) 115561.

[79] R. Zamponi, N. Van de Wyer, C. Schram, Benchmark assessment of an improved regularization technique for generalized inverse beamforming, in: 2018 AIAA/CEAS Aeroacoustics Conference, in: AIAA 2018-4106, American Institute of Aeronautics and Astronautics, Atlanta, Georgia, 2018.

[80] V. Ananthan, P. Bernicke, R. Akkermans, T. Hu, P. Liu, Effect of porous material on trailing edge sound sources of a lifting airfoil by zonal overset-LES, J. Sound Vib. 480 (2020) 115386.

[81] P. Bernicke, R. Akkermans, V. Ananthan, R. Ewert, J. Dierke, L. Rossian, A zonal noise prediction method for trailing-edge noise with a porous model, Int. J. Heat Fluid Flow 80 (2019) 108469.

[82] W.J.G. da Silva Pinto, F. Margnat, A shape optimization procedure for cylinders aeolian tone, Comput. & Fluids 182 (2019) 37–51.

[83] W.J.G.S. Pinto, F. Margnat, Y. Gervais, Influence of cross-section on the aeolian tone: a numerical study in the laminar regime, in: 25th AIAA/CEAS Aeroacoustics Conference, in: AIAA 2019-2532, AIAA, Delft, The Netherlands, 2019.

[84] W.J.G. da Silva Pinto, F. Margnat, Shape optimization for the noise induced by the flow over compact bluff bodies, Comput. & Fluids 198 (2020) 104400.

[85] W.J.G.S. Pinto, F. Margnat, C. Noûs, Aeolian tone level as a consequence of distance to the onset of unsteadiness: influence of bluff-body shape on the critical Reynolds number, in: Forum Acousticum, 7-11 December, Lyon, France, 2020.

[86] W.J.G.S. Pinto, F. Margnat, C. Noûs, Experimental study of the influence of the shape on the spanwise coherence length of the flow over a bluff body, in: Forum Acousticum, 7-11 December, Lyon, France, 2020.

[87] V. Ananthan, P. Bernicke, R. Akkermans, Aeroacoustic analysis of a circulation-controlled high-lift flap by zonal overset large-Eddy simulation, AIAA J. 58 (2020) 5294–5305.

[88] P. Bernicke, R. Akkermans, V. Ananthan, R. Ewert, J. Dierke, L. Rossian, A zonal noise prediction method for trailing-edge noise with a porous model, Int. J. Heat Fluid Flow 80 (2019) 108469.

[89] E. Talboys, C. Brücker, Upstream shear-layer stabilisation via self-oscillating trailing edge flaplets, Exp. Fluids 59 (10) (2018) 1–10.

[90] E. Talboys, T.F. Geyer, C. Brücker, An aeroacoustic investigation into the effect of self-oscillating trailing edge flaplets, J. Fluids Struct. 91 (2019) 102598.

[91] E. Talboys, T.F. Geyer, F. Prüfer, C. Brücker, A parametric study of the effect of self-oscillating trailing-edge flaplets on aerofoil self-noise, Appl. Acoust. 177 (2021) 107907.

[92] E. Talboys, T.F. Geyer, C. Brücker, Influence of self-oscillating trailing edge flaplets on turbulent boundary layer–trailing edge noise., in: 23rd Int. Congr. Acoust., Aachen, Germany, 2019.

[93] C. Teruna, F. Avallone, D. Ragni, A. Rubio-Carpio, D. Casalino, Numerical analysis of a 3-D printed porous trailing edge for broadband noise reduction, J. Fluid Mech. 926 (2021).

[94] L. Rego, F. Avallone, D. Ragni, D. Casalino, On the mechanisms of jet-installation noise reduction with flow-permeable trailing edges, J. Sound Vib. (2021) 116582.

[95] M. Daroukh, T. Le Garrec, C. Polacsek, Low-speed turbofan aerodynamic and acoustic prediction with an isothermal lattice Boltzmann method, AIAA J. 60 (2) (2022) 1152–1170.

[96] R.A. Loew, J.T. Lauer, J. McAllister, D.L. Sutliff, The advanced noise control fan, in: 25th AIAA Aerodynamic Measurement Technology and Ground Testing Conference, 5-8 June 2006, San Francisco, CA., in: AIAA 2006-3150, 2006.

[97] S. Palani, P. Murray, A. McAlpine, C. Richter, Optimisation of slanted septum core and multiple folded cavity acoustic liners for aero-engines, in: AIAA AVIATION 2021 FORUM, in: AIAA 2021-2172, AIAA, Chicago, IL & Online, 2021, pp. 1–19.

[98] S. Palani, P. Murray, A. McAlpine, D. Sasaki, C. Richter, Slanted septum and multiple folded cavity liners for broadband sound absorption, Int. J. Aeroacoust. 20 (5–7) (2021) 633–661.

[99] M. Staggat, A. Moreau, S. Guerin, Analytical prediction of boundary layer ingestion noise for an integrated turbofan, in: 26th International Congress on Sound and Vibration, ICSV, 2019,

[100] M. Barbarino, D. Bianco, A BEM-FMM approach applied to the combined convected Helmholtz integral formulation for the solution of aeroacoustic problems, Comput. Methods Appl. Mech. Engrg. 342 (2018) 585–603.
[101] F. Petrosino, M. Barbarino, M. Staggat, Aeroacoustics assessment of an hybrid aircraft configuration with rear-mounted boundary layer ingested engine, Appl. Sci. 11 (7) (2021) 2936.
[102] A. Proença, J. Lawrence, R. Self, Experimental investigation into the turbulence flowfield of in-flight round jets, AIAA J. 58 (8) (2020) 3339–3350.
[103] A. Proença, J. Lawrence, R. Self, Measurements of the single-point and joint turbulence statistics of high subsonic jets using hot-wire anemometry, Exp. Fluids 60 (4) (2019) 63.
[104] A. Proença, J. Lawrence, R. Self, Investigation into the turbulence statistics of installed jets using hot-wire anemometry, Exp. Fluids 61 (8) (2020) 220.
[105] M.J. Lighthill, On sound generated aerodynamically, General Theory. Proc. R. Soc. Lond. (1952) 564–587.
[106] S. Meloni, A. Di Marco, M. Mancinelli, R. Camussi, Wall-pressure fluctuations induced by a compressible jet flow over a flat plate at different mach numbers, Exp. Fluids 60 (3) (2019) 48.
[107] S. Meloni, M. Mancinelli, R. Camussi, J. Huber, Wall-pressure fluctuations induced by a compressible jet in installed configuration, AIAA J. 58 (7) (2020) 2991–3000.
[108] S. Meloni, J.L. Lawrence, A.R. Proenca, R.H. Self, R. Camussi, Wall pressure fluctuations induced by a single stream jet over a semi-finite plate, Int. J. Aeroacoust. 19 (3–5) (2020) 240–253.
[109] C. Polacsek, A. Cader, M. Buszyk, R. Barrier, F. Gea-Aguilera, H. Posson, Aeroacoustic design and broadband noise predictions of a fan stage with serrated outlet guide vanes, Phys. Fluids 32 (2020).
[110] A. Zarri, J. Christophe, S. Moreau, C. Schram, Influence of swept blades on low-order acoustic prediction for axial fans, Acoustics 2 (4) (2020) 812–832.
[111] A. Zarri, J. Christophe, C. Schram, Low-order aeroacoustic prediction of low-speed axial fan noise, in: 25th AIAA/CEAS Aeroacoustics Conference, 20-23 May 2019, Delft, NL, American Institute of Aeronautics and Astronautics, 2019, AIAA Paper 2019-2760.
[112] V. Kopiev, G. Faranosov, O. Bychkov, V. Kopiev, I. Moralev, P. Kazansky, Active control of jet-plate interaction noise for excited jets by plasma actuators, J. Sound Vib. 484 (2020) 115515.
[113] V.F. Kopiev, Y.S. Akishev, I.V. Belyaev, N.K. Berezhetskaya, V.A. Bityurin, G.A. Faranosov, M.E. Grushin, A.I. Klimov, V.A. Kopiev, I.A. Kossyi, I.A. Moralev, N.N. Ostrikov, M.I. Taktakishvili, N.I. Trushkin, M.Y. Zaytsev, Instability wave control in turbulent jet by plasma actuators, J. Phys. D: Appl. Phys. 47 (2014) 505201.
[114] Z.-N. Wang, A. Proenca, J. Lawrence, P.G. Tucker, R. Self, Large-Eddy-simulation prediction of an installed jet flow and noise with experimental validation, AIAA J. 58 (6) (2020) 2494–2503.
[115] A. Proenca, J. Lawrence, R. Self, Measurements of the single-point and joint turbulence statistics of high subsonic jets using hot- wire anemometry, Exp. Fluids 60 (2019) 63.
[116] J. Lawrence, M. Azarpeyvand, R. Self, Interaction between a flat plate and a circular subsonic jet, in: 17th AIAA/CEAS Aeroacoustics Conference (32nd AIAA Aeroacoustics Conference), 5-8 June 2011, Portland, Oregon, 2011, AIAA Paper 2011-2745.
[117] N. Hu, Coherence of wall pressure fluctuations in zero and adverse pressure gradients, J. Sound Vib. 511 (2021) 1–27.
[118] A. Smol'yakov, V. Tkachenko, Model of a field of pseudosonic turbulent wall pressures and experimental data, Akust. Zh. 37 (1991) 1199–1207.
[119] G. Corcos, The structure of the turbulent pressure field in boundary layer flows, J. Fluid Mech. 18 (1964) 353–378.
[120] S. Haxter, C. Spehr, Comparison of model prediction for coherence length to in-flight measurements at cruise conditions, J. Sound Vib. 390 (2017) 86–117.
[121] S.L. Prigent, E. Salze, E. Jondeau, C. Bailly, Spatial structure and wavenumber filtering of wall pressure fluctuations on a full-scale cockpit model, Exp. Fluids 61 (9) (2020) 1–14.
[122] D. Juvé, S.L. Prigent, E. Salze, P. Souchotte, C. Bailly, Opening lectures—Wall-pressure wavenumber-frequency spectra: Experimental challenges and recent advances, in: Flinovia—Flow Induced Noise and Vibration Issues and Aspects-III, Springer Nature, 2021, pp. 1–23.
[123] S.L. Prigent, E. Salze, C. Bailly, Deconvolution of wave-number-frequency spectra of wall pressure fluctuations, AIAA J. 58 (1) (2020) 164–173.
[124] W.J. Tzeng, F.Y. Wu, Theory of impedance networks: the two-point impedance and LC resonances, J. Phys. A: Math. Gen. 39 (27) (2006) 8579–8591.
[125] I. Davis, A. McKay, G.J. Bennett, A graph-theory approach to optimisation of an acoustic absorber targeting a specific noise spectrum that approaches the causal optimum minimum depth, Journal of Sound and Vibration 505 (2021) 116135.
[126] A. McKay, I. Davis, J. Killeen, G.J. Bennett, SeMSA: a compact super absorber optimised for broadband, low-frequency noise attenuation, Sci. Rep. 10 (1) (2020) 17967.
[127] D.-Y. Ma, Theory of microslit absorbers, Acta Acust. 25 (2001) 481–485.
[128] A. Aulitto, A. Hirschberg, I. Lopez-Arteaga, Influence of geometry on acoustic end-corrections of slits in microslit absorbers, J. Acoust. Soc. Am. 149 (2021) 3073–3085.
[129] A. Aulitto, A. Hirschberg, I.L. Arteaga, E.L. Buijssen, Effect of slit length on linear and non-linear acoustic transfer impedance of a micro-slit plate, Acta Acust. 6 (2022) 6.
[130] L. Hirschberg, S.J. Hulshoff, F. Bake, Sound production due to swirl–nozzle interaction: Model-based analysis of experiments, AIAA J. 59 (4) (2021) 1269–1276.
[131] L. Hirschberg, F. Bake, K. Knobloch, S.J. Hulshoff, Swirl-nozzle interaction experiments: Influence of injection-reservoir pressure and injection time, AIAA J. 59 (7) (2021) 2806–2810.
[132] L. Hirschberg, F. Bake, K. Knobloch, A. Rudolphi, S. Kruck, O. Klose, S.J. Hulshoff, Swirl-nozzle interaction experiment: Quasi-steady model based analysis, Exp. Fluids 62 (175) (2021) 1–16.
[133] B.J. Tester, The propagation and attenuation of sound in lined ducts containing uniform or 'plug' flow, J. Sound Vib. 28 (1973) 151–203.
[134] Z. Zhang, H. Bodén, M. Åbom, The cremer impedance: An investigation of the low frequency behavior, J. Sound Vib. 459 (2019) 114884.
[135] A.M. Spillere, L.A. Bonomo, J.A. Cordioli, E.J. Brambley, Experimentally testing impedance boundary conditions for acoustic liners with flow: Beyond upstream and downstream, J. Sound Vib. 489 (2020) 115676.
[136] S. Jacob, M. Åbom, A comment on the correct boundary conditions for the cremer impedance, JASA Express Lett. 1 (2021) 022801.
[137] M. Barbarino, F. Petrosino, A. Visingardi, A high-fidelity aeroacoustic simulation of a VTOL aircraft in an urban air mobility scenario, Aerosp. Sci. Technol. (2021) 107104.
[138] D. Casalino, M. Barbarino, A. Visingardi, Simulation of helicopter community noise in complex urban geometry, AIAA J. 49 (8) (2011) 1614–1624.
[139] M. Noeding, L. Bertsch, Application of noise certification regulations within conceptual design, MDPI Aerosp. Aircr. Noise 8 (2021) 1–23, Special Issue.
[140] V. Lafont, F. Méry, R. Roncen, F. Simon, E. Piot, Liner impedance eduction under shear grazing flow at a high sound pressure level, AIAA J. 58 (3) (2020) 1107–1117.
[141] V. Lafont, F. Méry, P. Reulet, F. Simon, Surface temperature measurement of acoustic liners in the presence of grazing flow and thermal gradient, Exp. Fluids 62 (2021) 82.
[142] A. Emmanuelli, J. Zheng, M. Huet, A. Giauque, T.L. Garrec, S. Ducruix, Description and application of a 2D-axisymmetric model for entropy noise in nozzle flows, J. Sound Vib. 472 (2020) 115163.
[143] M. Huet, A. Emmanuelli, T.L. Garrec, Entropy noise modelling in 2D choked nozzle flows, J. Sound Vib. 488 (2020) 115637.
[144] K. Pausch, S. Herff, W. Schröder, Noise sources of an unconfined and a confined swirl burner, J. Sound Vib. 475 (2020) 115293.
[145] K. Pausch, S. Herff, F. Zhang, H. Bockhorn, W. Schröder, Noise sources of lean premixed flames, Flow Turbul. Combust. 103 (2019) 773–796.